Induced Cell Death in Diverse Algal Species by the Exposure to Resin Nanoparticles

by

Ayat Jabr Salem Al-Azab

Student ID Number: 1228001

A dissertation submitted to the

Engineering Course, Department of Engineering,

Graduate School of Engineering,

Kochi University of Technology,

Kochi, Japan

in Partial Fulfillment of the Requirements for the degree of

Doctor of Philosophy

Assessment Committee:

Supervisor : Professor Takeshi Ohama

Co-Supervisor : Professor Seiji Tanaka

Co-Supervisor : Professor Kojiro Ishii

Yasuko Hayashi, Niigata University

Hitoshi Miyasaka, Sojo University

September 2021

ABSTRACT

The number and use of resin nanoparticles have been rapidly increased, which has led to growing awareness of their adverse effect on living organisms, particularly on aquatic organisms. It has been reported that resin nanoparticles made of isobutyl cyanoacrylate polymers (iBCA-NPs) acutely induce cell death in a wide range of microgreen algae; this was accompanied by excess accumulation of reactive oxygen species (ROS). In this study, analysis of the fundamental mechanism of how resin NPs induce cell death in algae, determination of how widely distributed algal species differ in their sensitivity, and investigation of transcriptome changes induced by iBCA-NPs were performed. First, to examine the potency of iBCA-NPs to induce cell death in diverse non-green algal species (e.g. species in the SAR and Hacrobia clades) and the difference in sensitivity to iBCA-NPs among the species, 18 non-green algal species were co-incubated with laboratory-prepared iBCA-NPs (mean diameter: 180 nm). After exposure to 100 mg L^{-1} iBCA-NPs for 24 h, cell death was induced in two of three *Bacillariophyceae* species, all three *Cryptophyceae* species, four of six Dinophyta species, three of four Haptophyta strains, and all three *Raphidophyceae* species. However, exposure to a concentration of 1 g L^{-1} iBCA-NPs induced cell death in all the examined species. ROS scavenger *N*-acetyl-L-cysteine (NAC) substantially delayed cell death induction, suggesting that ROS generation is a direct cause of induced cell death. The cells of the *Raphidophyceae* species that lack covering structures and a Haptophyta strain bearing no coccoliths were more sensitive than those of species bearing covering structures. This finding suggests that cell covering structures act as barriers against the invasion of NPs.

Second, to better understand the molecular mechanism of cell death induced in algae by iBCA-NPs, altered gene expression changes along with the increase of the cell death ratio were investigated in *Chlamydomonas reinhardtii* (Chlorophyceae) through chronological

transcriptome analyses using next generation sequencing. Transcriptome data indicated upregulation of genes coding for the antioxidant enzymes included in the oxidative stress response, such as glutathione peroxidase (GPX5), Fe-superoxide dismutase (Fe-SOD), and glutathione S-transferase (GSTS1) when the cell death ratio reached ~3%. Besides these genes, 9 out of 20 heat shock protein (HSP)-coding genes and Cre13.g605200, a gene identified to code for cell wall hydrolytic enzymes, were prominently upregulated (log_2 fold-change, up to 11.73). The tag-insertion mutant for the Cre13.g605200 gene showed considerable resistance to nanoparticle-induced cell death, suggesting that its overexpression is essential for the induction of acute cell death by iBCA-NPs.

Nucleosomal units of laddering DNA were barely detected in the smeary digested DNA of *C. reinhardtii* cells exposed to iBCA-NPs, this indicates that induced cell death is primarily a necrosis-like type, while it is also partly accompanied by the programmed cell death (PCD)-like type. Direct chemical reactions between the largely accumulated ROS and intracellular substances such as proteins, lipids, and DNA can be the cause of necrosis.

DEDICATION

This Dissertation is dedicated to my beloved parents…

For their unconditional love and continuous support

ACKNOWLEDGEMENTS

First and foremost, I would like to praise and thank Allah for giving me the blessings, strength and ability during my study and in completing this work. Second, I am sincerely grateful to my supervisor, **Prof. Takeshi Ohama** for giving me the opportunity to be one of the doctoral students in his laboratory. I would like to thank him for all the guidance, recommendations, support, and help that I got from him not only in my research life, but also in my daily life in Japan. Moreover, thanks to my supervisor for helping me to improve my troubleshooting skills in research.

I would like to extend my gratitude to my co-supervisors, **Prof. Seiji Tanaka** and **Prof. Kojiro Ishii** for their valuable help and important suggestions. My sincere thanks goes also to the committee members: **Prof. Hitoshi Miyasaka** and **Associate Prof. Yasuko Hayashi** for their insightful comments and recommendations.

Special thanks to all of the **International Relation Center members (IRC)** for their kindness and help they offered me throughout my study. Thanks for the **Special Scholarship Program (SSP)** for the financial support during my research and study in Kochi University of Technology (KUT). Moreover, I gratefully acknowledge International house's managers for their efforts to provide us the pleasant and comfortable environment all along our stay in the International house.

I would like also to express my special thanks to **Dr. Fean D. Sarian** for his support, practical suggestions and helpful advice, and for the brainstorming and scientific discussions that we had throughout our working in the lab. Thanks also should go to **Dr. Dwiyantari Widyaningrum**, **Dr. Yuichi Aoki**, and my lab member **Yuki Sori** for their help and contribution in this work. Further thanks to **Dr. Tomohito Yamasaki** for his valuable advice and suggestions.

Deepest thanks to my friends, **Sukma Wahyu Fitriani**, **Mustafa Sarr**, **Asma Khatun**, **Namal Bandara**, **Islam Hamama**, and **Noha Ismail** for supporting and encouraging me throughout my study, for the wonderful times we shared and the joy we had even in tough times. Moreover, I would like to thank all my friends in Jordan for their support in particular, my best friend **Bayan Al-Momani** who continuously encourages and supports me. And many thanks to my friend **Majed Al-Rajibi** for all the help and support that he gave it to me all over my study.

Last but not the least, my ultimate thanks is dedicated to my family: **my parents**, my sisters and brothers who always give me the strength and encouragement to peruse my passion in research.

TABLE OF CONTENTS

LIST OF TABLES

LIST OF FIGURES

LIST OF ABBRIVIATIONS

Description	Abbreviation
2',7'-dichlorodihydrofluorescein diacetate	H2DCFDA
2',7'-dichlorofluorescein	DCF
Bovine serum albumin	BSA
Complementary DNA	cDNA
Eukaryotic initiation factor	EIF1A
False discovery rate	FDR
Fe-superoxide dismutase	Fe-SOD
Fold change	FC
Gamete lytic enzyme	GLE
Glutathione peroxidase	GPX5
Glutathione S-transferase	GSTS1
Heat shock protein	HSP
HSF	Heat shock factor
Inhibitor of apoptosis-promoting Bax1	BAX1-I
Matrix metalloproteinase	MMP
N-acetyl-L-cysteine	NAC
Nanoparticles	NPs
National Institute for Environmental Science	NIES
Optical density	OD
Poly(isobutylcyanacrylate) nanoparticles	iBCA-NPs
Poly(ADP-ribose) polymerase 16	PARP16
Polycyanoacrylate nanoparticles	PCA-NPs
Polymerase chain reaction	PCR
Principal component analysis	PCA
Programmed cell death	PCD
Quantile-adjusted conditional maximum likelihood	qCML
Quantitative real-time PCR	RT-qPCR

Quantum dots	QDs
Reactive oxygen species	ROS
Reads per kilobase of exon per million mapped reads	RPKM
Sporangin	SPR
Standard error	SE
Superoxide dismutase	SOD
Transmission electron microscope	TEM
Tryban blue	TB
zygospore germination enzyme	Z-lysin

CHAPTER ONE: GENERAL INTRODUCTION

Background

Nanotechnology is defined as the engineering and manufacturing of materials at atomic and molecular scales with a length range of 1 to 100 nanometers [1,2]. Materials with nanoscale lengths differ from the bulk materials of the same composition by their small size, high surface area to volume ratio, and surface reactivity, making them attractive for various applications (e.g., electronics, cosmetics, paints, and medicine) [3,4]. However, the growth of the nanotechnology industry raises concerns about the release of engineered nanoparticles (ENPs) into different environments during their production, manufacturing, use, and disposal [5,6]. Therefore, investigation of their adverse effect on living organisms has become a major concern. Many studies have been performed to assess the adverse effect of ENPs on living organisms in the aquatic environment, which is considered to be the main sink for contamination with ENPs [7,8].

Algae are the primary producers in the aquatic ecosystem, forming the basis of the aquatic food web by providing nutrients and energy for other organisms [9,10]. Therefore, undesirable effects leading to disruption of the algal population can affect the structure and function of aquatic ecosystems [11]. Thus, investigation of the toxicological effect of ENPs on algae is essential.

1.1. Behavior and fate of engineered nanoparticles in the aquatic environment

In the aquatic environment, ENPs may undergo several chemical and physical processes, including aggregation/agglomeration, dissolution, sedimentation, and transformation, which are affected by several factors such as the exposure conditions (pH and ionic strength), the properties of ENPs (concentration, size, and charge), and the dissolved natural organic matter

(NOM) [8,12,13]. The aforementioned factors determine the fate of ENPs by altering their surface properties, resulting in either increasing or decreasing stability of ENPs, which ultimately influence their interaction with aquatic organisms by enhancing or reducing their toxicological effect [14]. For instance, both TiO_2-NPs and CeO-NPs exhibit a pH-dependent surface charge; they are negatively charged at basic pH and positively charged at acidic pH [15,16]. However, agglomeration of CeO-NPs occurs at pH 8 near the point of zero charge [16]. By contrast, high ionic strength favors the aggregation of ENPs [13,17]. A rapid agglomeration of TiO_2-NPs (4–5 nm) within a few minutes in a 16.5 mmol $L^{-}1$ NaCl solution at pH ~4.5 has been observed [18].

NOM is a complex of various organic compounds, derived from the decomposition of living organisms in an aquatic ecosystem [14]. It can be of large molecular weight (e.g. fluvic acid, humic acid and extracellular polymeric substances) or low molecular weight such as that in thiols, amines, and carboxylic compounds [19]. A coating of NOM on ENPs modifies the ENPs' surface properties such as charge and subsequently alters their behavior and fate in the aquatic system [13]. Adsorption of NOM on the surface of ENPs may increase the surface charge, thus resulting in steric repulsion between particles, which enhances their stability and bioavailability in the aquatic environment. The increased stability of ENPs will increase the probability of their interaction with aquatic organisms [20]. By contrast, adsorption of high-molecular weight NOM on ENPs causes the formation of large aggregates, resulting in sedimentation and removal of ENPs from the water column [13,17]. For instance, it has been reported that the stability of CeO-NPs is increased by humic acid at low ionic strength in the presence of both KCl and $CaCl_2$ salts [21]. Meanwhile, at high $CaCl_2$ concentration, aggregation of CeO-NPs was induced because of the bridging attraction of humic substances with NPs and Ca^{+2} [21].

1.2. Toxicological effect of engineered nanoparticles on algae

Previous studies described how ENPs interact with NOM, which influences their surface chemistry and their deposition in the aquatic system, given that NOM, such as proteins, lipids, or polysaccharides, is released from aquatic organisms [14]. This suggests that ENPs have the potency to interact with aquatic organisms through interaction with cellular molecules, which might lead to disruption of cellular metabolism and structure [4]. Several studies reported the effect of different ENPs (e.g., metal oxide, carbon nanotubes, quantum dots (QDs), and polymer-based nanoparticles) on algae [17,22–27] (Table 1.1). Among ENPs, metallic nanoparticles were the most studied nanoparticles, probably due to their intensive use in many applications, including paints, cosmetics, catalysts, sunscreen, and sensors. According to "The Nanotechnology Consumer Products Inventory," metals and metal oxides are the materials most often mentioned in the product inventory, including, silver (25 products), silica (14), titanium dioxide (8), zinc oxide (8), and cerium oxide (1) [28]. Based on previous studies, the toxicity of metal oxide nanoparticles towards algae is characterized by growth inhibition, reduction of photosynthesis and chlorophyll content, and increase of the intracellular ROS level [17,22,26,29,30]. This toxicity is mediated by four main mechanisms: (1) agglomeration of NPs due to the formation of hydrophobic and hydrogen bonds with the amino acid and chemical groups on the surface of algal cells [31–33]; (2) shading effect, where NP aggregate on the cell surface causing reduction of light available for photosynthesis and consequently inhibit growth of the algae [17,34,35]; (3) dissolution of metal ions, such as the release of Ag^{+} and Zn^{+2} from Ag-NPs and ZnO-NPs, respectively [17,22,24]; and (4) imposing of oxidative stress by induction of ROS generation [36–38].

Agglomeration, shading effect, and oxidative stress are also explained by the toxicity induced by carbon nanotubes (CNTs), which are characterized by growth inhibition and photosynthesis

reduction in several unicellular algae such as *Chlorella vulgaris* and *Pseudokirchneriella subcapitata* [27,39,40]. Contrarily, adsorption on the algal cell wall and formation of algae–NPs agglomerates explained the impaired growth caused by polystyrene nanoparticles (PS-NPs) [25,41].

Table 1.1. The toxicological effect of several kinds of engineered nanoparticles (ENPs) on algae.

Type of nanoparticles	Nanoparticles	Mean diameter (nm)	Algal specie	Toxic effect	References
Metal-based	Ag	20-100	*Thalassiosira pseudonana, Cyanobacterium Synechococcus sp.*	Growth inhibition	[23]
		25	*Chlamydomonas reinhardtii*	Photosynthesis inhibition	[17]
	TiO_2	25-70	*Pseudokirchneriella subcapitata*	Growth inhibition, lipid peroxidation	[22,34]
		5-10	*Karenia brevis, Skeletonema costatum*	ROS accumulation, Lipid oxidation, growth inhibition	[30]

Al_2O_3	9-172	*Scenedesmus* sp. *Chlorella* sp.	Reduction of chlorophyll content, growth inhibition	[29]
	82.6, 246.9	*Chlorella ellipsoids*	ROS accumulation, cell membrane damage	[37]
CuO	30	*Pseudokirchneriella subcapitata*	Growth inhibition	[22]
	30-40	*Chlamydomonas reinhardtii*	Accumulation of ROS, growth inhibition, decrease in carotenoid level	[26]
ZnO	30, 50-70	*Pseudokirchneriella subcapitata*	Growth inhibition	[22,24]
	19, 93	*Chlamydomonas reinhardtii*	Growth inhibition	[36]
	40-48	*Chlorella vulgaris*	Reduction of cell viability, lipid peroxidation	[42]

SiO_2	12.5-27.0	*Pseudokirchneriella subcapitata*	Growth inhibition	[31]
	10-20	*Scenedesmus obliquus*	Growth inhibition, reduction of chlorophyll content	[43]
NiO	20	*Chlorella vulgaris*	Growth inhibition, reduction of photosynthesis	[44]
CeO_2	14, 20, 29	*Pseudokirchneriella subcapitata*	Growth inhibition	[45]
	140	*Chlamydomonas reinhardtii*	Reduction of photosynthesis	[33]
Polystyrene (PS-NPs)	110	*Pseudokirchneriella subcapitata*	Growth inhibition	[25]

Carbon-based	Carbon nanotubes (CNTs)	5-15	*Chlorella vulgaris* *Pseudokirchneriella subcapitata*	Growth inhibition	[27]
	Single walled carbon nanotubes (SWCNTs)	1.2-1.4	*Chlamydomonas reinhradtii*	Growth inhibition, photosynthesis reduction	[46]
	Multi walled carbon nanotubes (MWCNTs)	60-80			
	Fullerence (C_{60})	<200	*Chlamydomonas Reinhardtii*	Affecting photosynthesis and respiration in cytosol	[47]

1.2.1. The physiological effect of engineered nanoparticles on algae

Algal cells are surrounded by porous and semipermeable cell walls with an average pore size of 5–20 nm [17]. The biochemical composition of algal cell walls varies among species [48,49]. It is mainly composed of cellulose, glycoproteins, and polysaccharides [17,50]. The algal cell wall acts as the first barrier to prevent the invasion of NPs; only NPs with a smaller size than the maximal pore size can move across the cell wall. Once the NPs pass through the cell wall and reach the plasma membrane, they might be internalized *via* endocytosis, where the plasma membrane forms a cavity-like structure surrounding NPs and then pulls them inside the cell. In addition to endocytosis, NPs can cross the plasma membrane by passive diffusion through ion channels or embedded transport proteins [51,52]. When the NPs enter the cell and are in contact with cellular organelles (e.g., mitochondria, chloroplast, and endoplasmic reticulum), they can cause damage or alteration to the function and structure of the organelles [53,54]. It has been reported that exposure to 100 mg L^{-1} CuO-NPs cause damage to the chloroplast structure and degradation of chlorophyll in *Chlorella sp.* and *Scenedesmus sp*. [55]. The damage of the chloroplast structure adversely affects the photosynthesis process and results in the inhibition of photosynthesis. Impairment of photosynthesis was reported in *Chlorella pyrenoidosa* cells that were exposed to TiO_2-NPs [56], in *Chlorella sp.* and *Scenedesmus sp.* treated with Al_2O_3-NPs [29], and in *C. vulgaris* cells exposed to Ag-NPs [57].

An increased level of ROS was also detected in algal cells following the exposure to ENPs, suggesting that ENPs induce toxicity to algae *via* oxidative stress [36–38]. To cope with this stress, antioxidant defense is activated to eliminate the excess accumulation of ROS, which includes the increased level of antioxidant enzymes such as superoxide dismutase (SOD), ascorbate peroxidase (APX), and glutathione reductase (GR) [26,42]. An increased level of SOD was reported in *C. vulgaris* cells exposed to ZnO-NPs in a dose-dependent manner, whereas the level of glutathione decreased in cells exposed to >100 mg L^{-1} ZnO-NPs [42].

Furthermore, the activity of APX and GR significantly increased in *C. renhardtii* cells exposed to >10 mg L^{-1} CuO-NPs, whereas elevated levels of catalase (CAT) and glutathione S-transferase (GSTS1) activity were detected when *C. reinhardtii* was exposed to 1 mg L^{-1} and 1,000 mg L^{-1}, respectively [26]. However, if the ROS level exceeds the capacity of antioxidant enzymes to detoxify the adverse effect of ROS, ROS will directly interact with the cellular components, including proteins, DNA, and lipids, resulting in DNA damage, protein oxidation, and lipid peroxidation [58]. The latter will reduce the integrity of the cell membrane, making it more permeable and less selective, which might facilitate the internalization of NPs [38]. Moreover, the physical interaction of NPs with a cell may introduce new pores, larger than the original pores, in the cell wall, increasing the likelihood of NP internalization into the cell [17].

Damage to the cell membrane was also demonstrated in *C. pyrenoidosa* exposed to CuO-NPs [54]. Besides that, TEM images confirmed the internalization of CuO-NPs and their deposition in vacuoles [54]. A lactate dehydrogenase (LDH) enzyme assay was performed to confirm the integrity of the cell membrane [59]. Detection of an increased level of LDH leakage indicates damage to the cell membrane, which can be the cause of cell death [37,42]. Leakage of LDH was detected in *C. vulgaris* exposed to ≥200 mg L-1 ZnO-NPs [42] and in *Chlorella ellipsoids* exposed to low concentration (1 µg ml^{-1}) of Al_2O_3-NPs [37], suggesting that damage of the cell membrane is induced by these NPs.

1.2.2. The molecular effect of engineered nanoparticles on algae

The growing and rapid development of genomic and transcriptomic technologies facilitate the analysis of transcriptome changes induced by ENPs in algae. The transcriptomic studies for the effect of ENPs revealed a remarkable downregulation of photosynthesis-related genes [56,60–62], indicating an alteration of chloroplast function. It has been reported that

exposure to 10 mg L^{-1} CeO_2-NPs significantly decreased the level of transcripts encoding light-harvesting proteins of photosystems I and II (LHCA3, 5, and 8; LHCB4 and 5; and LHCBM2, 3, 5, 6, and 7) in *C. reinhardtii* [62]. Moreover, the exposure to Ag-NPs repressed the expression of the reaction center protein gene of PSII (D1) in *Skeletonema costatum* cells [60]. Interestingly, the psbB gene-encoding chlorophyll protein was significantly upregulated (>2-fold of the control) after exposing *C. pyrenoidosa* cells to 20 mg L^{-1} TiO_2-NPs [56], which might be a compensatory mechanism for the reduction of chlorophyll pigment that was caused by TiO_2-NPs.

As previously mentioned, ENPs impose oxidative stress by increasing the level of intracellular ROS in algae. As a response to this stress, a defense mechanism is induced involving the upregulation of oxidative-responsive genes that maintain the cellular redox homeostasis. It was reported that CeO_2-NPs induced the expression of glutathione peroxidase (GPX) gene in *C. reinhardtii* cells, whereas genes encoding SOD, L-ascorbate peroxidase, GSTS1, GR, and two peroxiredoxin family genes were downregulated [62]. Unlike CeO_2-NPs, ZnO-NPs elevated the level of transcripts encoding GSTS1 and three heat shock protein (HSP) genes (HSP22C, HSP70A, and HSP 90A) that prevent the aggregation of proteins induced by the oxidative stress [61]. However, TiO_2-NPs, Ag-NPs, and QDs did not increase the level of transcripts encoding GSTS1, GPX, HSP22C, and HSP70A genes [61].

Moreover, it was reported that the exposure to Ag-NPs enhanced the expression of eight transcripts encoding hydroxyproline-rich glycoprotein components of *C. reinhardtii* cell wall, suggesting that repair of the cell wall takes place after the damage caused by Ag-NPs [61].

Polycyanoacrylate nanoparticles (PCA-NPs) are one of the ENPs used in medical applications as drug delivery systems [63,64]. They are considered to be a safe, non-toxic material for humans. However, some reports demonstrated that mild toxicity could be induced by PCA-NPs in animal cells [65,66]. Recently, Shirotake [67] reported that PCA-NPs derived

from isobutyl cyanoacrylate (iBCA-NPs) induced cell death in Gram-positive bacteria by causing autolysis, but induced cell death did not occur in Gram-negative bacteria.

To date, only one study investigated the toxicological effect of PCA-NPs on algae [68].

1.3. Cynaoacrylate

Cyanoacrylates are esters (alkyl side chains) of cyanoacrylic acid, where the alkyl side chains can be short (e.g., methyl and ethyl) or long (e.g., butyl and octyl) (Fig. 1.1) [69]. They are one of the most reactive monomers, synthesized for the first time by Ardis in 1949 [70]. In brief, cyanoacrylate was synthesized by reacting formaldehyde with alkyl cyanoacetate to obtain prepolymer. Then, heat was applied to the prepolymer to distil off the liquid monomer (Fig. 1.2). Different cyanoacrylate monomers can be obtained by altering the alkoxy carbonyl group (—COOR).

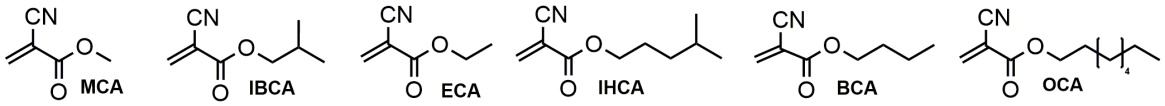

Figure 1.1. Chemical structure of different cyanoacrylate monomers. MCA, methyl cyanoacrylate; IBCA, isobutyl cyanoacrylate; ECA, ethyl cyanoacrylate; IHCA, isohexyl cyanoacrylate; BCA, butyl cyanoacrylate; OCA, octyl cyanoacrylate. Redrawn from [84].

Cyanoacrylate monomers can instantly polymerize in contact with nucleophiles such as water or weak bases [69,71]. Generally, cyanoacrylate polymerizes through three different mechanisms, i.e. anionic, zwitterionic, and free radical polymerization. Anionic and zwitterionic are the main processes of polymerization because of their rapid initiation at room temperature. By contrast, polymerization by free radical initiators can be employed in an acidic

aqueous solution, to suppress accidental anionic polymerization [71]. However, the free radical polymerization rate is lower than that of anionic or zwitterionic polymerization [71,72].

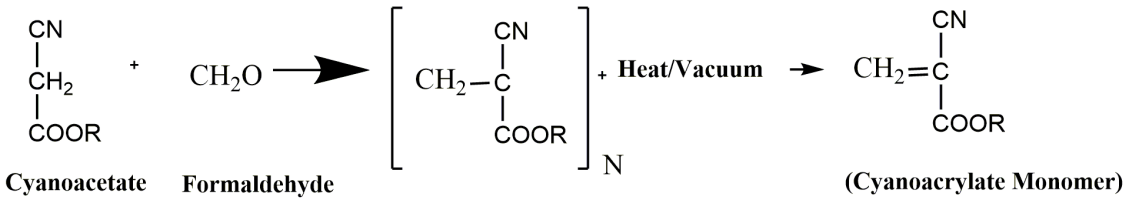

R== CH_3 Methyl

CH_2H_3 Ethyl

C_4H_9 Isobutyl, Butyl

Figure 1.2. Synthesis of cyanoacrylate monomer. Redrawn from [65].

1.3.1. Applications of cyanoacrylate

Coover et al. [73] discovered the adhesive properties of cyanoacrylate monomers, suggesting their use as adhesive materials for medical application. The utilization of cyanoacrylate as an adhesive material for the closure of skin wounds has grown, particularly because of the ability of cyanoacrylate to form strong and quick adhesion in wound closures by rapid anionic polymerization even with traces of nucleophiles [74–77]. They have been used as tissue adhesives for various medical applications, including repair of myocardial tears [78], pulmonary resections [79], abdominal closure after general surgery [80], and laparoscopic gastrointestinal surgery. Besides that, they have been used in the detection of latent fingerprints in criminal investigations [81] and as an electrolyte matrix for dye-sensitized solar cells [82].

Later, Couvreur et al. [83] developed a protocol to synthesize NPs from ethyl or butyl cyanoacrylate in a solution containing HCl, with dextran as a stabilizing agent; he then introduced polycyanoacrylate NPs (PCA-NPs) for the first time as carriers for drug delivery.

Synthesis of PCA-NPs is carried out through an aqueous dispersion polymerization approach, where the anionic polymerization takes place in the presence of a stabilizing agent (e.g., polysorbate 80 or dextran) [71]. The size of the nanoparticles can be controlled by changing the polymerization conditions, particularly the concentration of the stabilizing agent, which is the key factor in the determination of NP size [71]. It also provides steric repulsion between nanoparticles, preventing their aggregation [84].

The unique properties of PCA-NPs including their ability to adsorb different biological compounds, biocompatibility, biodegradability, and stability in the biological fluids [83–86] render them useful as drug delivery carriers. Furthermore, they provide controlled delivery of drugs and protect therapeutic agents from enzymatic degradation [87]. Several therapeutic agents and molecules can be entrapped in PCA-NPs, such as antibiotics [88,89], anti-cancer drugs [90–92], nucleic acids [93], and peptides [94,95].

1.3.2. Toxicity of polycyanoacrylate

Although cyanoacrylate polymers showed excellent performance as a tissue adhesive and drug delivery carriers, it was proved that short alkyl chain cyanoacrylate derivatives (e.g., methyl cyanoacrylate, and ethyl cyanoacrylate) could induce toxicity to animal tissues [65,66]. However, it was reported that the long alkyl chain cyanoacrylate derivatives (e.g., isobutyl cyanoacrylate) had no adverse effect on animal tissues. Neither inflammation nor necrosis was induced in tissues treated with a cyanoacrylate polymer derived from a long alky chain [96–98].

Toriumi et al. [65] reported that ethyl-2-cyanoacrylate induced tissue necrosis and acute inflammation in rat ear cells, whereas mild inflammation was induced in rat ear cells treated with butyl-2-cyanoacrylate. He speculated that the different toxicity effects of butyl-2-cyanoacrylate and ethyl-2-cyanoacrylate are due to the differences in their degradation rate.

The release of large quantities of toxic products, including formaldehyde and cyanoacetate following the rapid degradation of ethyl-2-cyanoacrylate, might be the cause of the observed acute inflammation in the treated tissue with ethyl-2-cyanoacrylate [65]. Supporting the speculation by Toriumi et al. [65] it was earlier reported that the rate of PCA-NP degradation depends on the alkyl chain of PCA. For instance, PCA with a short alkyl chain (e.g. methyl cyanoacrylate) degrades within hours compared to PCA with a long alkyl chain (e.g. isobutyl cyanoacrylate), which takes three days to be eliminated [99].

Moreover, Catherine et al. [66] reported that isohexyl cyanoacrylate NPs (IHCA-NPs) exhibited the least toxicity to fibroblast cells compared to methyl cyanoacrylate (MCA-NPs), ethyl cyanoacrylate NPs (ECA-NPs), and isobutyl cyanoacrylate NPs (iBCA-NPs). These results can be explained by the slow degradation of IHCA-NPs and the subsequent slow release of toxic degradation products.

Interestingly, Eiferman and Snyder [100] reported an antibacterial effect of cyanoacrylate *in vitro* and *in vivo*. They found that cyanoacrylate could induce toxicity to Gram-positive bacteria (e.g., *Staphylococcus aureus* and *Streptococcus pneumonia*) but not to Gram-negative bacteria. The induced toxicity to Gram-positive bacteria was through the binding of cyanoacrylate to free amino acid or hydroxyl groups existing within the cell wall. However, in the case of Gram-negative bacteria, the lipopolysaccharide capsule surrounding the cell wall acts as a barrier against the cyanoacrylate effect [100].

Recently, Widyaningrum et al. [68] reported that isobutylcyanoacrylate nanoparticles (iBCA-NPs) with a mean diameter of 25 nm induced acute cell death in microgreen algal species belonging to Chlorophyceae. The induced cell death was accompanied by the appearance of protoplast-like cells and an accumulation of ROS. It was observed that iBCA-NPs frequently collided with the *C. reinhardtii* cell wall without stable adherence to the cell wall. These collisions might cause uncontrolled secretion of cell wall hydrolytic enzymes that

partially hydrolyse the cell wall of *C. reinhardtii*. Thereafter, iBCA-NPs passed through the damaged cell wall and bound to different proteins on the plasma membrane, causing loss of the three-dimensional structure of proteins. As a consequence, the activation of different signalling pathways ended with an increase of the ROS level and eventually cell death [68]. This principal mechanism of induced toxicity by iBCA-NPs is different from that induced by a metal oxide, where shading effects and alterations of the nutrient exchange with the surrounding environment are the main causes of algal growth inhibition [34,35]. Meanwhile, neither the shading effect nor impairment of nutrient exchange was observed in the case of iBCA-NPs. However, both metal oxides and iBCA-NPs induce ROS production [37,38,68].

IBCA-NPs not only have the potency to induce toxicity to microgreen algae belonging to Chlorophyceae but also could induce toxicity to a wide range of algae. Herein (i.e., Chapter 2), we investigated the effect of iBCA-NPs with a mean diameter of 180 nm on 18 widely distributed non-green algal species (i.e., 19 strains belonging to SAR and Hacrobia clades). Detailed analyses were performed using *Prymnesium parvum* (Haptophyta) and *Rhodomonas atrorosea* (Cryptophyta).

However, to date, the molecular mechanism of cell death induction by iBCA-NPs in diverse algal species is still unknown. To better understand the effect of iBCA-NPs on the metabolic process in algal cells and the response of algal cells to the stress induced by NPs at the molecular level, it is essential for one to analyze the gene expression changes following the exposure to iBCA-NPs. Among microgreen algae, the genome of *C. reinhardtii* is well organized, containing 14,415 genes and 17,741 loci with protein-coding transcripts [101]. Besides that, the rapid doubling time (c.a. 8–12 h), well-defined media and growth requirements [102], availability of mutant strain library at the *Chlamydomonas* resource center (http://chlamy.org/), and well-established molecular techniques for genetic study [103,104] make *C. reinhardtii* an excellent model organism for analyzing the molecular effect of iBCA-

NPs on microgreen algae. In Chapter 3, we investigate the chronological transcriptome changes induced by the exposure of iBCA-NPs in *C. reinhardtii*, where cell mortality ranged from ~3% to ~30%, using next generation sequencing.

1.4. References

[1] S.E. Mcneil, Nanotechnology for the biologist, J. Leukoc. Biol. 78 (2005) 585–594. https://doi.org/10.1189/jlb.0205074.

[2] F. Sanchez, K. Sobolev, Nanotechnology in concrete – A review, Constr. Build. Mater. 24 (2010) 2060–2071. https://doi.org/10.1016/j.conbuildmat.2010.03.014.

[3] A. Nel, T. Xia, L. Mädler, N. Li, Toxic potential of materials at the nanolevel, Science 311 (2006) 622–627. https://doi.org/10.1126/science.1114397.

[4] A.M. Schrand, M.F. Rahman, S.M. Hussain, J.J. Schlager, D.A. Smith, A.F. Syed, Metal-based nanoparticle and their toxicity assessment, Wiley Interdiscip. Rev. Nanomed. Nanobiotechnol. 2 (2010) 21–24. https://doi.org/10.1002/wnan.103.

[5] F. Gottschalk, B. Nowack, The release of engineered nanomaterials to the environment, J. Environ. Monit. 13 (2011) 1145–1155. https://doi.org/10.1039/c0em00547a.

[6] N. Uddin, F. Desai, E. Asmatulu, Engineered nanomaterials in the environment : bioaccumulation , biomagnification and biotransformation, Environ. Chem. Lett. 18 (2020) 1073–1083. https://doi.org/10.1007/s10311-019-00947-0.

[7] J. Zhao, B. Xing, Environmental processes and toxicity of metallic nanoparticles in aquatic systems as affected by natural organic matter, Environ. Sci. Nano. 3 (2016) 240–255. https://doi.org/10.1039/C5EN00230C.

[8] D. Shevlin, N.O. Brien, E. Cummins, Science of the Total Environment Silver engineered nanoparticles in freshwater systems – Likely fate and behaviour through

natural attenuation processes, Sci. Total Environ. 621 (2017) 1033-1046. https://doi.org/10.1016/j.scitotenv.2017.10.123.

[9] J.W. Blunt, B.R. Copp, M.H. Munro, P.T. Northcote, M.R. Prinsep, Marine natural products, Nat. Prod. Rep. 20 (2003) 1–48.

[10] R. L. Chapman, Algae : the world ’s most important “ plants ”— an introduction, Mitig. Adapt. Strateg. Glob. Chang. 18 (2013) 5–12. https://doi.org/10.1007/s11027-010-9255-9.

[11] Y.H. Chang, C.R. Ku, H.L. Lu, Effects of aquatic ecological indicators of sustainable green energy landscape facilities, Ecol. Eng. 71 (2014) 144–153.

[12] W. Zhang, Y. Yao, K. Li, Y. Huang, Y. Chen, Influence of dissolved oxygen on aggregation kinetics of citrate-coated silver nanoparticles, Environ. Pollut. 159 (2011) 3757–3762. https://doi.org/10.1016/j.envpol.2011.07.013.

[13] A. Quigg, W. Chin, C. Chen, S. Zhang, Y. Jiang, A. Miao, K.A. Schwehr, C. Xu, P.H. Santschi, Direct and Indirect Toxic E ff ects of Engineered Nanoparticles on Algae: Role of Natural Organic Matter, ACS Sustain. Chem. Eng. 1 (2013) 686-702.

[14] G.V. Lowry, K.B. Gregory, S.C. Apte, J.R. Lead, Transformations of Nanomaterials in the Environment, Environ. Sci. Technol. 46 (2012) 6893–6899. https://doi.org/10.1021/es300839e.

[15] K.A. Dunphy Guzman, M.P. Finnegan, J.F. Banfield, Influence of Surface Potential on Aggregation and Transport of Titania Nanoparticles, Environ. Sci. Technol. 40 (2006) 7688–7693. https://doi.org/10.1021/es060847g.

[16] M. Baalousha, Y. Ju-Nam, P.A. Cole, J.A. Hriljac, I.P. Jones, C.R. Tyler, V. Stone, T.F. Fernandes, M.A. Jepson, J.R. Lead, Characterization of cerium oxide nanoparticles—Part 2: Nonsize measurements, Environ. Toxicol. Chem. 31 (2012) 994–1003. https://doi.org/https://doi.org/10.1002/etc.1786.

[17] E. Navarro, A. Baun, R. Behra, N.B. Hartmann, J. Filser, A.J. Miao, A. Quigg, P.H. Santschi, L. Sigg, Environmental behavior and ecotoxicity of engineered nanoparticles to algae, plants, and fungi, Ecotoxicology 17 (2008) 372–386. https://doi.org/10.1007/s10646-008-0214-0.

[18] R.A. French, A.R. Jacobson, B. Kim, S.L. Isley, R.L.E.E. Penn, Influence of Ionic Strength , pH , and Cation Valence on Aggregation Kinetics of Titanium Dioxide Nanoparticles, Environ. Sci. Technol. 43 (2009) 1354–1359.

[19] Q. Abbas, B. Yousaf, Amina, M.U. Ali, M.A.M. Munir, A. El-Naggar, J. Rinklebe, M. Naushad, Transformation pathways and fate of engineered nanoparticles (ENPs) in distinct interactive environmental compartments: A review, Environ. Int. 138 (2020) 105646. https://doi.org/https://doi.org/10.1016/j.envint.2020.105646.

[20] M. Baalousha, A. Manciulea, S. Cumberland, K. Kendall, J.R. Lead, Aggregation and surface properties of iron oxide nanoparticles: Influence of ph and natural organic matter, Environ. Toxicol. Chem. 27 (2008) 1875–1882. https://doi.org/https://doi.org/10.1897/07-559.1.

[21] K. Li, Y. Chen, Effect of natural organic matter on the aggregation kinetics of CeO_2 nanoparticles in KCl and $CaCl_2$ solutions: Measurements and modeling, J. Hazard. Mater. 209–210 (2012) 264–270. https://doi.org/https://doi.org/10.1016/j.jhazmat.2012.01.013.

[22] V. Aruoja, H.C. Dubourguier, K. Kasemets, A. Kahru, Toxicity of nanoparticles of CuO, ZnO and TiO2 to microalgae *Pseudokirchneriella subcapitata*, Sci. Total Environ. 407 (2009) 1461–1468.

[23] A.D. Burchardt, R.N. Carvalho, A. Valente, P. Nativo, D. Gilliland, C.P. Garc, R. Passarella, V. Pedroni, T. Lettieri, Effects of Silver Nanoparticles in Diatom *Thalassiosira pseudonana* and *Cyanobacterium Synechococcus sp.*, Environ. Sci.

Technol. 46 (2012) 11336-11344. https://doi.org/10.1021/es300989e.

[24] N.M. Franklin, N.J. Rogers, S.C. Apte, G.E. Batley, G.E. Gadd, P.S. Casey, Comparative toxicity of nanoparticulate ZnO, bulk ZnO, and $ZnCl_2$ to a freshwater microalga (*Pseudokirchneriella subcapitata*): The importance of particle solubility, Environ. Sci. Technol. 41 (2007) 8484–8490. https://doi.org/10.1021/es071445r.

[25] T.M. Nolte, N.B. Hartmann, J.M. Kleijn, J. Garnæs, D. Van De Meent, A.J. Hendriks, A. Baun, The toxicity of plastic nanoparticles to green algae as influenced by surface modification, medium hardness and cellular adsorption, Aquat. Toxicol. 183 (2017) 11-20. https://doi.org/10.1016/j.aquatox.2016.12.005.

[26] S.P. Melegari, F. Perreault, R.H.R. Costa, R. Popovic, W.G. Matias, Evaluation of toxicity and oxidative stress induced by copper oxide nanoparticles in the green alga *Chlamydomonas reinhardtii*, Aquat. Toxicol. 142 (2013) 431–440.

[27] F. Schwab, T.D. Bucheli, L.P. Lukhele, A. Magrez, B. Nowack, L. Sigg, K. Knauer, Are carbon nanotube effects on green algae caused by shading and agglomeration?, Environ. Sci. Technol. 45 (2011) 6136–6144. https://doi.org/10.1021/es200506b.

[28] A. Kahru, H. Dubourguier, I. Blinova, A. Ivask, K. Kasemets, Biotests and Biosensors for Ecotoxicology of Metal Oxide Nanoparticles: A Minireview, Sensors 8 (2008) 5153–5170. https://doi.org/10.3390/s8085153.

[29] I.M. Sadiq, S. Pakrashi, N. Chandrasekaran, A. Mukherjee, Studies on toxicity of aluminum oxide (Al_2O_3) nanoparticles to microalgae species: *Scenedesmus sp.* and *Chlorella sp.*, J. Nanoparticle Res. 13 (2011) 3287–3299. https://doi.org/10.1007/s11051-011-0243-0.

[30] F. Li, Z. Liang, X. Zheng, W. Zhao, M. Wu, Z. Wang, Toxicity of nano-TiO_2 on algae and the site of reactive oxygen species production, Aquat. Toxicol. 158 (2015) 1–13.

https://doi.org/10.1016/j.aquatox.2014.10.014.

[31] C.O.R.J. Anssen, ECOTOXICITY OF SILICA NANOPARTICLES TO THE GREEN ALGA *PSEUDOKIRCHNERIELLA SUBCAPITATA* : IMPORTANCE OF SURFACE AREA, Environ. Toxicol. Chem. 27 (2008) 1948–1957.

[32] Z. Wang, J. Li, J. Zhao, B. Xing, Toxicity and internalization of CuO nanoparticles to prokaryotic alga *Microcystis aeruginosa* as affected by dissolved organic matter., Environ. Sci. Technol. 45 (2011) 6032–6040. https://doi.org/10.1021/es2010573.

[33] L.A. Röhder, T. Brandt, L. Sigg, R. Behra, Influence of agglomeration of cerium oxide nanoparticles and speciation of cerium(III) on short term effects to the green algae *Chlamydomonas reinhardtii*, Aquat. Toxicol. 152 (2014) 121–130. https://doi.org/https ://doi.org/10.1016/j.aquatox.2014.03.027.

[34] D.M. Metzler, M. Li, A. Erdem, C.P. Huang, Responses of algae to photocatalytic nano-TiO_2 particles with an emphasis on the effect of particle size, Chem. Eng. J. 170 (2011) 538–546. https://doi.org/https://doi.org/10.1016/j.cej.2011.02.002.

[35] L. Chen, L. Zhou, Y. Liu, S. Deng, H. Wu, G. Wang, Toxicological effects of nanometer titanium dioxide (nano-TiO_2) on *Chlamydomonas reinhardtii*, Ecotoxicol. Environ. Saf. 84 (2012) 155–162. https://doi.org/10.1016/j.ecoenv.2012.07.019.

[36] C. Gunawan, A. Sirimanoonphan, W.Y. Teoh, C.P. Marquis, R. Amal, Submicron and nano formulations of titanium dioxide and zinc oxide stimulate unique cellular toxicological responses in the green microalga *Chlamydomonas reinhardtii*, J. Hazard. Mater. 260 (2013) 984–992. https://doi.org/https://doi.org/10.1016/j.jhazmat.2013.06.067.

[37] S. Pakrashi, S. Dalai, T.C. Prathna, S. Trivedi, R. Myneni, A.M. Raichur, N. Chandrasekaran, A. Mukherjee, Cytotoxicity of aluminium oxide nanoparticles towards fresh water algal isolate at low exposure concentrations, Aquat. Toxicol. 132–133 (2013)

34–45. https://doi.org/https://doi.org/10.1016/j.aquatox.2013.01.018.

[38] B. Xia, B. Chen, X. Sun, K. Qu, F. Ma, M. Du, Interaction of TiO_2 nanoparticles with the marine microalga *Nitzschia closterium*: Growth inhibition, oxidative stress and internalization, Sci. Total Environ. 508 (2015) 525–533. https://doi.org/https://doi.org/10.1016/j.scitotenv.2014.11.066.

[39] Z. Long, J. Ji, K. Yang, D. Lin, F. Wu, Systematic and Quantitative Investigation of the Mechanism of Carbon Nanotubes ' Toxicity toward Algae, Environ. Sci. Technol. 46 (2012) 8458-8466.

[40] E.K. Sohn, Y.S. Chung, S.A. Johari, T.G. Kim, J.K. Kim, J.H. Lee, Y.H. Lee, S.W. Kang, I.J. Yu, Acute toxicity comparison of single-walled carbon nanotubes in various freshwater organisms, Biomed Res. Int. 2015 (2015). https://doi.org/10.1155/2015/323090.

[41] X. Li, Interaction of silver and polystyrene nanoparticles with algae, École polytechnique fédérale de Lausanne, Lausanne, Switzerland, 2015. https://doi.org/10.5075/epfl-thesis-6818

[42] T.Y. Suman, S.R. Radhika Rajasree, R. Kirubagaran, Evaluation of zinc oxide nanoparticles toxicity on marine algae *chlorella vulgaris* through flow cytometric, cytotoxicity and oxidative stress analysis, Ecotoxicol. Environ. Saf. 113 (2015) 23–30. https://doi.org/https://doi.org/10.1016/j.ecoenv.2014.11.015.

[43] C. Wei, Y. Zhang, J. Guo, B. Han, X. Yang, J. Yuan, Effects of silica nanoparticles on growth and photosynthetic pigment contents of *Scenedesmus obliquus*, J. Environ. Sci. 22 (2010) 155–160. https://doi.org/https://doi.org/10.1016/S1001-0742(09)60087-5.

[44] N. Gong, K. Shao, W. Feng, Z. Lin, C. Liang, Y. Sun, Biotoxicity of nickel oxide nanoparticles and bio-remediation by microalgae *Chlorella vulgaris*, Chemosphere 83

(2011) 510–516. https://doi.org/10.1016/j.chemosphere.2010.12.059.

[45] K. Van Hoecke, J.T.K. Quik, J. Mankiewicz-Boczek, K.A.C. De Schamphelaere, A. Elsaesser, P. Van der Meeren, C. Barnes, G. McKerr, C.V. Howard, D. Van De Meent, K. Rydzyński, K.A. Dawson, A. Salvati, A. Lesniak, I. Lynch, G. Silversmit, B. De Samber, L. Vincze, C.R. Janssen, Fate and Effects of CeO_2 Nanoparticles in Aquatic Ecotoxicity Tests, Environ. Sci. Technol. 43 (2009) 4537–4546. https://doi.org/10.1021/es9002444.

[46] D.N. Matorin, A.V. Karateyeva, V.A. Osipov, E.P. Lukashev, N.K. Seifullina, A.B. Rubin, Influence of Carbon Nanotubes on Chlorophyll Fluorescence Parameters of Green Algae *Chlamydomonas reinhardtii*, Nanotechnol. Russ. 5 (2010) 320–327. https://doi.org/10.1134/S199507801005006X.

[47] E.V. Basiuk, O.E. Ochoa-olmos, L.F. De Mora-estrada, Ecotoxicological Effects of Carbon Nanomaterials on Algae , Fungi and Plants, J. Nanosci 11 (2011) 3016-3038. https://doi.org/10.1166/jnn.2011.3767.

[48] A. Popper, M. Ralet, D.S. Domozych, Plant and algal cell walls: diversity and functionality, Ann. Bot. 114 (2014) 1043–1048. https://doi.org/10.1093/aob/mcu214.

[49] I. Sørensen, F.A. Pettolino, A. Bacic, J. Ralph, F. Lu, M.A.O. Neill, Z. Fei, J.K.C. Rose, D.S. Domozych, W.G.T. Willats, The charophycean green algae provide insights into the early origins of plant cell walls, Plant J. 68 (2011) 201–211. https://doi.org/10.111 1/j.1365-313X.2011.04686.x.

[50] D. Domozych, M. Ciancia, J.U. Fangel, M.D. Mikkelsen, P. Ulvskov, W.G. Willats, The cell walls of green algae : a journey through evolution and diversity, Front. Plant Sci. 3 (2012) 82. https://doi.org/10.3389/fpls.2012.00082.

[51] C.G. England, A.M. Gobin, H.B. Frieboes, Evaluation of uptake and distribution of gold

nanoparticles in solid tumors., Eur. Phys. J. Plus. 130 (2015). https://doi.org/10.1140/epjp/i2015-15231-1.

[52] K. Nambara, K. Niikura, H. Mitomo, T. Ninomiya, C. Takeuchi, J. Wei, Y. Matsuo, K. Ijiro, Reverse Size Dependences of the Cellular Uptake of Triangular and Spherical Gold Nanoparticles, Langmuir 32 (2016) 12559-12567. https://doi.org/10.1021/acs.langmuir.6b02064.

[53] M. Bhuvaneshwari, V. Iswarya, S. Archanaa, G.M. Madhu, G.K.S. Kumar, R. Nagarajan, N. Chandrasekaran, A. Mukherjee, Cytotoxicity of ZnO NPs towards fresh water algae *Scenedesmus obliquus* at low exposure concentrations in UV-C, visible and dark conditions, Aquat. Toxicol. 162 (2015) 29–38. https://doi.org/https://doi.org/10.1016/j.aquatox.2015.03.004.

[54] J. Zhao, X. Cao, X. Liu, Z. Wang, C. Zhang, J.C. White, B. Xing, Interactions of CuO nanoparticles with the algae *Chlorella pyrenoidosa*: adhesion, uptake, and toxicity, Nanotoxicology 10 (2016) 1297–1305. https://doi.org/10.1080/17435390.2016.1206149.

[55] X. Che, R. Ding, Y. Li, Z. Zhang, H. Gao, W. Wang, Mechanism of long-term toxicity of CuO NPs to microalgae, Nanotoxicology 12 (2018) 923-939. https://doi.org/10.1080/17435390.2018.1498928.

[56] A. Middepogu, J. Hou, X. Gao, D. Lin, Effect and mechanism of TiO_2 nanoparticles on the photosynthesis of *Chlorella pyrenoidosa*, Ecotoxicol. Environ. Saf. 161 (2018) 497–506. https://doi.org/10.1016/j.ecoenv.2018.06.027.

[57] S. Zheng, Q. Zhou, C. Chen, F. Yang, Z. Cai, D. Li, Q. Geng, Y. Feng, H. Wang, Role of extracellular polymeric substances on the behavior and toxicity of silver nanoparticles and ions to green algae *Chlorella vulgaris*, Sci. Total Environ. 660 (2019) 1182–1190. https://doi.org/https://doi.org/10.1016/j.scitotenv.2019.01.067.

[58] J.G. Scandalios, Oxidative stress: Molecular perception and transduction of signals triggering antioxidant gene defenses, Brazilian J. Med. Biol. Res. 38 (2005) 995–1014. https://doi.org/10.1590/S0100-879X2005000700003.

[59] H.A. JENG, J. SWANSON, Toxicity of Metal Oxide Nanoparticles in Mammalian Cells, J. Environ. Sci. Heal. Part A. 41 (2006) 2699–2711. https://doi.org/10.1080/10934520600966177.

[60] J. Huang, J. Cheng, J. Yi, Impact of silver nanoparticles on marine diatom *Skeletonema costatum*, J. Appl. Toxicol. 36 (2016) 1343–1354. https://doi.org/10.1002/jat.3325.

[61] D.F. Simon, R.F. Domingos, C. Hauser, C.M. Hutchins, W. Zerges, K.J. Wilkinson, Transcriptome sequencing (RNA-seq) analysis of the effects of metal nanoparticle exposure on the transcriptome of *Chlamydomonas reinhardtii*, Appl. Environ. Microbiol. 79 (2013) 4774–4785. https://doi.org/10.1128/AEM.00998-13.

[62] N.S. Taylor, R. Merrifield, T.D. Williams, J.K. Chipman, R. Jamie, M.R. Viant, N.S. Taylor, R. Merrifield, T.D. Williams, J.K. Chipman, Molecular toxicity of cerium oxide nanoparticles to the freshwater alga *Chlamydomonas reinhardtii* is associated with supra-environmental exposure concentrations, Nanotoxicology 10 (2016) 32-41. https://doi.org/10.3109/17435390.2014.1002868.

[63] M.N.V.R. Kumar, Nano and Microparticles as Controlled Drug Delivery Devices, J. Pharm. Pharm. Sci. 3 (2000) 234-258.

[64] F.D. Jaeghere, E. Doelker, R. Gurny, Encyclopedia of Control Drug Delivery, in: E. Mathiowitz (Ed.), Nanoparticles, John Wiley & Sons, New York, 1999, pp. 641–663.

[65] D.M. Toriumi, W.F. Raslan, M. Friedman, M.E. Tardy, Histotoxicity of Cyanoacrylate Tissue Adhesives: A Comparative Study, Arch. Otolaryngol. Neck Surg. 116 (1990) 546–550. https://doi.org/10.1001/archotol.1990.01870050046004.

[66] L. Catherine, R.H. Moiler, F. Puisieux, P. Couvreur, Alkylcyanoacrylate drug carriers : II . Cytotoxicity of cyanoacrylate nanoparticles with different alkyl chain length, Int. J. Pharm. 84 (1992) 13–22.

[67] S. Shirotake, A new cyanoacrylate colloidal polymer with novel antibacterial mechanism and its application to infection control, J. Nanomedine Biother. Discov. 4 (2014) 1–7.

[68] D. Widyaningrum, D. Iida, Y. Tanabe, Y. Hayashi, S.D. Kurniasih, T. Ohama, Acutely induced cell mortality in the unicellular green alga *Chlamydomonas reinhardtii* (Chlorophyceae) following exposure to acrylic resin nanoparticles, J. Phycol. 55 (2019) 118–133. https://doi.org/10.1111/jpy.12798.

[69] B.J. Vote, M.J. Elder, Cyanoacrylate glue for corneal perforations : a description of a surgical technique and a review of the literature, J. Clin. Exp. Ophthalmol. 28 (2000) 437–442.

[70] A.E., Ardis, US. Patents No. 2467926 and 2467927, New formulation of 2-octylCA tissue adhesive versus commercially available methods. Am. J. Surg. 188 (1949), 307-313.

[71] D.R. Robello, T.D. Eldridge, M.T. Swanson, Degradation and Stabilization of Polycyanoacrylates, J. Polym. Sci. A. Polym. Chem. 37 (1999) 4570–4581.

[72] M.G. Han, S. Kim, S.X. Liu, Synthesis and degradation behavior of poly(ethyl cyanoacrylate), Polym. Degrad. Stab. 93 (2008) 1243–1251.https://doi.org/10.1016/j.polymdegradstab.2008.04.012.

[73] H.W. Coover, Chemistry and performance of cyanoacrylate adhesives, J. Soc. Plast. Eng. 15 (1959) 413–417.

[74] F. Leonard, R.K. Kulkarni, G. Brandes, J. Nelson, J.J. Cameron, Synthesis and Degradation of Poly(alkyl α-Cyanoacrylates), J. Appl. Polym. Sci. 10 (1966) 259–272.

[75] A.J. Singer, H.C. Thode, A review of the literature on octylcyanoacrylate tissue adhesive, Am. J. Surg. 187 (2004) 238–248. https://doi.org/https://doi.org/10.1016/j.amjsurg.2003.11.017.

[76] W.H. Eaglstein, T. Sullivan, Cyanoacrylates for Skin Closure, Dermatol. Clin. 23 (2005) 193–198. https://doi.org/10.1016/j.det.2004.09.003.

[77] A.J. Singer, J. V Quinn, J.E. Hollander, The cyanoacrylate topical skin adhesives, Am. J. Emerg. Med. 26 (2008) 490–496. https://doi.org/https://doi.org/10.1016/j.ajem.2007.05.015.

[78] J. Padró, J. Mesa, J. Silvestre, J. Larrea, J. Caralps, F. Cerrón, A. Aris, Subacute cardiac rupture: Repair with a sutureless technique, Ann. Thorac. Surg. 55 (1993) 20–24. https://doi.org/https://doi.org/10.1016/0003-4975(93)90468-W.

[79] S. Sabanathan, J. Eng, J. Richardson, The use of tissue adhesive in pulmonary resections, Eur. J. Cardio-Thoracic Surg. 7 (1993) 657–660. https://doi.org/10.1016/1010-7940(93)90264-C.

[80] A. Qureshi, P.J. Drew, A.C. Roberts, J.R.T. Monson, G.S. Duthie, n-Butyl cyanoacrylate adhesive for skin closure of abdominal wounds : preliminary results, Ann. R. Coll. Surg. Engl. 79 (1997) 414–415.

[81] D.L. Exline, C.Wallace, C.Roux, C. Lennard, M.P. Nelson, P.J. Treado, Forensic Applications of Chemical Imaging: Latent Fingerprint Detection Using Visible Absorption and Luminescence, J. Forensic Sci. 48 (2003) 1047–1053. https://www.astm.org/DIGITAL_LIBRARY/JOURNALS/FORENSIC/PAGES/JFS2002333.htm.

[82] S. Lu, R. Koeppe, S. Günes, N.S. Sariciftci, Quasi-solid-state dye-sensitized solar cells with cyanoacrylate as electrolyte matrix, Sol. Energy Mater. Sol. Cells. 91 (2007) 1081–1086. https://doi.org/https://doi.org/10.1016/j.solmat.2007.03.002.

[83] P. Couvreur, B. Kante, M. Roland, P. Guiot, P. BAuduin, P. Speiser, Polycyanoacrylate nanocapsules as potential lysosomotropic carriers: preparation, morphological and sorptive properties, J. Pharm. Pharmacol. 31 (1979) 331–332. https://doi.org/10.1111/j.2042-7158.1979.tb13510.x.

[84] G. Yordanov, Poly(alkyl cyanoacrylate) nanoparticles as drug carriers 33 years later, Bulg. J. Chem. 1 (2012) 61-72. https://www.researchgate.net/publication/260795492.

[85] P. Couvreur, Polyalkylcyanoacrylates as colloidal drug carriers, Crit. Rev. Ther. Drug Carrier Syst. 5 (1988) 1–20. http://europepmc.org/abstract/MED/3293806.

[86] C. Vauthier, C. Dubernet, E. Fattal, H. Pinto-Alphandary, P. Couvreur, Poly(alkylcyanoacrylates) as biodegradable materials for biomedical applications, Adv. Drug Deliv. Rev. 55 (2003) 519–548.

[87] A. Graf, A. McDowell, T. Rades, Poly(alkycyanoacrylate) nanoparticles for enhanced delivery of therapeutics – is there real potential?, Expert Opin. Drug Deliv. 6 (2009) 371–387. https://doi.org/10.1517/17425240902870413.

[88] H. Pinto-Alphandary, A. Andremont, P. Couvreur, Targeted delivery of antibiotics using liposomes and nanoparticles: research and applications, Int. J. Antimicrob. Agents. 13 (2000) 155–168. https://doi.org/https://doi.org/10.1016/S0924-8579(99)00121-1.

[89] K.O. Kisich, S. Gelperina, M.P. Higgins, S. Wilson, E. Shipulo, E. Oganesyan, L. Heifets, Encapsulation of moxifloxacin within poly(butyl cyanoacrylate) nanoparticles enhances efficacy against intracellular Mycobacterium tuberculosis, Int. J. Pharm. 345 (2007) 154–162. https://doi.org/https://doi.org/10.1016/j.ijpharm.2007.05.062.

[90] J.L. Arias, M.A. Ruiz, M. López-Viota, Á. V Delgado, Poly(alkylcyanoacrylate) colloidal particles as vehicles for antitumour drug delivery: A comparative study, Colloids Surfaces B Biointerfaces. 62 (2008) 64–70. https://doi.org/https://doi.org/10.1

016/j.colsurfb.2007.09.018.

[91] B. Petri, A. Bootz, A. Khalansky, T. Hekmatara, R. Müller, R. Uhl, J. Kreuter, S. Gelperina, Chemotherapy of brain tumour using doxorubicin bound to surfactant-coated poly(butyl cyanoacrylate) nanoparticles: Revisiting the role of surfactants, J. Control. Release. 117 (2007) 51–58. https://doi.org/https://doi.org/10.1016/j.jconrel.2006.10.015.

[92] J. Kreuter, H. R. Hartmann, Comparative study on the cytostatic effects and the tissue distribution of 5-fluorouracil in a free form and bound to polybutylcyanoacrylate nanoparticles in sarcoma 180-bearing mice, Oncology 40 (1983) 363–366.

[93] G. Lambert, E. Fattal, H. Pinto-Alphandary, A. Gulik, P. Couvreur, Polyisobutylcyanoacrylate nanocapsules containing an aqueous core as a novel colloidal carrier for the delivery of oligonucleotides, Pharm. Res. 17 (2000) 707–714. https://doi.org/10.1023/A:1007582332491.

[94] Q. Zhang, Z. Shen, T. Nagai, Prolonged hypoglycemic effect of insulin-loaded polybutylcyanoacrylate nanoparticles after pulmonary administration to normal rats, Int. J. Pharm. 218 (2001) 75–80. https://doi.org/https://doi.org/10.1016/S0378-5173(01)00614-7.

[95] A. Graf, K.S. Jack, A.K. Whittaker, S.M. Hook, T. Rades, Protein delivery using nanoparticles based on microemulsions with different structure-types, Eur. J. Pharm. Sci. 33 (2008) 434–444. https://doi.org/https://doi.org/10.1016/j.ejps.2008.01.013.

[96] K.H. Siedentop, Tissue adhesive Histoacryl (2-cyano-butyl-acrylate) in experimental middle ear surgery, Am. J. Otol. 2 (1980) 77–87. http://europepmc.org/abstract/MED/7193980.

[97] M.L. Ronis, J.D. Harwich, R. Fung, M. Dellavecchia, Review of cyanoacrylate tissue glues with emphasis on their otorhinolaryngological applications, Laryngoscope. 94

(1984) 210–213. https://doi.org/https://doi.org/10.1288/00005537-198402000-00012.

[98] M.E. Sachs, Enbucrilate as Cartilage Adhesive in Augmentation Rhinoplasty, Arch. Otolaryngol. 111 (1985) 389–393. https://doi.org/10.1001/archotol.1985.00800080075009.

[99] L. Grislain, P. Couvreur, V. Lenaerts, M. Roland, D. Deprez-Decampeneere, P. Speiser, Pharmacokinetics and distribution of a biodegradable drug-carrier, Int. J. Pharm. 15 (1983) 335–345. https://doi.org/https://doi.org/10.1016/0378-5173(83)90166-7.

[100] R.A. Eiferman, J.W. Snyder, Antibacterial Effect of Cyanoacrylate Glue, Arch. Ophthalmol. 101 (1983) 958–960. https://doi.org/10.1001/archopht.1983.01040010958022.

[101] S.S. Merchant, S.E. Prochnik, O. Vallon, E.H. Harris, S.J. Karpowicz, G.B. Witman, A. Terry, A. Salamov, L.K. Fritz-laylin, L. Maréchal-drouard, W.F. Marshall, L. Qu, D.R. Nelson, A.A. Sanderfoot, M.H. Spalding, V. V Kapitonov, Q. Ren, P. Ferris, E. Lindquist, H. Shapiro, S.M. Lucas, J. Grimwood, The Chlamydomonas Genome Reveals the Evolution of Key Animal and Plant Functions, Science 318 (2007) 245–252.

[102] J. Kropat, A. Hong-Hermesdorf, D. Casero, P. Ent, M. Castruita, M. Pellegrini, S.S. Merchant, D. Malasarn, A revised mineral nutrient supplement increases biomass and growth rate in *Chlamydomonas reinhardtii*, Plant J. 66 (2011) 770–780. https://doi.org/10.1111/j.1365-313X.2011.04537.x.

[103] J. Neupert, D. Karcher, R. Bock, Generation of Chlamydomonas strains that efficiently express nuclear transgenes., Plant J. 57 (2009) 1140–1150. https://doi.org/10.1111/j.1365-313X.2008.03746.x.

[104] H. Tunçay, J. Findinier, T. Duchêne, V. Cogez, C. Cousin, G. Peltier, S.G. Ball, D.

Dauvillée, A forward genetic approach in *Chlamydomonas reinhardtii* as a strategy for exploring starch catabolism., PLoS One 8 (2013) e74763. https://doi.org/10.1371/journal.pone.0074763.

CHAPTER TWO: A RESIN CYANOACRYLATE NANOPARTICLE AS AN ACUTE CELL DEATH INDUCER TO BROAD SPECTRUM OF MICROALGAE

2.1. Introduction

The use and number of engineered resin nanoparticles (NPs), e.g., poly(alkyl)-cyanoacrylate NPs, polystyrene NPs, and polypropylene NPs, have been rapidly increasing. Their physical and chemical properties render them suitable for use in industrial and medical applications, such as in cosmetics, pigmented inks, and crack-resistant paints. However, the potential adverse effects of residual resin NPs on ecosystems are currently a serious concern [1,2].

Historically, studies on the effects of metal oxide NPs such as TiO_2 preceded those on resin NPs [3]. To date, *in vitro* experiments have shown that metal oxide NPs, carbon NPs, quantum dots, and dendrimers can induce growth inhibition and photosynthesis reduction in various green algal species [4–8]; however, they do not induce acute cell death.

Polycyanoacrylate NPs (PCA-NPs) are resin NPs that are promising for use in medical industries as drug delivery systems owing to their biocompatibility, biodegradability, and ability to adsorb active biological compounds such as antibiotics, antibodies, and enzymes [9,10].

Recently, we reported that poly(isobutylcyanoacrylate) resin NPs (iBCA-NPs) with a mean diameter of 25 nm possess the ability to rapidly induce cell mortality in green microalgae at a concentration of 100 mg L^{-1}. For example, cell mortality was induced in 19 of 25 investigated Volvocales species [11].

Algae are primary producers in aquatic ecosystems. They form the basis of the aquatic food web by providing oxygen to other organisms as well as absorbing trace metals and synthesizing nutrients [12]. Therefore, any change of algae population will eventually affect the function and structure of aquatic ecosystems [13]. Thus, it is essential to analyze the fundamental mechanism of how resin NPs induce algal cell mortality and determine how widely distributed algal species differ in their sensitivity. In this study, we evaluated the effects of iBCA-NP exposure on 18 widely distributed non-green algal species (i.e., 19 strains belonging to SAR and Hacrobia clades). Detailed analyses were performed using *Prymnesium parvum* (Haptophyta) and *Rhodomonas atrorosea* (Cryptophyta).

2.2. Materials and Methods

2.2.1. Nanoparticles

A detailed method for the preparation of iBCA-NPs with a mean diameter of 180 nm has been previously reported [11]. Briefly, an isobutylcyanoacrylate monomer (Aronalpha 501, Toagosei Co., Ltd. Japan) was added dropwise until it reached 1% concentration (w/v) in acidic water (pH = 2.0) containing 1.0% (w/v) dextran 60,000 (041-30525, Wako Pure Chemical Industries, Japan) as a dispersant while stirring at 600 rpm. The solution was stirred for 2 h and then neutralized using 0.5 M NaOH. The prepared NPs were stored at 4°C until use.

2.2.2. Preparation of surface-pre-coated poly(isobutylcyanoacrylate) resin nanoparticles

To determine the effect of pre-coating the surface of iBCA-NPs on algal cells, 15 mg of lyophilized powder of bovine serum albumin (BSA) (A7906, Sigma, USA) or skim milk (b199-219, Yukijirushi-Megumiruku, Japan) was added to 1% (w/v) iBCA-NP (w/v) solution (final concentration of 1.5%) and incubated for 72 h at 4°C. Then, pre-coated iBCA-NPs were added

to cells at 100 mg L^{-1}, and the cell mortality inducing ability was compared between non-coated iBCA-NPs and coated iBCA-NPs.

2.2.3. Zeta potential and size distribution of poly(isobutylcyanoacrylate) resin nanoparticles

Distribution of nanoparticles' diameter was measured using the dynamic light scattering method, and zeta potentials were measured based on the electrophoresis method using zeta potential and a particle size analyzer (ELSZ-2000ZS, Otsuka Electronics, Japan) following the manufacturer's instructions.

2.2.4. Algal species and their cultivation

The 18 algal species (19 strains) used in this study were obtained from the National Institute for Environmental Science (NIES, Tsukuba, Japan). Three species of *Bacillariophyceae*, three species (four strains containing two strains of the same species) of Haptophyta (*Prymnesiophyceae*), six species of Dinophyta (*Dinophyceae*), three species of *Raphidophyceae*, and three species of Cryptophyta (*Cryptophyceae*) were used in this study (Table 2.1). All algal strains were cultured in the NIES-recommended medium under constant fluorescent light (i.e., 30 μmol photons m^{-2} s^{-1}). Algal species were classified according to the NIES catalog.

2.2.5. Exposure of algal cells to poly(isobutylcyanoacrylate) resin nanoparticles

To investigate the effects of iBCA-NP exposure on non-green microalgal species, 1% iBCA-NP solution was added at the final concentration of 100 mg L^{-1} or 1 g L^{-1} to cells in log-phase growth (OD_{750} = 0.8–1.2) and co-incubated with gentle rotation for 24 h. For negative

control, co-incubation was conducted with only dextran 60,000-containing medium, which was used as a dispersant to prepare 180-nm iBCA-NPs.

2.2.6. Light microscopy

An Olympus microscope (BX63, Olympus, Tokyo, Japan) was used for bright-field, dark-field, and fluorescence microscopy. The specific mirror unit Olympus U-FBWA was used for fluorescence microscopy, whereas the specific condenser U-DCD (Olympus, Tokyo, Japan) was used for dark-field microscopy.

A laser confocal microscope (TCS SP8, Leica Microsystems CMS GmbH, Mannheim, Germany) was used to observe coccolith structures, which is a structure that covers cells in Haptophyta species. Samples were excited at 552 nm using 10% laser intensity. Autofluorescence of haptophyte chlorophyll was observed using a HyD1 detector (emission wavelength, 600–670 nm). Bright-field images were recorded using a photomultiplier tube trans detector.

2.2.7. Observation of *Rhodomonas atrorosea* using transmission electron microscopy

Cells were treated with 50 mg L^{-1} iBCA-NPs for 1 or 2 h, collected by centrifugation (2,000 × *g*, 5 min), and fixed in 1/15 M phosphate buffer (pH 7.4) containing 4% glutaraldehyde for 4 h at 4°C. The collected cells (2,000 × *g*, 5 min) were embedded in 2% agarose (Sea Plaque GTG, Takara Bio, Japan) at 45°C. The solidified gel was immersed in 1/15 M phosphate buffer (pH 7.4) for 1 h at 4°C. Post-fixation was performed in 1/15 M phosphate buffer containing 2% osmium tetroxide at 4°C for 2 h, and then samples were washed several times with distilled water for 1 h at 4°C. Next, samples were stained with 2% uranyl acetate at 4°C and then washed with distilled water for 1 h at 4°C. Samples were dehydrated using a graded ethanol series

(25%–100%) and finally embedded in Quetol-651 (Nisshin EM, Tokyo, Japan). Ultrathin sections of Quetol-651 blocks were stained with 2% uranyl acetate for 5 min at room temperature, followed by staining with lead citrate solution for 10 min at room temperature. Sections were observed using a transmission electron microscope (TEM) (Hitachi H-7650, Hitachi, Japan) at 80 kV.

2.2.8. Trypan blue staining assay

We used the trypan blue (TB) dye exclusion test to distinguish between dead and viable cells. This assay is based on the principle that living cells possess an intact plasma membrane that excludes the dye [14]. The TB solution (0.4% w/v, Wako Chem., Japan) was directly added to the cell suspension at a final concentration of 0.2% (w/v). After 5 min, the cells were observed using bright-field microscopy. Cells stained dark or light blue were regarded as dead. The cell death ratio was calculated by counting the total number of dead cells out of 100 cells.

2.2.9. Reactive oxygen species accumulation analysis

2',7'-dichlorodihydrofluorescein diacetate (H2DCFDA) (D668, Sigma, USA) was used to measure the accumulated reactive oxygen species (ROS) level. H2DCFDA solution (10 μM) was added to cells, followed by incubation for 15 min. Samples were then washed three times using a culture medium to reduce the background interference. H2DCFDA was converted to 2',7'-dichlorofluorescein (DCF) by ROS, and the fluorescence of DCF was measured using a fluorescence photometer (FL-2500, Hitachi, Japan) based on the Ex/Em wavelengths of DCF (495/515 nm). The abovementioned method was applied to *Prymnesium parvum, Cryptomonas ovata*, and *Rhodomonas atrorosea*, which were exposed to iBCA-NPs at a final concentration of 100 mg L^{-1}.

To investigate whether accumulated ROS is the primary cause of cell death, we exposed *P. parvum* cells to 100 mg L^{-1} of iBCA-NPs in a culture medium with and without the addition of 1 mM *N*-acetyl-L-cysteine (NAC) (Wako Pure Chemical Industries, Japan), which is a well-known ROS scavenger [15]. We determined the difference in the cell death ratio between these two conditions.

2.2.10. Cell growth curve

To investigate the adverse physiological effects of a low concentration of iBCA-NPs on cell growth, cells were exposed to iBCA-NPs at the final concentration of 10 mg L^{-1} or 100 mg L^{-1}. After co-incubation, cells were centrifuged (1,000 × *g*, 10 min), and the cell pellets were suspended in fresh culture medium. This step was repeated three times to remove residual NPs. Finally, 200 µL of the washed cells were inoculated in 20 mL of fresh medium. We assayed cell growth by measuring the turbidity at OD_{750} using a photometer (U-1900, Hitachi, Japan). The following equation was used to calculate the cell density in cells/mL based on the measured optical density value (GeneArt cryopreservation method Catalog # A24228, Life Technologies, USA): Cell concentration (cells mL^{-1}) = $[(OD_{750} - 0.88) / 9] \times 10^8$.

2.2.11. Statistical analyses

Cell death ratios and ROS levels were statistically compared using student's t-test and two-way analysis of variance. The differences between mean values were considered significant when the p-value was <0.05. We used GraphPad Prism version 7.03 (GraphPad Software, San Diego, California, USA) for all statistical analyses.

2.3. Results and Discussion

2.3.1. Particle size distribution and zeta potential of poly(isobutylcyanoacrylate) resin nanoparticles

The mean diameter of the synthesized monodisperse iBCA-NPs was 180.55 ± 0.07 nm (Appendix A, Fig. 1). The zeta potential of iBCA-NPs in the ESM culture medium was −2.12 ± 0.50 mV, whereas that of *P. parvum* cells (Haptophyta) in the medium was −15.97 ± 0.44 mV. The zeta potential of the skim milk-coated iBCA-NPs in the culture medium was −19.77 ± 2.13, whereas that of iBCA-NPs coated with BSA was −14.49 ± 2.33.

2.3.2. Induced abnormal swimming pattern in *Prymnesium parvum* (Haptophyta) after exposure to poly(isobutylcyanoacrylate) resin nanoparticles

In the co-incubation culture of *P. parvum* cells with iBCA-NPs at 500 mg L^{-1}, we observed the scattered light trails of NPs using dark-field microscopy. The NPs occasionally collided with the cells and bounced off their surfaces. Neither stable adhesion nor hetero aggregate of the cells and NPs was observed, possibly because both were negatively charged (Appendix A, Video 1A). Following 15 min of co-incubation, almost all cells started to exhibit abnormal swimming patterns. In addition, some cells adopted a spherical shape, suggesting cell wall degradation (Appendix A, Video 1B). After 1 h of co-incubation, most cells stopped swimming. The change in cellular redox poise is a key factor in determining the swimming direction of *Chlamydomonas reinhardtii*, with cells changing their swimming direction by switching between positive and negative phototaxis [16,17]. Therefore, acutely induced abnormal swimming patterns in *P. parvum* can reflect the disordered poise of redox in the cell.

2.3.3. Species-dependent sensitivity assay using poly(isobutylcyanoacrylate) resin nanoparticles at 100 mg L^{-1} and 1 g L^{-1}

To assay the sensitivity of various non-green algal species to NPs, we exposed cells in log-phase growth to iBCA-NPs at 100 mg L^{-1} or 1 g L^{-1} for 24 h in the recommended culture medium. Cell mortality was determined using TB staining.

After exposure to 100 mg L^{-1} iBCA-NPs for 24 h, the ratio of cells stained with TB reached >70% in two of the three *Bacillariophyceae* species, all three Cryptophyta species, four of the six Dinophyta species, all three Haptophyta species (except one of the two strains of *Emiliania huxleyi*), and all three tested *Raphidophyceae* species (Fig. 2.1). Then, we exposed the resistant algal species to a higher concentration (1 g L^{-1}) for 24 h. This exposure induced >70% cell death in all investigated samples (Table 2.1).

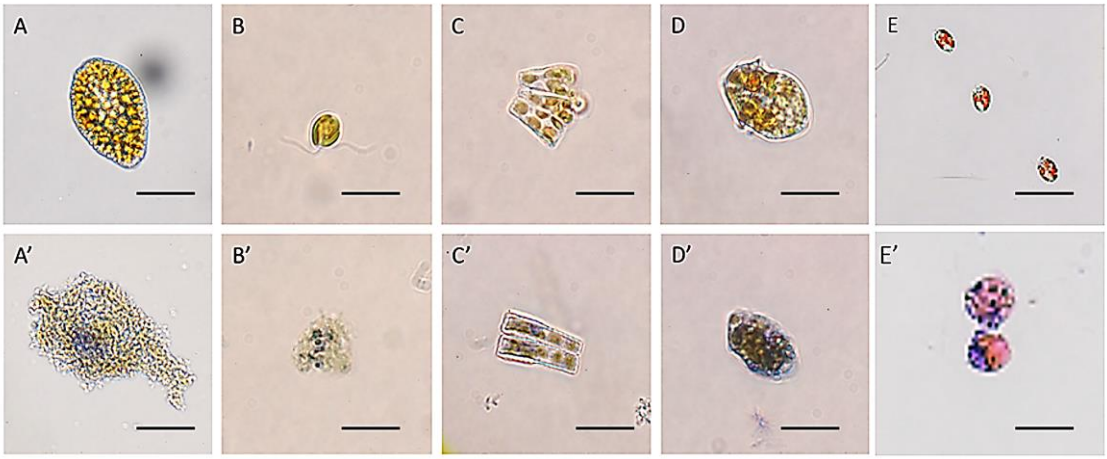

Figure 2.1. Induced cell death following exposure to poly(isobutylcyanoacrylate) resin nanoparticles (iBCA-NPs) at 100 mg L^{-1} (A′ , B′ , C′ , D′ , E′) and incubation in dextran-containing medium as the control (A, B, C, D, E). After 24 h of incubation, cells were stained with trypan blue (TB). (A) and (A′) *Chattonella marina* (Raphidophyceae); (B) and (B′) *Prymnesium parvum* (Haptophyta); (C) and (C′) *Thalassionema nitzschioides* (Bacillariophyceae); (D) and (D′) *Heterocapsa triquetra* (Dinophyta); (E) and (E') *Rhodomonas atrorosea* (Cryptophyta); bar, 10 µm.

IBCA-NP concentrations of 100 mg L^{-1} and 1 g L^{-1} were used to investigate the sensitivity of the different algal species. However, there are currently no reliable environmental concentrations of resin NPs to which the used concentrations can be directly compared with. To the best of our knowledge, only one report has described the concentration of NPs, both from natural sources (e.g., clay particles) as well as manufactured resin NPs, in aquatic environments [18]. In the paper, NP concentrations were assessed at nine different locations in Sweden (rivers, lakes, and coastal areas) by tracking the weakly scattering particles using a high-sensitivity camera. The NP concentrations were found to be from 0.5×10^{11} to 2×10^{12} particles L^{-1}. In contrast, 100 mg L^{-1} of iBCA-NP contains approximately 2.9×10^{13} particles L^{-1} (density of iBCA-NP = ca. 1.125). Therefore, the concentration of resin NPs used in this experiment must be much higher than that of NPs in most aquatic locations where there is no specific source of NP litter. Thus, the obtained cell mortality ratios by the following exposure to iBCA-NP at 100 mg L^{-1} and 1,000 mg L^{-1} must be under extreme conditions.

Table 2.1. List of investigated algal species, extracellular coverings, and their sensitivity to poly(isobutylcyanoacrylate) resin nanoparticles.

Species	**Strain**	**Classification**[a]	**Extracellular Coverings**	**Cell death**[b]		
				Dispersant	100 mg L^{-1}	1000 mg L^{-1}
Thalassionema nitzschioides	NIES-534	Heterokontophyta and *Bacillariophyceae*	Frustule (silica)	No	Yes[c]	ND[d]
Chaetoceros debilis	NIES-3710	Heterokontophyta and *Bacillariophyceae*	Frustule (silica)	No	Yes	ND
Odontella longicruris	NIES-590	Heterokontophyta and *Bacillariophyceae*	Frustule (silica)	No	No	Yes
Calyptrosphaera sphaeroidea	NIES-1308	Haptophyta and *Prymnesiophyceae*	Coccolith (-)	No	Yes	ND
Prymnesium parvum	NIES-1017	Haptophyta and *Prymnesiophyceae*	Unmineralized plate-scale	No	Yes	ND
Emiliania huxleyi	NIES-1310	Haptophyta and *Prymnesiophyceae*	Coccolith (-)	No	Yes	ND
	NIES-2778		Coccolith (+)	No	No	ND

Amphidinium carterae	NIES-331	Dinophyta and *Dinophyceae*	No covering	No	Yes	ND
Karenia mikimotoi	NIES-2411	Dinophyta and *Dinophyceae*	No covering	No	Yes	ND
Prorocentrum dentatum	NIES-900	Dinophyta and *Dinophyceae*	Thecal plates (*Amphiesma*)	No	Yes	ND
Heterocapsa triquetra	NIES-7	Dinophyta and *Dinophyceae*	Thecal plates (*Amphiesma*)	No	Yes	ND
Coolia monotis	NIES-615	Dinophyta and *Dinophyceae*	Thecal plates (*Amphiesma*)	No	No	Yes
Gambierdiscus sp.	NIES-2764	Dinophyta and *Dinophyceae*	Thecal plates (*Amphiesma*)	No	No	Yes
Olisthodiscus luteus	NIES-15	Heterokontophyta and *Raphidophyceae*	No covering	No	Yes	ND
Chattonella marina	NIES-1	Heterokontophyta and *Raphidophyceae*	No covering	No	Yes	ND

Heterosigma akashiwo	NIES-5	Heterokontophyta and *Raphidophyceae*	No covering	No	Yes	ND
Chroomonas caudata	NIES-712	Cryptophyta and *Cryptophyceae*	Periplast	No	Yes	ND
Cryptomonas ovata	NIES-274	Cryptophyta and *Cryptophyceae*	Periplast (proteinaceous)	No	Yes	ND
Rhodomonas atrorosea	NIES-699	Cryptophyta and *Cryptophyceae*	Periplast (proteinaceous)	No	Yes	ND

[a]Classification was in accordance with the list of the National Institute for Environmental Studies

[b]Incubation time was 24 h

[c]>70% cell death

[d]Not determined

2.3.4. Effect of cell coverings on cell mortality

Among the four investigated Haptophyta strains (i.e., three species), *E. huxleyi* NIES−2778, which bears a thick accumulation of coccoliths, was resistant (only ~15% cell mortality at 100mg L^{-1} iBCA-NP for 24 h). In contrast, *E. huxleyi* NIES-1310 and *Calyptros phaera sphaeroidea*, which bear no coccoliths, and *P. parvum*, which bears only 2–3 thin layers of unmineralized plate scales [19,20], showed >70% cell mortality after 24 h of incubation.

Notably, two strains of *E. huxleyi*, NIES-1310 (bearing no coccoliths) and NIES-2778 (bearing thick accumulation of coccoliths), showed considerably different sensitivities (Fig. 2.2). This finding strongly suggests that the accumulated thick coccolith layer works as a mechanical barrier against iBCA-NP.

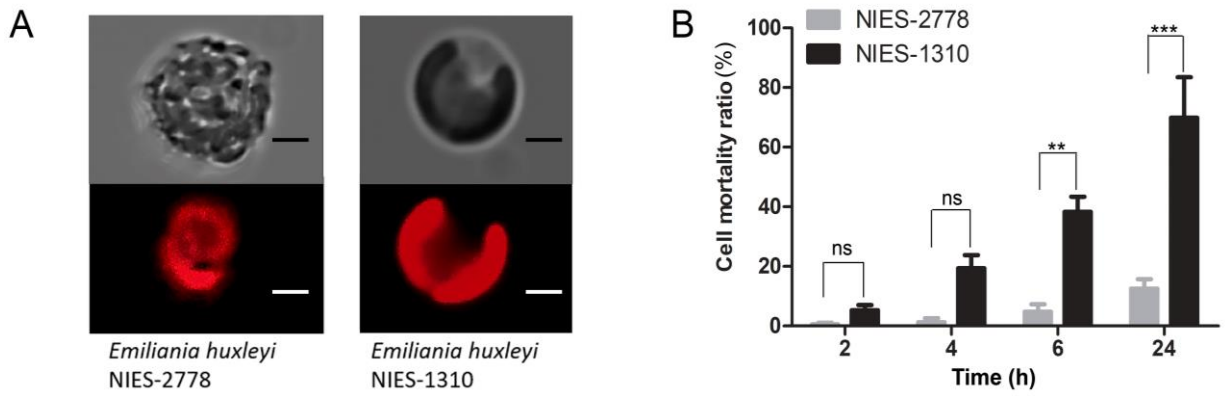

Figure 2.2. The mechanical barrier effect of accumulated coccoliths on cell death induction. (A) Laser microscopic images of two *Emiliania huxleyi* strains, naked NIES-1310, and coccolith-bearing NIES-2778. Upper panels are bright-field images and lower lower panels are the corresponding fluorescence images; bar, 1 μm. (B) Different cell death ratios in two strains of *E. huxleyi*. The naked strain NIES-1310 and coccolith-bearing strain NIES-2778 were exposed to 100 mg L^{-1} poly(isobutylcyanoacrylate) resin nanoparticles (iBCA-NPs). Cell death was assayed using the trypan blue (TB) staining method. Results are shown as the mean ratios (±SE) calculated from three independent experiments. Asterisks denote a significant difference in mean values between the two strains (two-way analysis of variance, ** $p < 0.01$, *** $p < 0.001$, ns = $p > 0.05$).

Supporting the barrier effect of cell coverings, two *Raphidophyceae* species with no cell covering structure [21–23] (i.e., *Chattonella marina* and *Olisthodiscus luteus*) showed high sensitivity to iBCA-NP, with >70% cell mortality after a 24 h of incubation with 100 mg L^{-1} of iBCA-NPs (Table 2.1).

One of the three tested *Bacillariophyceae* species, *Odontella longicruris* showed higher resistance than *Thalassionema nitzschioides* and *Chaetoceros debilis* (Table 2.1). The pores in the *O. longicruris* silica cell covering (frustule) are ~250 nm in diameter [24], whereas those in *T. nitzschioides* are ~500 nm [25] and those in *C. debilis* are of undetermined size. Considering that the smallest size of iBCA-NPs was ~70 nm and the largest size was ~450 nm (Appendix A, Fig. 1), the frustule of *T. nitzschioides* (~500 nm) did not function as a mechanical barrier against the invasion of iBCA-NPs, whereas that of *O. longicruris* (~250 nm) must have some mechanical barrier effect.

Among the six tested *Dinophyceae* species, two species (*Coolia monotis* and *Gambierdiscus* sp.), which bear thecal plates, required treatment of 1 g L^{-1} iBCA-NPs to induce >70% cell death, whereas >70% cell death was induced by only 100 mg L^{-1} iBCA-NPs in the other four species (i.e., *Amphidinium carterae*, *Karenia mikimotoi*, *Prorocentrum dentatum*, and *Heterocapsa triquetra*) (Table 2.1). Among the four rather sensitive species, two (*A. carterae* and *K. mikimotoi*) do not bear thecal plates, whereas the other two (*P. dentatum* and *H. triquetra*) bear thecal plates. Therefore, further investigation is required to elucidate the factors that determine sensitivity of *Dinophyceae* species to resin NPs.

As the control, we incubated algal cells with dextran 60,000-containing medium, which was used as a dispersant to prepare iBCA-NPs. For example, 0.1% (w/v) dextran 60,000 was added to the culture medium as a control for 0.1% iBCA-NPs, and 1% (w/v) dextran was added to the culture medium for 1% iBCA-NPs. The cell death induced by co-incubation with dextran

60,000 was consistently below 5% in all species. Therefore, cell death could be attributed to NPs but not dextran.

2.3.5. Reduced potency of poly(isobutylcyanoacrylate) resin nanoparticles by surface coating with skim milk or bovine serum albumin

The Haptophyta species *P. parvum* was exposed to 100 mg L^{-1} iBCA-NPs immersed in BSA solution or skim milk to coat the surface of NPs, and the cell death-inducing potency of the coated iBCA-NPs was compared with that of non-coated iBCA-NPs. We found that the potency of coated NPs was considerably reduced. For instance, after 8 h of exposure to non-coated iBCA-NPs, the cell death ratio was ~37%, while it was only ~9% and ~10% after exposure to iBCA-NPs immersed in skim milk and BSA, respectively (Fig. 2.3).

It has been reported that *n*-butyl-cyanoacrylate-NPs (*n*BCA-NPs) can adsorb BSA and proteins contained in rat serum [26]. Moreover, it can deliver adsorbed proteins such as *β*-galactosidase, RhoG, and mouse anti-*α*-synuclein monoclonal antibody H3C to neurons [27]. Therefore, the surface of iBCA-NPs immersed in 100 mg L^{-1} skim milk or BSA should have been coated with the included proteins.

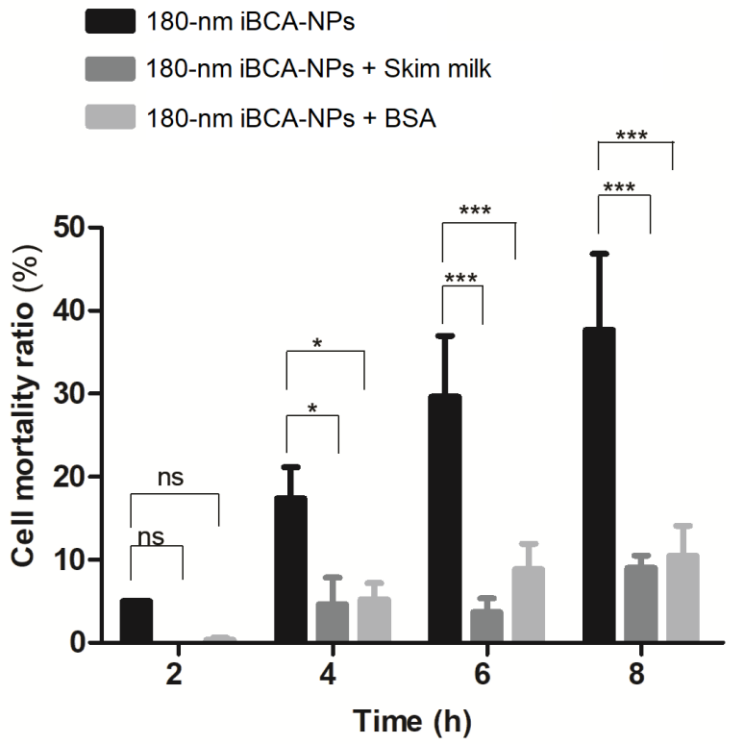

Figure 2.3. Comparison of the cell death-inducing potency between non-coated and poly(isobutylcyanoacrylate) resin nanoparticles (iBCA-NPs) coated with skim milk or bovine serum albumin (BSA). Results are shown as the mean ratios (±SE) calculated from three independent experiments. Asterisks denote significant differences between the two treatments (two-way analysis of variance, * $p < 0.05$, *** $p < 0.001$, ns = $p > 0.05$).

The substantially reduced potency of coated iBCA-NPs is likely because pre-coating interfered with the ability of NPs to bind to target molecules, which is essential to induce cell death.

2.3.6. Correlation between reactive oxygen species accumulation and cell mortality

We measured the time-dependent increase in the fluorescence of DCF, the converted product of nonfluorescent H2DCFDA by esterase and ROS, using a fluorescence spectrometer. In *P. parvum*, fluorescence intensity increased with increased exposure time. It reached a peak at 2 h, and the fluorescence intensity was approximately three times higher than that of the control. The fluorescence intensity then decreased after exposure for 3 h (Fig. 2.4A). Consistent with spectrofluorescence data, fluorescence-positive cells were most frequently observed at 2 h of exposure using fluorescence microscopy (Fig. 2.4C).

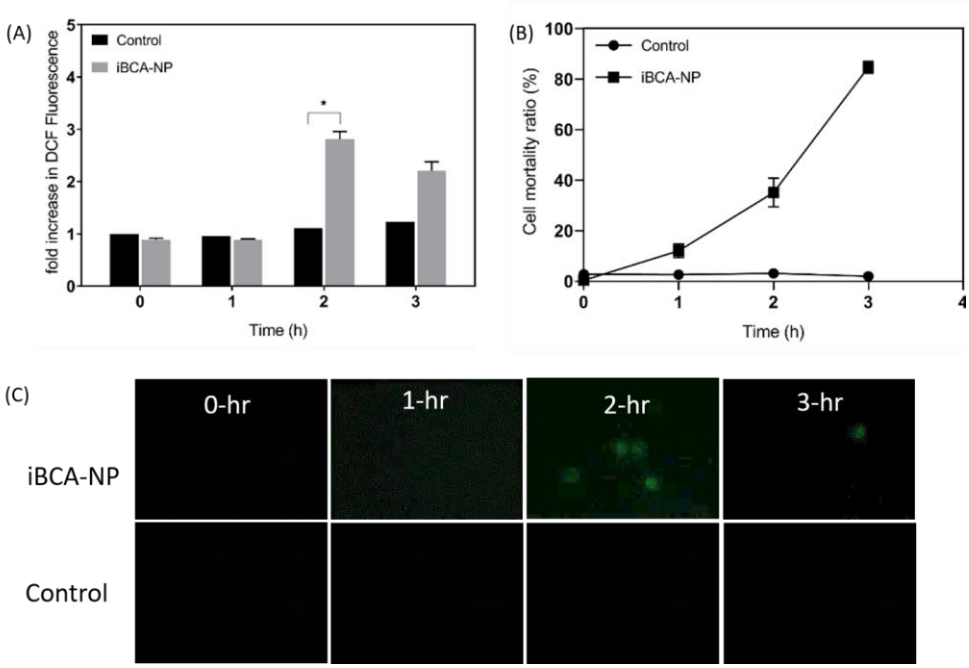

Figure 2.4. Time-course changes in 2',7'- dichlorofluorescein (DCF) fluorescence level, cell mortality, and appearance of reactive oxygen species (ROS)-positive cells. (A) Increase in DCF fluorescence in *Prymnesium parvum* following the exposure of poly(isobutylcyanoacrylate) resin nanoparticles (iBCA-NPs) at 100 mg L^{-1}. The fluorescence was measured using a fluorescence spectrometer. Two-way analysis of variance, * $p < 0.05$. (B) Time-course change in the cell mortality ratio following the exposure of iBCA-NPs at 100 mg L^{-1}. (C) Microscopic observation of DCF fluorescence in *P. parvum* cells exposed to 100 mg L^{-1} of iBCA-NPs. Control is the result of cells incubated in the dextran-containing medium that is contained in the iBCA-NP solution as a dispersant.

The decrease in the number of fluorescence-positive cells and DCF levels following longer incubations is likely because DCF cannot be retained inside the cell when the plasma membrane is severely damaged. This is consistent with the observation that cells darkly stained with TB were consistently DCF fluorescence-negative, whereas cells slightly stained with TB or unstained cells were DCF fluorescence-positive. This finding also suggests that ROS accumulation precedes plasma membrane disruption. We also detected DCF fluorescence-positive cells in Cryptophyta species (i.e., *C. ovata* and *R. atrorosea*) after exposure to 100 mg L^{-1} iBCA-NPs for 1 h (Appendix A, Fig. 2).

The addition of membrane-permeable NAC before iBCA-NP treatment substantially reduced *P. parvum* cell death. The cell death ratio in *P. parvum* in the medium with and without NAC after 7 h of exposure to iBCA-NPs (100 mg L^{-1}) was ~5% and ~50%, respectively (Fig. 2.5). These results showed that ROS accumulation was a direct cause of resin NP-induced cell

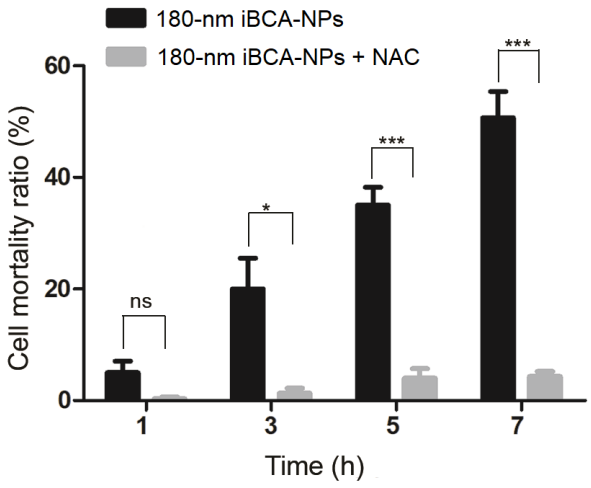

Figure 2.5. Effect of the reactive oxygen species (ROS) scavenger N-acetyl-L-cysteine (NAC) on cell death. NAC (1 mM final concentration) was added 45 min before exposure of *Prymnesium parvum* cells to 100 mg L^{-1} poly(isobutylcyanoacrylate) resin nanoparticles (iBCA-NPs). Results are shown as the mean ratios (±SE) calculated from three independent experiments. Asterisks denote significant differences between the two treatments at a given time (two-way analysis of variance, * $p < 0.05$, *** $p < 0.001$, ns = $p > 0.05$).

death. ROS accumulation can induce oxidative modifications in proteins, particularly methionine and cysteine residues [28,29], which results in the formation of protein aggregates and activation of chaperone-mediated autophagy [30–32].

In the present study, we detected changes in the color of *R. atrorosea* cells caused by NP exposure. The cell color changed from brownish to greenish (Appendix A, Fig. 3). This might be caused by the degradation or twisted conformation of phycobiliprotein, which is densely packed in the thylakoid lumen, or that of the integral membrane Chl-a/c2 carotenoid protein complexes [33].

2.3.7. Transmission electron microscopy observation of fine structure changes in *Rhodomonas atrorosea* (Cryptophyta)

The width of mitochondria in unexposed *R. atrorosea* cells was 0.3–0.4 μm (Fig. 2.6A), whereas swollen mitochondria (width > 1.0 μm) were often detected after 1 h of exposure to 100 mg L^{-1} iBCA-NPs (Fig. 2.6B–E). These mitochondria often lacked cristae in the middle (Fig. 2.6B, D), and many had cristae only at their peripheral regions (Fig. 2.6C, E). Enlarged vacuoles were also detected, which were more prominent after 2 h of exposure (Fig. 2.6F, G) than after 1 h of exposure (Fig. 2.6B–F). However, chloroplast enlargement was not as prominent in both 1-h and 2-h-exposed cells. We previously reported that lysis of *C. reinhardtii* cells was induced by co-incubation with 25-nm-sized iBCA-NPs. In *C. reinhardtii*, cell lysis was often accompanied by extreme enlargement of vacuoles, whereas the enlargement of mitochondria was not detected [11].

Disordered chloroplasts or those with partial thylakoid loss were also prominently detected in the exposed cells (Fig. 2.6D). Such prominently disordered chloroplasts were not detected in *C. reinhardtii* exposed to 25-nm-sized iBCA-NPs [11].

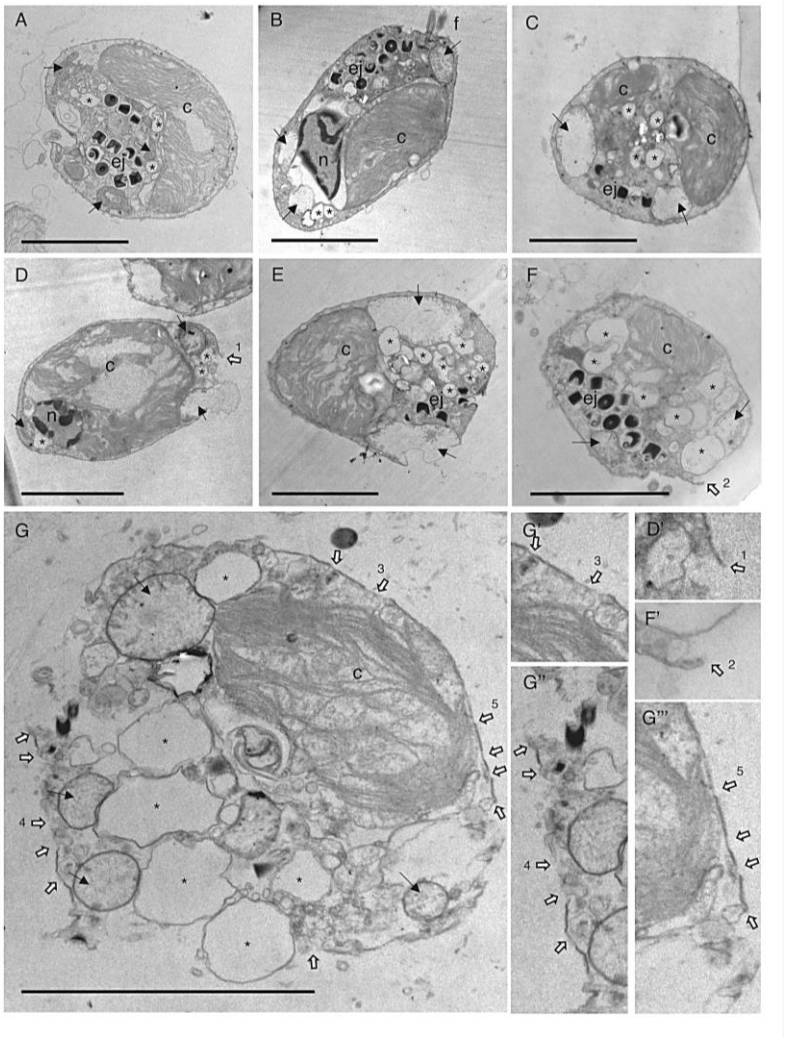

Figure 2.6. Transmission electron microscopy (TEM) image of *Rhodomonas atrorosea* cells exposed to 100 mg L^{-1} poly(isobutylcyanoacrylate) resin nanoparticles (iBCA-NPs). (A) Unexposed cells. (B through E) 1-h-exposed cells. (F and G) 2-h-exposed cells. Enlarged images of specific areas are shown with one or several apostrophes ('). Black arrows, mitochondria; white arrows in G, G', G'', and G''', places where lack plasma membrane and cell wall; c, chloroplast; n, nucleus; ej, ejectosome; f, flagellum; *, vacuole; bar, 5 μm.

One of the possible reasons is that chloroplast disorder in *R. atrorosea* is related to the degradation or twisted conformation of phycobiliprotein which is densely packed in the thylakoid lumen. Most of the observed plasma membrane ruptures after 1 h of exposure appeared to stem from increased turgor pressure in extremely enlarged mitochondria (arrow in Fig. 2.6D, E). Regions that seemed to be lacking a cell wall and plasma membrane were prominently enlarged and observed more often after 2 h of exposure (white arrows in Fig. 2.6F, G, F', G', G'', and G''') than after 1 h of exposure (white arrows in Fig. 2.6D, D').

Electron transport systems in chloroplasts and mitochondria are major ROS producers in plants [34,35]. Abnormal structures in these organelles suggest that defects in them caused ROS release into the cytoplasm, as detected by DCF fluorescence in *P. parvum* cells exposed to NPs (Fig. 2.4C).

IBCA-NPs served as an ROS inducer in both *R. atrorosea*, and *C. reinhardtii*, but the induced defects in fine structures exhibited species-specific differences. This finding might reflect the difference in the affected metabolic pathways and the proteins embedded in organelle membranes.

2.3.8. Relationship between nanoparticle concentration and induced cell death ratio in *Prymnesium parvum* (Haptophyta)

We analyzed the relationship between cell death and mass concentration (w/v) of NPs using *P. parvum* (Haptophyta species). Cell death increased along with an increase in iBCA-NP concentration (w/v). Cell death ratios after 4 h of exposure at final concentrations of 50 mg L^{-1}, 100 mg L^{-1}, and 250 mg L^{-1} were 52%, 72%, and 95%, respectively (Appendix A, Fig. 4). A longer incubation period induced more cell death. Following 24 h of incubation with 10 mg

L^{-1}, 25 mg L^{-1}, 50 mg L^{-1}, and 100 mg L^{-1} iBCA-NPs, the cell death ratio reached ~5%, ~45%, ~85%, and 100%, respectively (Fig. 2.7).

At 10 mg L^{-1} concentration of iBCA-NPs, the *P. parvum* cell death ratio was 5% even after 24 h of exposure, which was not significantly different from that of the unexposed cells (Fig. 2.7). We investigated if the TB-negative cells incurred any physiological damage using *P. parvum* cells co-incubated with 10 mg L^{-1} iBCA-NPs for 24 h.

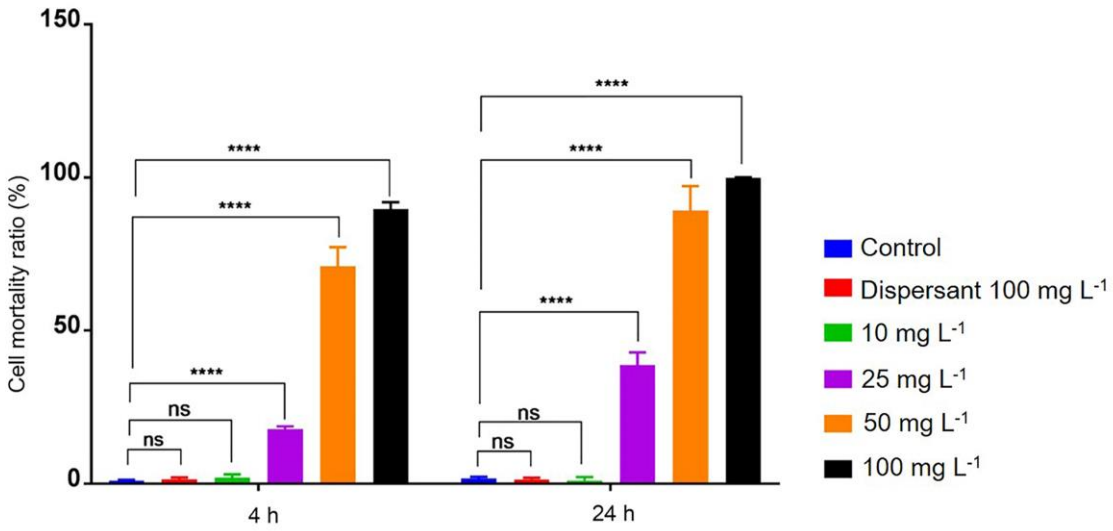

Figure 2.7. Ratios of cell death induced by various concentrations of poly(isobutylcyanoacrylate) resin nanoparticles (iBCA-NPs) in *Prymnesium parvum* cells following 4 h or 24 h of exposure. Cells incubated in dextran-containing medium were used as the control. Results are shown as the mean ratios (±SE) calculated from three independent experiments. Asterisks denote significant differences between the two strains (two-way analysis of variance, **** $p < 0.0001$, ns = $p > 0.05$).

The *P. parvum* cells co-incubated with 10 mg L^{-1} iBCA-NPs, which had been washed three times with fresh medium, required 12 days to initiate logarithmic cell growth. In contrast, untreated and dispersant-treated cells entered log-phase growth within a shorter period (5 days) (Fig. 2.8). Therefore, even the TB-negative cells must have been severely affected by the

accumulated ROS. Interestingly, in the logarithmic phase, iBCA-NP-exposed and unexposed cells exhibited no significant differences in growth rate, suggesting that the ROS. Interestingly, in the logarithmic phase, iBCA-NP-exposed and unexposed cells exhibited no significant differences in growth rate, suggesting that the ROS damage induced by iBCA-NPs was tentative and did not cause genetic changes.

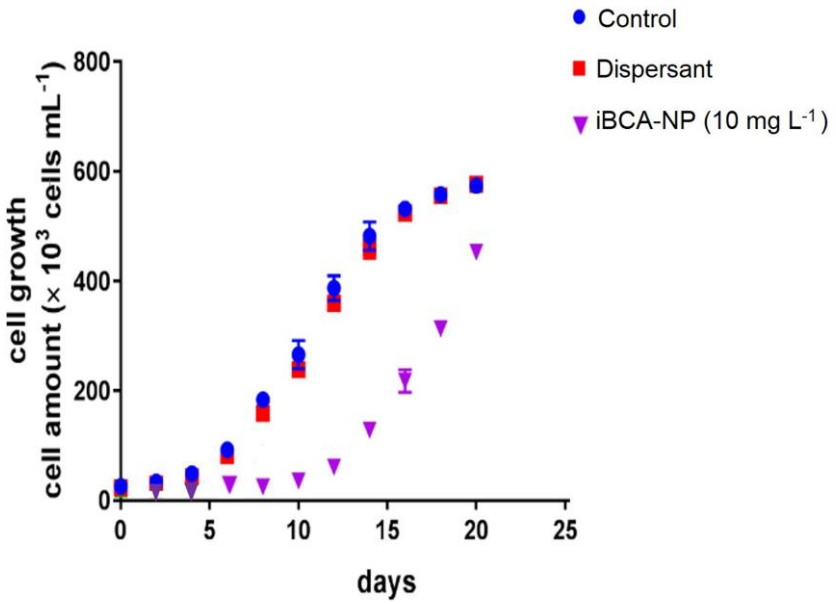

Figure 2.8. Growth curve of *Prymnesium parvum* cells inoculated in fresh medium after exposure to poly(isobutylcyanoacrylate) resin nanoparticles (iBCA-NPs). *P. parvum* cells that had been exposed to 10 mg L-1 of iBCA-NPs for 24 h were washed and inoculated in fresh medium. Cells not exposed to nanoparticles were used as a control.

2.3.9. The hypothesized mechanism of how resin nanoparticles induce cell mortality

Non-resin NPs such as metal oxide NPs (e.g., ZnO, CuO, and TiO_2), carbon nanotubes [36], and semiconductor quantum dots, have the potency to induce growth inhibition in green microalgae but no potency to induce acute cell death [37,38]. All these NPs quickly generated

hetero-aggregates composed of NPs and cells [39–42]. Therefore, nutrient exchange inhibition and the light shade effect are considered the primary effects of these NPs [6,43–45].

However, the dark-field observation of *P. parvum* cells co-incubated with iBCA-NPs showed that NPs occasionally collided with the cells and bounced off their surfaces without stable adherence. Therefore, sealing of the cell surface by NPs cannot be the primary cause of the induced cell death in cyanoacrylate resin NPs.

Our results suggest that cell coverings such as the coccolith of Haptophyta species and silica-made frustules of Heterokontophyta species act as mechanical barriers to prevent cell mortality. A critically different sensitivity was observed between the two strains of *E. huxleyi*, which is probably attributable to the presence/absence of coccoliths.

The barrier effect of cell coverings leads to the hypothesis that NPs need to penetrate cell coverings to induce cell death. This hypothesis was also supported by TEM observations, revealing that the cell wall of NP-sensitive *R. atrorosea* was damaged after exposure to iBCA-NPs (Fig. 2.6). In addition, in another NP-sensitive species, i.e., *P. parvum*, protoplast-like spherical cells were detected after 15 min of exposure to iBCA-NPs (Appendix A, Video 1A). The importance of the invasion of NPs suggests that the target molecule of the NP is present within cell coverings.

Because of the weak specific affinity of iBCA-NPs to proteins [46–49], once NPs penetrate cell coverings, they must find multiple proteins, e.g., G protein-coupled receptors, ion channel-coupled receptors, and cytokine receptors, on the plasma membrane to which they can bind. The binding of NPs to such proteins must induce functional loss in the proteins by altering their three-dimensional structures [48]. The functional loss in proteins triggers responses that eventually lead to ROS accumulation, as observed in this study.

The iBCA-NPs coated with BSA or skim milk showed considerably reduced potency to induce cell death. This is likely because the protein binding sites of iBCA-NPs were occupied by proteins present in skim milk or BSA. Therefore, the pre-coated NPs exhibited reduced potency to bind the target proteins located on the cell wall or plasma membrane.

The abovementioned hypothesis accurately explains why a resin iBCA-NP can induce cell death in diverse algal species with species- or strain-specific differences in sensitivity. Therefore, it is essential to determine the mechanisms involved in the interactions between resin NPs and proteins for the appropriate regulation of resin NP disposal.

2.4. References

[1] E. Navarro, A. Baun, R. Behra, N.B. Hartmann, J. Filser, A.J. Miao, A. Quigg, P. H. Santschi, L. Sigg, Environmental behavior and ecotoxicity of engineered nanoparticles to algae, plants, and fungi, Ecotoxicology. 17 (2008) 372–386.https://doi.org/10.1007/s10646-008-0214-0.

[2] M.A. Maurer-Jones, I.L. Gunsolus, C.J. Murphy, C.L. Haynes, Toxicity of engineered nanoparticles in the environment, Anal. Chem. 85 (2013) 3036–3049. https://doi.org/10.1021/ac303636s.

[3] K. Hund-Rinke, M. Simon, Ecotoxic effect of photocatalytic active nanoparticles (TiO2) on algae and daphnids (8 pp), Environ. Sci. Pollut. Res. 13 (2006) 225–232.

[4] A. Nel, T. Xia, L. Mädler, N. Li, Toxic potential of materials at the nanolevel, Science 311 (2006) 622–627. https://doi.org/10.1126/science.1114397.

[5] E.Y. Krysanov, D.S. Pavlov, T.B. Demidova, Y.Y. Dgebuadze, Effect of nanoparticles on aquatic organisms, Biol. Bull. 37 (2010) 406–412.

[6] F. Schwab, T.D. Bucheli, L.P. Lukhele, A. Magrez, B. Nowack, L. Sigg, K. Knauer, Are carbon nanotube effects on green algae caused by shading and agglomeration?, Environ. Sci. Technol. 45 (2011) 6136–6144. https://doi.org/10.1021/es200506b.

[7] S.P. Melegari, F. Perreault, R.H.R. Costa, R. Popovic, W.G. Matias, Evaluation of toxicity and oxidative stress induced by copper oxide nanoparticles in the green alga Chlamydomonas reinhardtii, Aquat. Toxicol. 142 (2013) 431–440.

[8] T.Y. Suman, S.R. Rajasree, R. Kirubagaran, Evaluation of zinc oxide nanoparticles toxicity on marine algae Chlorella vulgaris through flow cytometric, cytotoxicity and oxidative stress analysis, Ecotoxicol. Environ. Saf. 113 (2015) 23–30.

[9] J. Kreuter, H.R. Hartmann, Comparative study on the cytostatic effects and the tissue distribution of 5-fluorouracil in a free form and bound to polybutylcyanoacrylate nanoparticles in sarcoma 180-bearing mice, Oncology. 40 (1983) 363–366.

[10] C. Vauthier, C. Dubernet, E. Fattal, H. Pinto-Alphandary, P. Couvreur, Poly(alkylcyanoacrylates) as biodegradable materials for biomedical applications, Adv. Drug Deliv. Rev. 55 (2003) 519–548.

[11] D. Widyaningrum, D. Iida, Y. Tanabe, Y. Hayashi, S.D. Kurniasih, T. Ohama, Acutely induced cell mortality in the unicellular green alga Chlamydomonas reinhardtii (Chlorophyceae) following exposure to acrylic resin nanoparticles, J. Phycol. 55 (2019) 118–133. https://doi.org/10.1111/jpy.12798.

[12] J.W. Blunt, B.R. Copp, M.H. Munro, P.T. Northcote, M.R. Prinsep, Marine natural products, Nat. Prod. Rep. 20 (2003) 1–48.

[13] Y.H. Chang, C.R. Ku, H.L. Lu, Effects of aquatic ecological indicators of sustainable green energy landscape facilities, Ecol. Eng. 71 (2014) 144–153.

[14] W. Strober, Trypan Blue Exclusion Test of Cell Viability, Curr. Protoc. Immunol. 111 (2015) A3.B.1-A3.B.3. https://doi.org/10.1002/0471142735.ima03bs111.

[15] J.F. Curtin, M. Donovan, T.G. Cotter, Regulation and measurement of oxidative stress in apoptosis, J. Immunol. Methods. 265 (2002) 49–72.

[16] K.I. Wakabayashi, S.M. King, Modulation of Chlamydomonas reinhardtii flagellar motility by redox poise, J. Cell Biol. 173 (2006) 743–754. https://doi.org/10.1083/jcb.200603019.

[17] K.I. Wakabayashi, Y. Misawa, S. Mochiji, R. Kamiya, Reduction-oxidation poise regulates the sign of phototaxis in Chlamydomonas reinhardtii, Proc. Natl. Acad. Sci. U. S. A. 108 (2011) 11280–11284. https://doi.org/10.1073/pnas.1100592108.

[18] J.A. Gallego-urrea, J. Tuoriniemi, T. Pallander, M. Hassellöv, Measurements of nanoparticle number concentrations and size distributions in contrasting aquatic environments using nanoparticle tracking analysis, Environ. Chem. 7 (2010) 67–81. https://doi.org/10.1071/EN09114.

[19] I. Manton, G.F. Leedale, Observations on the fine structure of Prymnesium parvum Carter, Arch. Microbiol. 45 (1963) 285–303.

[20] I. Manton, Observations on scale production in Prymnesium parvum, J. Cell. Sci. 1 (1966) 375–380.

[21] G. Hasle, E. Syvertsen, K. Steidinger, K. Tangen, C. Tomas, Identifying Marine Diatoms and Dinoflagellates, 1st ed., Academic Press, San Diego, California, 1996.

[22] H.A. Bowers, C. Tomas, T. Tengs, J.W. Kempton, A.J. Lewitus, D.W. Oldach, RAPHIDOPHYCEAE [CHADEFAUD EX SILVA] SYSTEMATICS AND RAPID IDENTIFICATION: SEQUENCE ANALYSES AND REAL-TIME PCR ASSAYS 1, J.

Phycol. 42 (2006) 1333–1348.

[23] D.M. Anderson, Approaches to monitoring, control, and management for harmful algal blooms (HABs), Ocean. Coast. Manag. 52 (2009) 342-347.

[24] A.S. Lavigne, I. Sunesen, E.A. Sar, Morphological, taxonomic and nomenclatural analysis of species of Odontella, Trieres and Zygoceros (Triceratiaceae, Bacillariophyta) from Anegada Bay (Province of Buenos Aires, Argentina), Diatom Res. 30 (2015) 307–331.

[25] E.A. Sar, I. Sunesen, P.V. Fernández, Marine diatoms from Buenos Aires coastal waters (Argentina). II. Thalassionemataceae and Rhaphoneidaceae, Rev. Chil. Hist. Nat. 80 (2007) 63–79.

[26] A.K.O. Åslund, E. Sulheim, S. Snipstad, E. Von Haartman, H. Baghirov, N. Starr, M. Kvale Løvmo, S. Lelú, D. Scurr, C.D.L. Davies, R. Schmid, Ý. Mørch, Quantification and Qualitative Effects of Different PEGylations on Poly(butyl cyanoacrylate) Nanoparticles, Mol. Pharm. 14 (2017) 2560–2569. https://doi.org/10.1021/acs.molpharmaceut.6b01085.

[27] L. Hasadsri, J. Kreuter, H. Hattori, T. Iwasaki, J.M. George, Functional protein delivery into neurons using polymeric nanoparticles, J. Biol. Chem. 284 (2009) 6972–6981. https://doi.org/10.1074/jbc.M805956200.

[28] P. Moradas-Ferreira, V. Costa, P. Piper, W. Marger, The molecular defences against reactive oxygen species in yeast, Mol. Microbiol. 19 (1996) 651–658.

[29] C.M. Cremers, U. Jakob, Oxidant sensing by reversible disulfide bond formation, J. Biol. Chem. 288 (2013) 26489–26496. https://doi.org/10.1074/jbc.R113.462929.

[30] T.C. Squier, Oxidative stress and protein aggregation during biological aging, Exp.

Gerontol. 36 (2001) 1539–1550. https://doi.org/10.1016/S0531-5565(01)00139-5.

[31] R. Kiffin, C. Christian, E. Knecht, A.M. Cuervo, Activation of chaperone-mediated autophagy during oxidative stress, Mol. Biol. Cell. 15 (2004) 4829–4840. https://doi.org/10.1091/mbc.E04-06-0477.

[32] L.R.C.Vasconcellos, F.F. Dutra, M.S. Siqueira, H.A. Paula-Neto, J. Dahan, E. Kiarely, L.A.M. Carneiro, M.T. Bozza, L.H. Travassos, Protein aggregation as a cellular response to oxidative stress induced by heme and iron, Proc. Natl. Acad. Sci. U. S. A. 113 (2016) E7474–E7482. https://doi.org/10.1073/pnas.1608928113.

[33] D. Bruce, J. Biggins, S. Charbonneau, M. Thewalt, Excitation Energy Transfer in *Cryptomonas Ovata*. Preillumination Dependent Changees in 77K Picosecond Time Resolved Fluorescence Emission Spectra, in: Biggins J. (Ed.), Prog. Photosynth. Res., Springer, Dordrecht, 1987.

[34] B.S. Tiwari, B. Belenghi, A. Levine, Oxidative stress increased respiration and generation of reactive oxygen species, resulting in ATP depletion, opening of mitochondrial permeability transition, and programmed cell death, Plant Physiol. 128 (2002) 1271–1281. https://doi.org/10.1104/pp.010999.

[35] K. Das, A. Roychoudhury, Reactive oxygen species (ROS) and response of antioxidants as ROS-scavengers during environmental stress in plants, Front. Environ. Sci. 2 (2014). https://doi.org/10.3389/fenvs.2014.00053.

[36] E.K. Sohn, Y.S. Chung, S.A. Johari, T.G. Kim, J.K. Kim, J.H. Lee, Y.H. Lee, S. W. Kang, I.J. Yu, Acute toxicity comparison of single-walled carbon nanotubes in various freshwater organisms, Biomed Res. Int. 2015 (2015). https://doi.org/10.1155/2015/323090.

[37] K. Miazek, W. Iwanek, C. Remacle, A. Richel, D. Goffin, Effect of metals, metalloids and metallic nanoparticles on microalgae growth and industrial product biosynthesis: A review, Int. J. Mol. Sci. 16 (2015) 23929–23969. https://doi.org/10.3390/ijms161023929.

[38] G. Libralato, E. Galdiero, A. Falanga, R. Carotenuto, E. De Alteriis, M. Guida, Toxicity effects of functionalized quantum dots, gold and polystyrene nanoparticles on target aquatic biological models: a review., Molecules. 22 (2017) 1439–1446.

[39] N.M. Franklin, N.J. Rogers, S.C. Apte, G.E. Batley, G.E. Gadd, P.S. Casey, Comparative toxicity of nanoparticulate ZnO, bulk ZnO, and ZnCl2 to a freshwater microalga (Pseudokirchneriella subcapitata): The importance of particle solubility, Environ. Sci. Technol. 41 (2007) 8484–8490. https://doi.org/10.1021/es071445r.

[40] V. Aruoja, H.C. Dubourguier, K. Kasemets, A. Kahru, Toxicity of nanoparticles of CuO, ZnO and TiO2 to microalgae Pseudokirchneriella subcapitata, Sci. Total Environ. 407 (2009) 1461–1468. https://doi.org/10.1016/j.scitotenv.2008.10.053.

[41] P. Chen, B.A. Powell, M. Mortimer, P.C. Ke, Adaptive interactions between zinc oxide nanoparticles and Chlorella sp., Environ. Sci. Technol. 46 (2012) 12178–1285.

[42] M. Thakkar, S. Mitra, L. Wei, Effect on growth, photosynthesis, and oxidative stress of single walled carbon nanotubes exposure to marine alga Dunaliella tertiolecta, J. Nanomater. 2016 (2016).

[43] P. Bhattacharya, S. Lin, J.P. Turner, P.C. Ke, Physical adsorption of charged plastic nanoparticles affects algal photosynthesis, J. Phys. Chem. C. 114 (2010) 16556–16561. https://doi.org/10.1021/jp1054759.

[44] X. Li, Interaction of silver and polystyrene nanoparticles with algae, École polytechnique fédérale de Lausanne, Lausanne, Switzerland, 2015. https://doi.org/10.5075/epfl-thesis-

6818

[45] T.M. Nolte, N.B. Hartmann, J.M. Kleijn, J. Garnæs, D. van de Meent, A. Jan Hendriks, A. Baun, The toxicity of plastic nanoparticles to green algae as influenced by surface modification, medium hardness and cellular adsorption, Aquat. Toxicol. 183 (2017) 11–20. https://doi.org/10.1016/j.aquatox.2016.12.005.

[46] A. Gessner, A. Lieske, B.R. Paulke, R.H. Müller, Functional groups on polystyrene model nanoparticles: influence on protein adsorption, J. Biomed. Mater. Res.A. 65 (2003) 319–326.

[47] M. Lundqvist, J. Stigler, G. Elia, I. Lynch, T. Cedervall, K.A. Dawson, Nanoparticle size and surface properties determine the protein corona with possible implications for biological impacts, Proc. Natl. Acad. Sci. USA. 105 (2008) 14265–14270.

[48] S.R. Saptarshi, A. Duschl, A.L. Lopata, Interaction of nanoparticles with proteins: relation to bio-reactivity of the nanoparticle, J. Nanobiotechnology. 11 (2013) 26.

[49] X. Sun, Z. Feng, L. Zhang, T. Hou, Y. Li, The selective interaction between silica nanoparticles and enzymes from molecular dynamics simulations, PLoS One. 9 (2014) e107696.

CHAPTER THREE: CHRONOLOGICAL TRANSCRIPTOME CHANGES INDUCED BY EXPOSURE TO CYANOACRYLATE RESIN NANOPARTICLES IN *CHLAMYDOMONAS REINHARDTII*

3.1. Introduction

There is a growing interest for engineered resin nanoparticles [e.g. poly(alkyl-cyanoacrylate) nanoparticles and polystyrene nanoparticles] as well as metal oxide nanoparticles worldwide [1,2]. Physical and chemical properties of nanoparticles render them suitable for use in both industry and medicine, such as production of cosmetics, pigmented inks, and crack-resistant paints as well as drug delivery carriers. However, there is a serious concern that wasted resin nanoparticles that are inappropriately discarded in water can be harmful to aquatic living organisms [3–6]. Microalgae are organisms that play a vital role in aquatic ecosystems as a basic producer. Therefore, it is important to analyze the molecular mechanism underlying the effect of nanoparticles on algae.

Resin nanoparticles composed of cyanoacrylate polymers with no prominent inflammatory effects and biodegradability in animals have been investigated as potential carrier materials for drug delivery [7,8]. Unexpectedly, it was found that isobutyl cyanoacrylate nanoparticles (iBCA-NPs) induce acute cell death of gram-positive bacteria [9], green microalgae belonging to the class Chlorophyceae [10], and various non-green algal species belonging to the SAR supergroup and the cryptomonads–haptophytes assemblage [11]. The molecular mechanism underlying cell death induced by iBCA-NPs in such a wide range of microorganisms remains to be elucidated.

We reported earlier that coincubation of iBCA-NPs with microalgae did not allow inducing their mutual agglomerates or stable binding of nanoparticles to the cell surface [10,11]. In contrast, metal oxide nanoparticles were found to inhibit algal cell growth by the generation of heteroaggregates composed of both cells and nanoparticles [12,13]. Either shading or hampering the exchange of smooth materials provided from outside (e.g. oxygen, carbon dioxide, and nutrients) can be the primary reason for such a growth inhibition [14–17]. We also reported that exposure to iBCA-NPs potently induce both protoplast-like cells and ROS burst in *Chlamydomonas reinhardtii* [10]. These findings suggest that there is a principal difference between metal oxides and resin nanoparticles with respect to their working mechanisms to affect the exposed cells.

In this study, we investigated the chronological transcriptome changes induced by the exposure of *C. reinhardtii* to iBCA-NPs, where cell mortality was *a priori* found between ~3% and ~30%.

3.2. Materials and Methods

3.2.1. Strains and culture conditions

All *C. reinhardtii* strains used in this study were purchased from *Chlamydomonas* center (University of Minnesota, USA): a wild type strain CC-124, a mutant strain without cell walls CC-400, mapped tag-insertion mutants (LMJ.RY0402.158615 and LMJ.RY0402.051804) of matrix metalloproteinase (MMP) genes, and their parental strain CC-5325. All these strains were cultured in TAP medium under constant fluorescent light (84 µmol photons m^{-2} s^{-1}) at 25°C with gentle shaking. Cells at the mid-log growth phase (OD_{750} of approximately 0.8) were used for the experiments, unless mentioned otherwise.

3.2.2. Preparation of resin nanoparticles

Two different sizes of iBCA-NPs, ca. 30 and 180 nm in mean diameters, were synthesized. Both of them were composed of poly(isobutylcyanoacrylate) polymers and were synthesized as per previous reports [18,19] with some modifications. In brief, the 30-nm iBCA-NPs were synthesized by dropwise addition of the monomer (Aronalpha 501, Toagosei Co. Ltd., Tokyo, Japan) to acidic water with stirring at 600 rpm (pH adjusted to 2.0–2.3 by HCl), which contained 0.16% (w/v) anionic surfactant NEOPELEX G-15 (sodium dodecyl benzene sulfonate, Kao Corporation, Tokyo, Japan) and 1.25% (v/v) non-ionic surfactant Tween 20 (Kao Corporation, Tokyo, Japan) as dispersants. The 180-nm iBCA-NPs were synthesized in water (pH adjusted to 2.0–2.3 by HCl) containing 1.0% (w/v) dextran 60,000 (041-30525; Wako Pure Chemical, Osaka, Japan) while stirring at 600 rpm. The monomer was added until the weight reached 1% (w/v), after which the solution was subjected to stirring for another 2 h. Subsequently, the solution was neutralized by the addition of 0.5 M NaOH. The prepared solutions containing nanoparticles were stored at 4°C until use.

3.2.3. Preparation of 30-nm poly(isobutylcyanoacrylate) resin nanoparticles suspended in reduced concentrations of detergents

The 30-nm iBCA-NPs were suspended in water containing the two detergents used for their synthesis. Reduction of free detergents (i.e., non-adsorbed detergents on the surface) was achieved by sedimentation of nanoparticles followed by their resuspension in the original volume of distilled water. Cycles of ultracentrifugation were conducted as shown below.

Aliquots of 52 mL of the 30-nm iBCA-NPs suspension were added to two polycarbonate tubes, which were subsequently centrifuged (303,000×g for 2 h, Himac CP90α ultracentrifuge, Hitachi, Japan) using P50AT2 angle rotor. After the centrifugation, supernatants were discarded, and pellets were resuspended in the original volume of distilled water. The suspensions were

subjected to shaking overnight to disperse the pellets and subsequently sonicated (Sonics Vibra-Cell VC130 Ultrasonic Processor, Sonics & Materials Inc., USA) at 130 Watts for 2 min to completely disperse the nanoparticles. Next, the solution was centrifuged again at 303,000×*g* for 2 h. The resultant second pellets were suspended in 52 mL distilled water, dispersed again, and a portion of the suspension was used for cell exposure and the remaining volume was again centrifuged at 303,000×*g* for 2 h.

The supernatant prepared after the third centrifugation cycle was used to measure the concentration of NEOPELEX G-15 using the Nanogram SDS Assay Kit (ProFoldin, USA) following the manufacturer's instructions.

3.2.4. Zeta potential measurement and nanoparticle size distribution

Size distribution of nanoparticles was measured based on dynamic light scattering method, whereas zeta potentials were measured using electrophoresis method on an ELSZ-2000ZS device (Otsuka Electronics, Japan) following the user's manual.

3.2.5. Cell exposure to poly(isobutylcyanoacrylate) resin nanoparticles

C. reinhardtii wild type cells (CC-124) were cultured at 24°C under constant fluorescent light exposure (84 μmol photons m^{-2} s^{-1}) with gentle shaking (120 rpm) until reaching the mid-log phase (a density of 2×10^6–4×10^6 cells mL^{-1}). Thereafter, cells were exposed to the detergent-reduced 30-nm iBCA-NPs at a concentration of 300 mg L^{-1} or to the 180-nm iBCA-NPs at a concentration of 100 mg L^{-1} without dextran reduction, which was used as a dispersant.

Control cells for the 30-nm iBCA-NP treatment were cultured in TAP medium containing 0.003% NEOPELEX G-15 and 0.023% Tween 20. The detergents' concentrations matched those of the twice centrifuged 30-nm iBCA-NP solution at a concentration of 300 mg

L^{-1} (see above), while for the control treatment of 100 mg L^{-1} 180-nm iBCA-NP solution, 100 mg L^{-1} dextran 60,000 was used.

For the nanoparticle treatment, cells were incubated with gentle shaking (10 rpm) under dim light (~20 μmol photons m^{-2} s^{-1}) until the cell mortality reached specific ratios: ~3% (Stage-1), ~15% (Stage-2), and ~30% (Stage-3). The cells were harvested for gene expression analyses by exhaustive RNA-sequencing or quantitative reverse transcription PCR (RT-qPCR). Additionally, we obtained the transcriptome data of mere TAP-cultured cells in the mid-log phase (a density of ~3×10^6 cells mL^{-1}).

3.2.6. Cell mortality measurement and detection of reactive oxygen species accumulation

To distinguish between dead and viable cells, we used trypan blue (TB) staining method [20]. This assay is based on the principle that living cells possess intact cell membranes bearing potency to exclude the dye. The TB solution (0.4% w/v, Wako Chem., Japan) was directly added to the cell suspension at a final concentration of 0.2% (w/v). After 5 min, we observed the cells by bright-field microscopy using Olympus BX63 (Olympus, Japan) without employing the washing step. Dark- or light blue-stained cells were considered perished. The cell death ratio was calculated by counting the total number of stained cells out of 100 cells.

To detect the accumulated reactive oxygen species (ROS) in cells, a cell-permeable probe, non-fluorescent compound 2′,7′-dichlorodihydrofluorescein diacetate (H2DCFDA) (D668, Sigma) was used. The H2DCFDA solution was added to the cell culture (10 μM at the final concentration), incubated for 15 min, and then washed thrice with fresh culture medium to reduce the background probe. The fluorescence of 2′,7′-dichlorofluorescein (DCF), which is produced from H2DCFDA by ROS, was detected using a fluorescence microscope coupled with an Olympus U-FBWA filter unit (Olympus, Tokyo, Japan).

3.2.7. Total RNA isolation

For total RNA isolation, the harvested cell samples reaching the specific cell mortality ratios (Stage-1 through Stage-3) were centrifuged (2,000×*g*, 5 min) and then resuspended in 1 mL ice-cold TAP medium. The suspended cell pellets were centrifuged once again (9,500×*g*, 2 min). After complete supernatant removal, total RNA was extracted using TRI-reagent (Molecular Research Center, Inc., USA) following the manufacturer's instructions (TRI-reagent - Manufacturer's protocol, 1995). Thereafter, the extracted total RNA was purified using the RNeasy plant mini kit (Qiagen, Manchester, England). Both RNA quantity and quality were checked by measuring the absorbance at 280 nm and 260 nm using Nanodrop ND-1000 (Thermo Fisher Scientific Inc., MA, USA).

3.2.8. Construction and sequencing of complementary DNA libraries

Complementary DNA (cDNA) libraries were prepared using the KAPA Stranded mRNA-Seq Kit (Kapa biosystems, MA, USA). A total of 750 ng RNA per sample was used for 12 cycles of PCR amplification. The concentration of the generated cDNA libraries was measured on Qubit using the dsDNA HS Assay Kit (Thermo Fisher Scientific Inc., MA, USA), whereas the quality of cDNA libraries was confirmed on Fragment Analyzer using the dsDNA 915 Reagent Kit (Advanced Analytical Technologies Inc., IA, USA). The generated cDNA libraries were sequenced using Illumina NextSeq 500 (San Diego, CA, USA) under the 2 × 76 bp run. The obtained reads were filtered using Sickle software (ver.1.33), which removed the bases having quality values of <20 and discarded the sequences with fragment lengths of 30 bases or less along with their paired sequences. The filtered reads were then mapped using the Hisat22 aligner to the reference *C. reinhardtii* genome v. 5.5 (strain CC-503 cw92 mt^{+}) that

contains 14,415 genes [21]. Three independent 30-nm iBCA-NP-treated samples for each stage (Stage-1 through Stage-3) were analyzed. Analyses were also performed for the control samples.

3.2.9. Analysis of differentially expressed transcripts

After alignment of the obtained cDNA libraries, differentially expressed genes were predicted using "edgeR" package (ver. 3.10), which uses quantile-adjusted conditional maximum likelihood (qCML) to retrieve differentially expressed genes in an experiment using one-factor comparison (i.e., control *vs*. treatment). Log_2 fold-change (Log_2-FC) and false discovery rate (FDR) were calculated [22]. Differentially expressed transcripts were defined with FDR of <0.05 and Log_2-FC of ≥1 or ≤−1, unless otherwise noted. Gene annotation was retrieved from *Phytozome* v. 12.1/ *Chlamydomonas reinhardtii* v. 5.5.

3.2.10. Principal component analysis (PCA)

To provide a systematic view of RNA-seq data among untreated and treated cells, PCA was performed for the 17,741 genes expressed in at least one sample by using the prcomp function in the R environment (v. 3.6.2; R Core Team, Vienna, Austria).

3.2.11. Gene expression analysis of the 180-nm poly(isobutylcyanoacrylate) resin nanoparticle-exposed cells by quantitative reverse transcription PCR (RT-qPCR)

Considering the observed drastic changes in gene expression after application of the 30-nm iBCA-NPs, seven genes were selected to further assess their expression changes during exposure to a concentration of 100 mg L^{-1}. PCR primers for the candidate genes were designed using Primer-Blast (https://www.ncbi.nlm.nih.gov/tools/primer-blast/) and their sequences are

listed in Table 1 of Appendix B.

cDNA was generated using the qPCR RT Kit (ReverTra Ace, TOYOBO, Osaka, Japan) following the manufacturer's protocol. Thereafter, qPCR was conducted using the KOD SYBR qPCR Mix (TOYOBO, Osaka, Japan) according to the manufacturer's instructions with the designed primers. cDNA level of the *C. reinhardtii* eukaryotic initiation factor (EIF1A) gene was used for the normalization. cDNA amplifications were performed in the StepOne Real Time PCR System (ABI, USA). The obtained data were analyzed using the Pfaffl method [23].

3.2.12. Analysis of stress-inducible expression of Cre13.g605200 gene by quantitative reverse transcription PCR (RT-qPCR)

To investigate the conditions that can induce the overexpression of the Cre13.g605200 gene, wild type *C. reinhardtii* cells in the mid-log phase (a density of $2 \times 10^6 - 4 \times 10^6$ cells mL^{-1}) were incubated in TAP medium containing either 2.5 mM H_2O_2 or 200 mM NaCl. Total RNA was isolated when the cell mortality reached approximately 30% to be used for analyzing the gene expression change of Cre13.g605200 by RT-qPCR.

3.2.13. Profiling DNA degradation after exposure to either 180-nm poly(isobutylcyanoacrylate) resin nanoparticles or H_2O_2

To characterize the effect of 180-nm iBCA-NPs on DNA degradation, cell wall-deficient *C. reinhardtii* cells (CC-400) were exposed to 100 mg L^{-1} 180-nm iBCA-NPs. In addition, algae of the same cell type were exposed to 50 mM H_2O_2 to investigate the effect of the oxidative stress. After exposure, total DNA was isolated according to Pollock et al. [24] with several modifications.

Briefly, the cells collected after centrifugation at 1,000×*g* for 5 min were resuspended in SDS-EDTA-Proteinase K solution [2% (w/v) SDS, 200 mM NaCl, 40 mM EDTA (pH 8.0), 100 mM Tris-Cl (pH 8.0), 0.2% (v/v) *β*-mercaptoethanol, and 20 mg mL^{-1} Proteinase K (25530015, ThermoFisher Scientific, MA, USA)]. After incubation at 65℃ for 1 h, DNA was extracted with phenol–chloroform–isoamyl alcohol (25:24:1, v/v) mixture and centrifuged at 2,500×*g* for 5 min at room temperature. The upper aqueous phase was mixed with chloroform-isoamyl alcohol (24:1, v/v) mixture and centrifuged at 2,500×*g* for 3 min at room temperature. Nucleic acids contained in the aqueous phase were then precipitated with 2 volumes of absolute ethanol and rinsed with 70% ethanol. The pellets were resuspended in TE buffer [10 mM Tris-HCl (pH 7.4), 1 mM EDTA] containing 0.5 mg mL^{-1} heat-treated RNase A and incubated at 40°C for 30 min. The isolated DNA samples were resolved by 0.8% (w/v) agarose gel electrophoresis, followed by staining with SYBR Green I (5760A, Takara Bio Inc., Japan). A 470 nm LED transilluminator (LTi-ExLB, Biotools Inc., Japan) was used to visualize DNA.

3.2.14. Molecular phylogenetic tree construction

Amino acid sequences of 31 genes, annotated to code for cell wall lytic enzymes, were retrieved from *Phytozome* v. 12.1/ *Chlamydomonas reinhardtii* v. 5.5 using the key terms: “matrix metalloproteinase” and “cell wall lytic enzyme.” Multiple alignment of the amino acid sequences coded by these 31 genes was performed using ClustalW (ver. 2.1) [25]. Based on the aligned sequences, a maximum likelihood tree was generated using the MEGAX software (ver. 10.1.8) [26] with 100 bootstrap iterations.

3.2.15. Partially purification of Cre13.g605200 enzyme

The crude enzyme was prepared from cell free supernatant of the treated CC-124 cells with 300 mg L^{-1} 30-nm iBCA-NPs. Briefly, cell free supernatant was obtained by centrifugation at 5,200 × *g* for 5 min. Thereafter, crude enzyme was precipitated at 4°C by the addition of ammonium sulfate slowly to reach 60% saturation, and kept on stirring for 30 min. The precipitated proteins were collected by centrifugation at 13,500 ×*g* for 20 min at 4°C, the pellets were then suspended with protein buffer solution [10 mM Tris-acetate (pH 7.5), 200 mM NaCl, 0.05% (v/v) β-mercaptoethanol], and transferred to dialysis membrane with MW cutoff 1 kDa (Repligen, USA) to remove ammonium sulfate. Dialysis was performed against protein buffer solution at 4°C overnight with three changes of the buffer solution. Afterwards, samples were analyzed by sodium dodecyl sulfate polyacrylamide gel electrophoresis (SDS-PAGE). Samples were mixed with SDS-PAGE sample buffer [125 mM Tris-HCl (pH 6.8), 20% (v/v) glycerol, 4% (w/v) SDS, 10% (v/v) β-mercaptoethanol, 0.05% (w/v) bromophenol blue] in a ratio of 1:1, and heated in a boiling water bath for 5 min, then they were resolved by polyacrylamide gel for ~15 min at constant voltage (100 V) until the loading dye reach the resolving gel, followed by running them at 200 V for ~45 min. After gel electrophoresis, the partial purified enzymes were stained with PageBlue™ Protein Staining solution (Thermo Fisher Scientific, MA, USA) for 30 min with gentle shaking.

The gel band corresponding to the candidate enzyme was excised and analyzed by liquid chromatography- tandem mass spectrometry (LC-MS/MS) (Antegral Co., Japan).

3.2.16. Experimental design

All the abovementioned experiments to investigate gene expression changes were performed thrice using independently prepared cell samples to obtain statistically robust data (3 biological replicates).

3.3. Results

3.3.1. Characteristics of the 30-nm poly(isobutylcyanoacrylate) resin nanoparticles suspended in a reduced concentration of detergents

We prepared 30-nm iBCA-NPs suspended in a reduced concentration of detergents used for nanoparticle synthesis to reduce their effect in further experiments. The removal of detergents not adsorbed on the nanoparticle surface was performed by sedimentation and resuspension of the pellet. The concentration of NEOPELEX G-15 present in the supernatant after 3rd centrifugation cycle was reduced to approximately 1/18th of the initial concentration. Assuming that the dilution factor would be the same as for Tween 20, TAP medium containing 0.003% (w/v) of NEOPELEX G-15 and 0.023% (w/v) of Tween 20 was used for the control treatment of detergent-reduced 30-nm iBCA-NP exposure at 300 mg L^{-1}.

Zeta potential of the twice centrifuged 30-nm iBCA-NP [1% (w /v)] was changed from −16.43 ± 0.32 mV before centrifugation to −21.85 ± 0.58 mV afterward. Moreover, through two cycles of precipitation, the mean diameter of the 30-nm iBCA-NPs increased from the original 30.15 ± 0.08 nm to 94.40 ± 4.06 nm (Appendix B, Fig. 1).

Conversely, zeta potential of the 180-nm iBCA-NP [1% (w /v)] suspended in original 1.0% (w/v) dextran 60,000 was −7.50 ± 0.17 mV and the mean diameter was 180.96 ± 7.83 nm.

3.3.2. Time-course change of cell mortality after exposure to 30-nm poly(isobutylcyanoacrylate) resin nanoparticles

We exposed *C. reinhardtii* wild type, mid-log phase cells to detergent-reduced 30-nm iBCA-NPs at a concentration of 300 mg L^{-1}. TB-positive cell ratio increased during the exposure (Fig. 3.1A), which was accompanied by the generation of swollen and spherical

protoplast-like cells, as previously reported by us [10,11]. The number of DCF-positive cells, which indicated the accumulation of ROS, also increased (Fig. 3.1B). Observed morphological and biochemical changes at stipulated time-points were summarized as shown below.

Stage-1 containing ~3% of TB-stained cells: After 2–3 min of the addition of iBCA-NPs, swimming pattern of the cells' behavior changed to swirling (Appendix B, Video 1), and after 10 min, all cells stopped swimming. At this stage, the TB-stained cell ratio was ~3% (Appendix B, Table 2) and spherical protoplast-like cells reached ~30%, while the ROS fluorescent positive cell ratio was ~1% (Appendix B, Table 3). This stage was termed as Stage-1.

Stage-2 containing ~15% of TB-stained cells: After exposure for 60 min, the TB-positive cell ratio reached ~15% (Appendix B, Table 2) and the ROS fluorescent positive cell ratio was ~10% (Appendix B, Table 3). Many cells (~35%) contained prominently enlarged vacuoles, and we could detect nanoparticles trapped inside (Appendix B, Video 2) for some cells. This stage was termed as Stage-2.

Stage-3 containing ~30% of TB-stained cells: After exposure for 120 min, the TB-positive cell ratio reached ~30% (Appendix B, Table 2) and the ROS fluorescent positive cell ratio was ~24% (Appendix B, Table 3). This stage was termed as Stage-3.

The increase of both protoplast-like and TB-positive cells was twice lower after exposure to centrifuged 30-nm iBCA-NPs than that after exposure to non-centrifuged ones. However, the visible cell abnormalities (swirling swimming pattern, protoplast-like spherical cell shape, ROS accumulation, and TB-staining ability) and their chronological appearance were exactly the same as for non-centrifuged 30-nm iBCA-NPs (Fig. 3.1) [10].

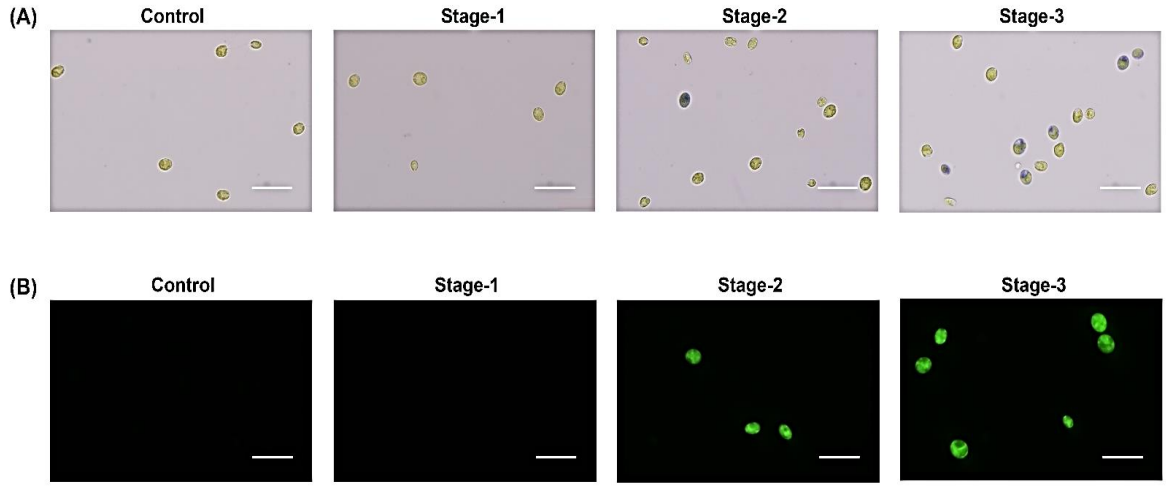

Figure 3.1. Chronological microscopic cell observation to show induced cell death and reactive oxygen species (ROS) by exposure to detergent-reduced poly(isobutylcyanoacrylate) resin nanoparticles (iBCA-NPs) at 300 mg L^{-1}. (A) Bright-field microscopic observation of cells stained by trypan blue (TB). (B) Microscopic observation of 2',7'- dichlorofluorescein (DCF) fluorescence. Bar, 20 µm.

Moreover, the exposure of cells to the 180-nm iBCA-NPs at a concentration of 100 mg L^{-1}, which were synthesized using dextran, induced the same abnormal features in exactly the same order as that induced by the 30-nm iBCA-NPs. However, the increase in the TB-positive ratio of these cells was approximately half of the double-centrifuged 30-nm iBCA-NPs at a concentration of 300 mg L^{-1} (Appendix B, Table 4).

3.3.3. Characteristics of transcriptome changes

To detect the metabolic pathways that were significantly affected by exposure to the resin nanoparticles, we performed three independent transcriptome analyses for cells (3 biological replicates) at each stage as well as for control samples. We obtained approximately 1.24×10^7 reads for each cell stage and approximately 1.57×10^7 and 1.59×10^7 reads for the

two types of control samples, i.e., cells cultured in the TAP medium which contained detergents and those cultured in the detergent-free TAP medium, respectively (Table 3.1).

Table 3.1. Summary of RNA-seq mapping results for two types of controls and 30-nm poly(isobutylcyanoacrylate) resin nanoparticles (iBCA-NPs) treated cells.

Treatment	Total number of reads	Total number of mapped reads	Ratio of mapped reads	Transcript abundance	
				Up-regulated[a]	Down-regulated[b]
Stage-1	13,349,033	10,705,130	80.19%	3763 (26%)	4462 (31%)
Stage-2	12,779,381	10,089,158	78.89%	4129 (29%)	5619 (39%)
Stage-3	10,932,449	8,952,130	81.82%	4162 (29%)	6049 (42%)
Detergents containing TAP culture-control	15,716,726	9,720,031	61.84%		
TAP culture control	15,972,714	14,241,268	89.16%		

[a]Number of significantly upregulated genes was based on the criteria that Log_2-FC ≥ 1, Log_2-FC ≤ -1 and FDR < 0.05. Percentages are shown in parenthesis.

[b]Number of significantly downregulated genes was based on the criteria that Log_2-FC ≥ 1, Log_2-FC ≤ -1 and FDR < 0.05. Percentage are shown in parenthesis.

Then, we conducted PCA for the harvested cell samples reaching specific cell mortality ratios (Stage-1, -2, and -3) and also cultured in only surfactants containing TAP medium (Surf6) using gene expression profiles obtained by RNA-seq analysis. In the PCA plot, the first and second principal components (PC1 and PC2) accounted for 80.54% and 5.44% variability in the RNA-seq dataset, respectively (Fig. 3.2). Clear segregations of iBCA-NPs-treated samples from the control samples were observed along with the first principal component, reflecting the nanoparticles-induced transcriptional alteration in *C. reinhardtii*. Of note, although the variance was slight, iBCA-NP treated samples were also separated by treatment duration along with the PC2 axis.

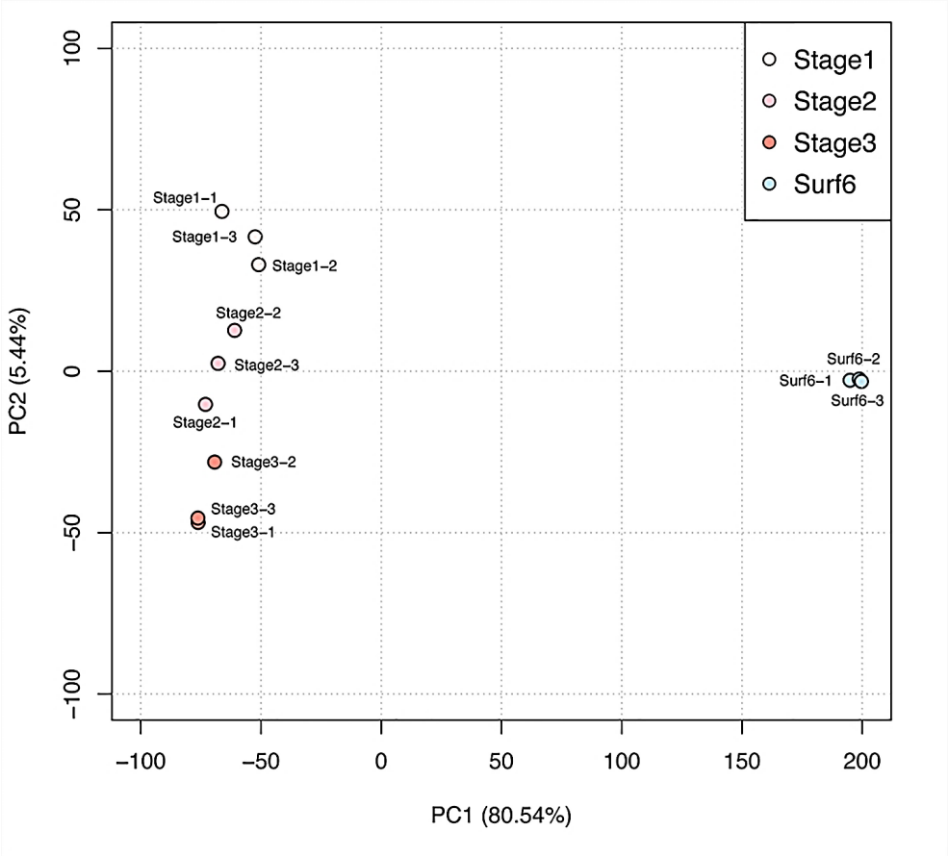

Figure 3.2. Principal component analysis (PCA) of RNA-seq data of *Chlamydomonas reinhardtii* obtained by exposure to 30-nm poly(isobutylcyanoacrylate) resin nanoparticles (iBCA-NPs) at three exposure periods: Stage-1, Stage-2, and Stage-3. Surf6-1,-2, -3: Cells cultured in TAP containing 0.003% NEOPELEX G-15 and 0.023% Tween 20 for 2 h. Three independent experiments were carried out.

Approximately 78% of reads were uniquely mapped to the *C. reinhardtii* reference genome, among which 17,741 loci have been found to contain protein-coding transcripts. Therefore, the coverage ratio of our RNA-sequence data was approximately 500 per locus for cells treated by nanoparticles and ~700 for both controls (Table 3.1).

The Stage-1transcriptome contained approximately 26% of upregulated genes, whereas 31% of genes were downregulated based on the following criteria: Log_2-FC of ≥1, Log_2-FC value of ≤ −1 and FDR of <0.05. These ratios did not significantly change even at Stage-2 and Stage-3 (Table 3.1).

3.3.4. Overexpression of the oxidative stress-responsive genes

We observed that the increase of ROS accumulation in DCF-positive cells was followed by increased number of TB-positive cells. Therefore, we focused on the change in the expression of the genes coding for enzymes involved in ROS detoxification.

Expression of the genes coding for glutathione S-transferase (GSTS1, coded by Cre16.g688550), glutathione peroxidase 5 (GPX5, Cre10.g458450), and Fe-superoxide dismutase (Fe-SOD, Cre10.g436050) was very prominently increased: the log_2-FC for the gene coding for GSTS1 at Stage-1 was 10.29, whereas that for GPX5 and Fe-SOD genes were 6.95 and 4.75, respectively, compared with the control cells cultured in the detergent-containing TAP medium with reliable significance (p-value < 0.05). Moreover, their log_2-FCs maintained high levels at Stage-1 through Stage-3 (Table 3.2).

Table 3.2. List of log_2-FC levels for heat shock protein and redox enzyme coding genes after exposure to 30-nm poly(isobutylcyanoacrylate) resin nanoparticles (iBCA-NPs) against TAP cultured control cells containing detergents.

Gene ID	Annotated gene function	Stage-1	Stage-2	Stage-3
Cre16.g688550	Glutathione S-transferase (GSTS1)	10.29	10.26	10.18
Cre10.g436050	Fe superoxide dismutase (Fe-SOD)	4.75	4.82	4.76
Cre10.g458450	Glutathione peroxidase (GPX5)	6.95	6.96	7.24
Cre07.g318800	Heat shock protein 22A (HSP22A)	14.22	15.57	16.18
Cre07.g318850	Heat shock protein 22B (HSP22B)	14.40	15.37	16.01
Cre03.g145787	Heat shock protein 22C (HSP22C)	13.04	13.84	14.21
Cre01.g020575	Heat shock protein 22D (HSP22D)	12.04	12.99	13.04
Cre14.g617450	Heat shock protein 22E (HSP22E)	11.92	12.93	13.41
Cre14.g617400	Heat shock protein 22F (HSP22F)	11.77	12.70	13.25
Cre07.g318600	Heat shock protein 22H (HSP22H)	3.82	4.30	5.72
Cre08.g372100	Heat shock protein 70A (HSP70A)	4.68	5.13	5.18
Cre06.g250100	Heat shock protein 70B (HSP70B)	4.03	4.22	4.07
Cre09.g393200	Heat shock protein 70C (HSP70C)	3.82	3.99	3.88
Cre16.g677000	Heat shock protein 70E (HSP70E)	4.67	4.91	4.77
Cre09.g386750	Heat shock protein 90A (HSP90A)	4.91	5.03	5.23

Reads per kb of transcript per million mapped reads (RPKM) for GSTS1-, GPX5-, and Fe-SOD-coding genes were 2710 ± 313.29, 4858 ± 383.87, and 1883 ± 222.20, respectively, and these RPKM qualified as 115th, 99th, and 138th among 16,711 transcript detected genes at Stage-1, respectively. Such an enhanced expression of the genes coding for antioxidant enzymes seemed reasonable to restore the redox balance disrupted by ROS accumulation.

3.3.5. Overexpression of heat shock protein (HSP) genes

Twenty HSP genes (8 of them belonging to the HSP22, 9 to the HSP70, and 3 to the HSP90 family) were coded in the *C. reinhardtii* genome. Ten genes out of these (6 from the HSP22 family, three from the HSP70 family, and one from the HSP90 family) were largely overexpressed (log_2-FC > 4.0) when the cells were exposed to the 30-nm iBCA-NPs.

At Stage-1, six HSP22 family genes (HSP22B, HSP22A, HSP22C, HSP22D, HSP22E, and HSP22F) were found to be highly overexpressed, having the following log_2-FC values: 14.40, 14.22, 13.04, 12.04, 11.92, and 11.77, respectively (Table 3.2). Moreover, their transcripts were found to be extremely abundant in the treated cells as shown by their RPKM values at Stage-1: 2093 ± 333, 3335 ± 464, 1143 ± 181, 82 ± 4.93, 3640 ± 666, and 2128 ± 401 for HSP22B, HSP22A, HSP22C, HSP22D, HSP22E, and HSP22F genes, respectively. Their RPKM values ranked 131st, 110th, 168th, 882nd, 108th, and 129th among the detected genes at Stage-1, respectively.

Our transcriptome data also revealed that overexpression of genes coding for the heat shock factors HSF1 (Cre09.g387150) and HSF2 (Cre07.g354500) were also elevated in response to the 30-nm iBCA-NPs exposure: $\log_2$-FCs at Stage-1 were 3.41 and 2.01 for HSF1 and HSF2, respectively. Therefore, the observed overexpression of HSPs-coding genes seemed to be intermediated by the elevated activity of HSFs.

3.3.6. Overexpression of cell wall lytic enzymes-coding genes

Considering that the exposure to the 30-nm iBCA-NPs induced protoplast-like cells, we focused on genes whose function is annotated as "cell wall lytic enzyme," based on the Pfam annotation (https://pfam.xfam.org/). We succeeded in extracting 31 genes coding for cell wall lytic enzymes using *Phytozome* v. 12.1/ *Chlamydomonas reinhardtii* v. 5.5 (Table 3.3). None of the detected transcripts corresponded to Cre17.g715800 at any stage or in the control samples, suggesting that this gene is a pseudogene.

Transcriptomic data of Stage-1 cells showed that expression of 11 out of 31 genes referenced in Table 3.3 were upregulated: six were significantly upregulated having $\log_2$-FC of >3.0, whereas the others were <3.0 with a *p*-value of <0.05. Among these, Cre13.g605200 was the most upregulated gene at all stages: the $\log_2$-FCs were 11.12, 11.54, and 11.73 at Stage-1, -2, and -3, respectively, compared with the control cells cultured in the detergent-containing TAP medium. The $\log_2$-FC value of Cre13.g605200 at Stage-1 was ranked 16th among the detected genes at the same stage, suggesting a large amount of the enzyme. It is noteworthy that $\log_2$-FCs for the remaining five cell wall lytic enzyme genes at Stage-1 were limited to 3.08, 5.30, 3.88, 4.74, and 3.29 for Cre03.g201550, Cre03.g201950, Cre09.g407050, Cre17.g708450, and Cre17.g728750, respectively.

Table 3.3. List of log_2-FC for 31 cell wall lytic enzyme genes after exposure to 30-nm poly(isobutylcyanoacrylate) resin nanoparticles (iBCA-NPs) against TAP cultured cells containing detergents.

Gene ID	Stage-1	Stage-2	Stage-3
Cre02.g078950	-1.67	-1.04	-0.64*
Cre02.g142366	1.66	1.92	2.91
Cre03.g170850	-0.57*	-1.04	-1.72
Cre03.g201550	3.08	2.92	3.11
Cre03.g201950	5.30	4.92	4.49
Cre05.g232600	-0.22*	-0.75	-1.00
Cre06.g278152	-0.83	-0.69	-0.03*
Cre06.g278153	-4.18	-7.41	-1.59*
Cre06.g278161	0.48*	0.28*	1.25
Cre06.g278165	2.49	2.67	2.60
Cre06.g292050	-3.77	-4.21	-7.85
Cre07.g324500	-1.90	-1.87	-4.08
Cre09.g393700	2.60	2.14	1.86
Cre09.g396772	-3.40	-3.56	-2.57
Cre09.g407050	3.88	-2.00*	-1.96*
Cre10.g421350	2.49	1.47	0.84*
Cre11.g467600	-3.63	-6.85	-2.55

Cre11.g467608	-2.98	-7.12	-7.06
Cre11.g467683	-1.76*	-5.90	-5.84
Cre11.g467684	-2.73	-3.05	-4.67
Cre13.g605200	11.12	11.54	11.73
Cre14.g625850	-4.41	-2.40	-0.81*
Cre16.g680902	-2.68	-2.19*	-5.84
Cre17.g708450	4.74	4.61	4.61
Cre17.g718450	-4.01	-7.23	-2.93
Cre17.g718468	-0.37*	-0.98	-0.35*
Cre17.g718500	0.56	0.38*	0.19*
Cre17.g728750	3.29	3.84	3.61

* p-value ≥ 0.05

Interestingly, moderate overexpression of Cre13.g605200 was also detected by exposure to either 2.5 mM H_2O_2 or 200 mM NaCl, where cell mortality reached ~30%: the log_2-FC values were 4.67 for treatment with H_2O_2 and 3.02 for treatment with 200 mM NaCl (Fig. 3.3).

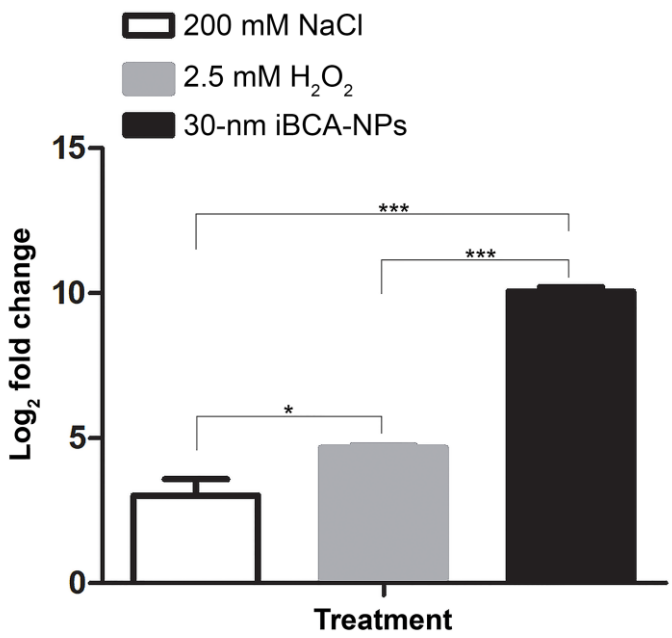

Figure 3.3. Gene expressions change of Cre13.g605200 triggered by three different stresses. *Chlamydomonas reinhardtii* cells were exposed either to 2.5 mM H_2O_2, 200 mM NaCl, or 300 mg L^{-1} 30-nm poly(isobutylcyanoacrylate) resin nanoparticles (iBCA-NPs) until the cell death ratio reached ~30%. Data were normalized using eukaryotic translation initiation factor 1A (EIF1A) whose expression was stable through the stages (RPKMs for EIF1A in Stage-1, -2, and -3 were 881.51 ± 23.52, 888.39 ± 36.96, and 1011.52 ± 72.74, respectively). Results are shown as the mean ratios (± SE) from three independent replicates. * p-value < 0.05, *** p-value < 0.001.

3.3.7. Phylogenetic origin of Cre13.g605200 gene and its overexpression

The coded amino acid sequence of Cre13.g605200 was manually aligned with three well-studied cell wall lytic enzymes: gamete lytic enzyme (GLE), sporangin (SPR), and zygospore germination enzyme (Z-lysin). Expected product of Cre13.g605200 contained a cysteine- switch, a zinc-binding, a Met-turn, and a calcium binding motif (Fig. 3.4), which are shared among GLE, SPR, and Z-lysin [27,28].

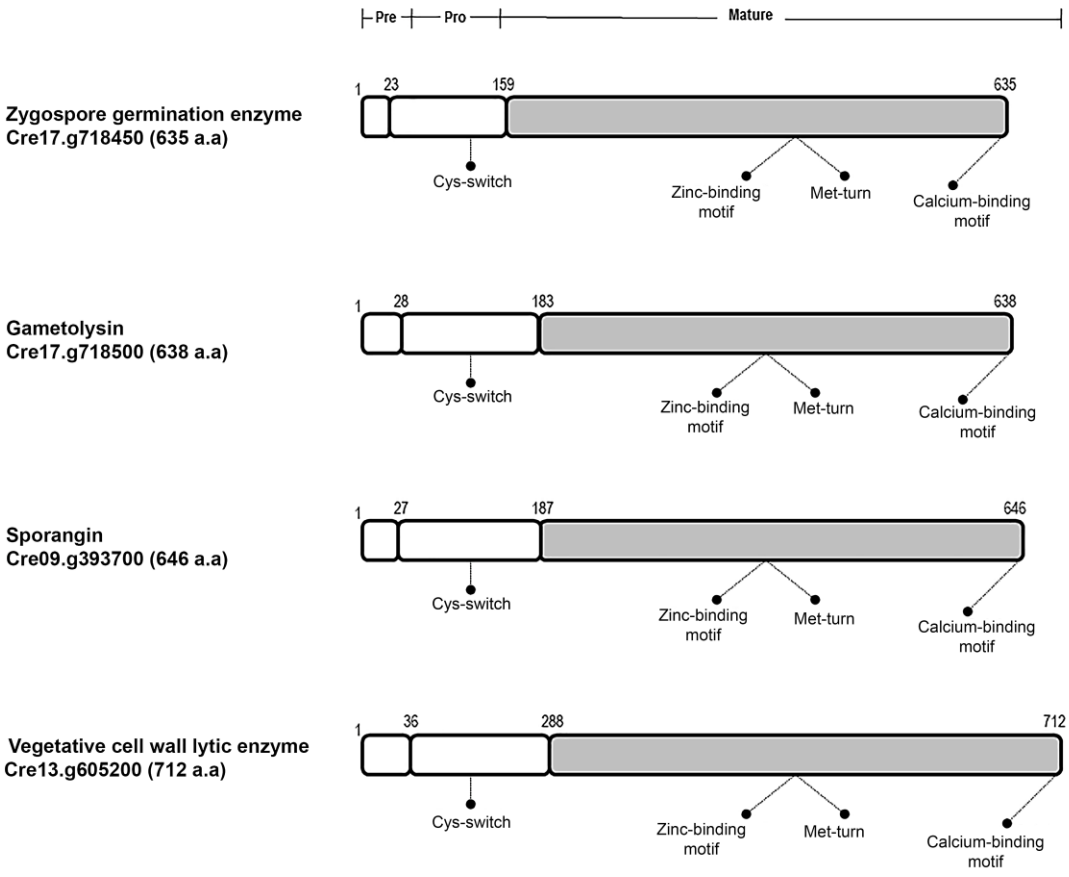

Figure 3.4. Domain architectures for three types of cell wall hydrolytic enzymes and for Cre13.g605200. Cys-switch: Specific region for applicability of the activation mechanism to the members of the matrix metalloproteinase gene family; Met-turn: Conserved methionine site lying within a hydrophobic base for the zinc-binding site. Numbers shown on the top of the domain architectures refer to the amino acid position counted from the N-terminus. The schematic diagrams for zygospore germination enzyme, gametolysin, and sporangin were redrawn from Kubo [27]. a.a: amino acid residue.

In summary, the deduced amino acid sequence of Cre13.g605200 displayed ~42%, ~40%, and ~34% similarity to GLE, SPR, and Z-lysin, respectively, whereas if the pre- and pro-regions were excluded, these similarities were 41%, ~ 40%, and ~ 34%, respectively. Interestingly, besides high similarity in amino acid sequences among these four proteins, length and position of introns in the genes coding for these sequences are extremely diverse (Appendix B, Fig. 2).

To investigate the origin of Cre13.g605200, molecular phylogenetic tree of 31 cell wall lytic enzymes was constructed using whole amino acid sequences by maximum likelihood method [29]. Within the tree, the protein coded by this gene is located in the clade containing GLE coded by Cre17.g718500, SPR coded by Cre09.g393700, and the protein coded by Cre17.g718468 with a robust bootstrap support of 100% (Fig. 3.5).

In this clade, the protein coded by Cre13.g605200 was excluded from the core clade composed of GLE, SPR, and the enzyme coded by Cre17.g718468 with 100% bootstrap support. Unexpectedly, Z-lysin is located out of the Cre13.g605200-containing clade, although it bears all representative motifs found in GLE and SPR.

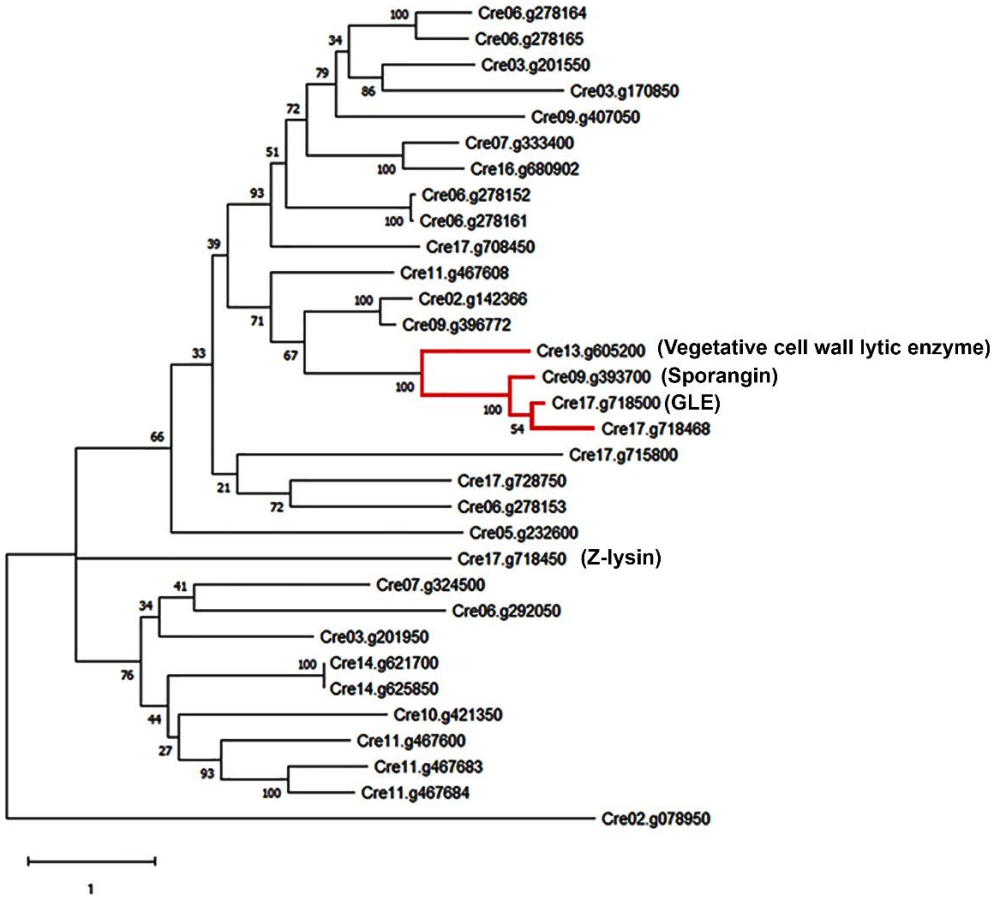

Figure 3.5. Maximum likelihood tree of 31 cell wall hydrolytic enzymes based on amino acid sequences. Multiple sequence alignment was carried out using ClustalW. Bootstrap values are shown as results of 100 bootstrap iterations. Scale bar shows one amino acid substitution per site.

Among GLE, SPR, and Z-lysin, only GLE has cell wall-degrading activity for vegetative growing cells [30,31], whereas the gene coding for this enzyme was found to be slightly downregulated after exposure to 30-nm iBCA-NPs despite the appearance of protoplast-like cells at Stage-1; the $\log_2$-FC value of the GLE-coding gene at this stage was 0.56 and the RPKM was limited to 25.78 ± 2.81. Conversely, RPKM of Cre13.g605200 was as high as 411.10 ± 52.84, 405.80 ± 32.21, and 342.70 ± 37.78 at Stage-1, -2, and -3, respectively. These results suggest that the appearance of protoplast-like cells is mainly attributed to the cell wall hydrolytic activity coded by Cre13.g605200. The same idea was strongly supported by the fact that Cre13.g605200 tag-mutant showed limited appearance of protoplast-like cells as well as strong resistance to nanoparticle exposure (see Section 3.3.8).

The expression of Cre09.g393700, which codes for a sporangial cell wall-specific hydrolytic enzyme (SPR), showed no drastic change. The $\log_2$-FCs at each stage were as follows: Stage-1 = 2.60, Stage-2 = 2.14, and Stage-3 = 1.86. Z-lysin gene (Cre17.g718450), which codes for a zygospore cell wall-specific hydrolytic activity enzyme, clearly decreased as shown by the $\log_2$-FCs: Stage-1 = −4.01, Stage-2 = −7.23, and Stage-3 = −2.93.

3.3.8. Cell mortality in the tag-inserted mutants for Cre13.g605200 gene

We compared the contribution levels of GLE-coding and Cre13.g605200 genes in the cell mortality caused by iBCA-NP exposure, considering our hypothesis that the conversion of vegetative cells to protoplasts is essential for this process [10] and that neither SPR nor Z-lysin has roles in the hydrolysis of walls of vegetative cells.

Strains LMJ.RY0402.158615 (a tag-insertion mutant at an exon of Cre13.g605200) and LMJ.RY0402.051804 (a tag-insertion mutant at an exon of the GLE-coding gene) were selected from the CLiP mutant library [32]. We compared the cell mortality of these strains after exposure to the 30-nm iBCA-NPs at a concentration of 100 mg L^{-1}. Consequently, cell mortality of the tag-mutant (LMJ.RY0402.051804) for the GLE-coding gene was found not to be significantly different from that of the CC-5325 mother cells (Fig. 3.6A), whereas the

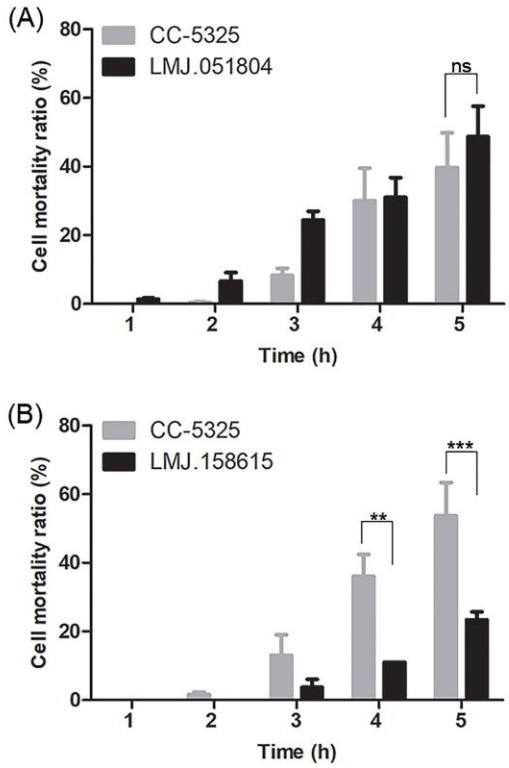

Figure 3.6. Cell mortality in tag-inserted mutants. (A) Cell mortality of the strain LMJ.RY0402.051804, a tag-inserted gametolysin gene (Cre17.g718500) mutant, after exposure to 30-nm poly(isobutylcyano acrylate) resin nanoparticles (iBCA-NPs) at a concentration of 100 mg L^{-1}. (B) Cell mortality of the strain LMJ.RY0402.158615, a tag-inserted Cre13.g605200 gene mutant, after exposure to 30-nm iBCA-NPs at a concentration of 100 mg L^{-1}. CC-5325 is a parental strain of both tag-mutants.; ** p-value < 0.01, *** p-value < 0.001, ns = p > 0.05.

mortality of the Cre13.g605200 tag-mutant was clearly reduced (Fig. 3.6B). Such a clearly visible tolerance of the Cre13.g605200-mutant indicates that its overexpression largely contributed to the cell mortality rate, whereas the overexpression of the GLE-coding gene has a negligible impact.

3.3.9. Analysis of amino acid sequence of Cre13.g605200 protein using liquid chromatography- tandem mass spectrometry (LC-MS/MS)

The enzyme coded by Cre13.g605200 gene was partially purified from 30 nm-iBCA-NPs-treated samples and analyzed by SDS-PAGE. SDS-PAGE showed that the enzyme fraction contains three polypeptide with a molecular weight ranged from ~40 to ~55 kDa (Appendix B, Fig. 3). Based on the calculated molecular weight of the mature protein coded by Cre13.g605200 gene, most probably the major polypeptide with a molecular weight ~ 55 kDa is corresponding to Cre13.g605200 protein. To confirm that, amino acid sequence of the major polypeptide was analyzed by LC-MS/MS. Five major proteins, including the abundant proteins in *C.reinhardtii* cell, ribulose-1,5-bisphosphate carboxylase/oxygenase (large subunit) and beta-1 tubulin, were detected by LC-MS/MS and identified by National Center for Biotechnology Information (NCBI) database (https://www.ncbi.nlm.nih.gov) (data not shown). However, LC-MS/MS failed to detect the protein coded by Cre13.g605200 gene suggesting that the concentration of Cre13.g605200 protein might be insufficient to be detected by LC-MS/MS.

3.3.10. Expression of programmed cell death-related genes

We analyzed the gene expression changes of PCD-related genes induced by exposure of 30-nm iBCA-NPs. We focused on the genes that have been annotated as “PCD” in

Phytozome v. 12.1/ *Chlamydomonas reinhardtii* v. 5.5, i.e., a gene coding for endonuclease G (Cre08.g362750), metacaspase type I (Cre12.g517451), metacaspase type II (Cre03.g184700), and poly(ADP-ribose) polymerase 16 (Cre17.g738550) as well as an inhibitor of apoptosis-promoting *Bax1* gene (*BAX1-I*) (Cre01.g061807) and *p53* gene (Cre01.g032350). Hereafter, we designated the genes that work to promote PCD progress with (*Pro*) and those that work to repress PCD reaction with (*Anti*) based on the analyses in land plants and animals [33–36].

Both metacaspase type I (*Pro*)-coding gene and *BAX1-I* (*Anti*)-coding gene were upregulated with peaks at Stage-1 and Stage-3, respectively, whereas metacaspase type II (*Pro*)-coding gene was prominently depressed at any stage. Poly(ADP-ribose) polymerase 16 (*Anti*)-coding gene was depressed at least at Stage-1 and Stage-3, whereas the expression of the endonuclease G (*Pro*)-coding gene was not largely upregulated at least at Stage-3. Moreover, p53 (*Pro*) gene was slightly upregulated from Stage-1 through Stage-3 (Table 3.4).

Table 3.4. Log_2-FC of programmed cell death related genes by exposure to 30-nm poly(isobutylcyanoacrylate) resin nanoparticles (iBCA-NPs) against TAP cultured control cells containing detergents.

Gene ID	Annotated gene function	Stage-1	Stage-2	Stage-3
Cre12.g517451	Metacaspase type I	5.52	5.17	4.81
Cre03.g184700	Metacaspase type II	-1.09	-1.95	-2.19
Cre08.g362750	Endonuclease G	-0.24*	-0.09*	0.71
Cre17.g738550	poly (ADP-ribose) polymerase 16 (PARP16)	-2.13	-1.61*	-6.76
Cre01.g061807	inhibitor of apoptosis-promoting Bax1	5.39	5.55	5.86
Cre01.g032350	p53-induced protein	1.39	1.53	1.52

* p-value ≥ 0.05.

To investigate whether the induced cell death can be classified as PCD-like cell death, we investigated the status of the isolated DNA after cells were coincubated with the nanoparticles. Laddering DNA of nucleosome units, which is a hallmark of PCD [37], was barely detected in the smeared DNA isolated from the *C. reinhardtii* cells exposed to 100 mg L^{-1} of the 180-nm iBCA-NP for 4–6 h (Fig. 3.7A), whereas much clear laddered DNA was noted in cells treated with 50 mM H_2O_2 for 3 h (Fig. 3.7B). This finding strongly supports the hypothesis that cell death induced by iBCA-NPs is primarily a necrosis-like type, while it is also partly related to the PCD-like type [38].

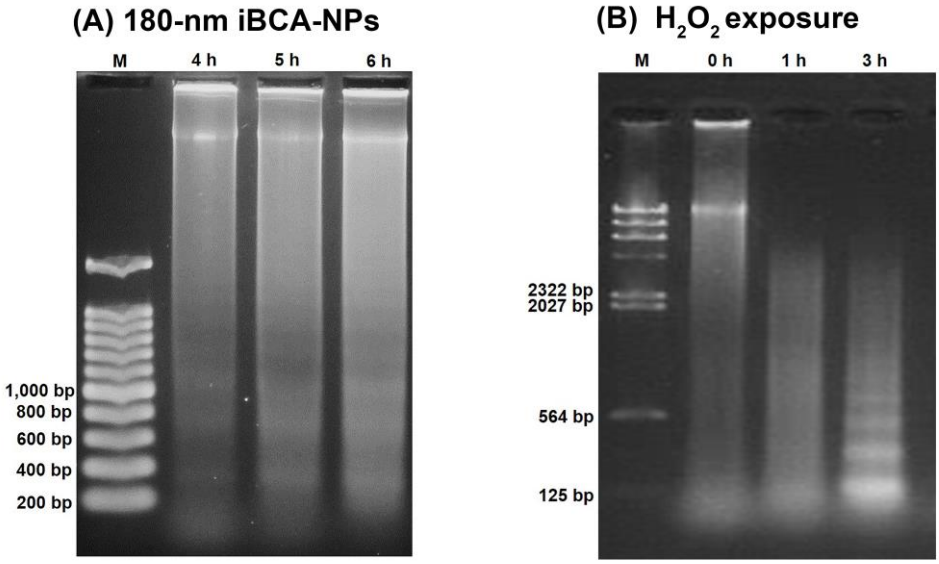

Figure 3.7. Genome DNA analyses after exposure to either poly(isobutylcyanoacrylate) resin nanoparticles (iBCA-NPs) or H_2O_2. (A) *Chlamydomonas reinhardtii* CC-400 wall-deficient mutant cells were exposed to 100 mg L^{-1} 180-nm iBCA-NPs for 4, 5, or 6 h. Subsequently, the isolated DNA was stained with SYBR green after agarose gel electrophoresis. (B) *Chlamydomonas reinhardtii* CC-124 wild type cells were exposed to 50 mM H_2O_2 for 0 h, 1 h, or 3 h. After exposure, the isolated DNA was stained with SYBR green after agarose gel electrophoresis.

3.3.11. Comparison of the exposure effects of 30 nm- and the 180-nm poly(isobutylcyanoacrylate) resin nanoparticles

The 30 nm- and 180-nm iBCA-NPs were composed of the same monomer, isobutyl cyanoacrylate, but synthesized using different detergents. We investigated whether the 180-nm iBCA-NPs have potency to induce overexpression of the genes that were found largely overexpressed by 300 mg L^{-1} 30-nm iBCA-NPs. RT-qPCR analyses were conducted for transcripts coding for HSP22A, HSP22C, GPX5, Fe-SOD, GLE, SPR, and Cre13.g605200 of the cells exposed to 100 mg L^{-1} 180-nm iBCA-NPs for 3 h. After exposure to 100 mg L^{-1} of 180-nm iBCA-NPs, the expression of Cre13.g605200 was prominently elevated at all cell stages (log_2-FCs: Stage-1 = 5.26, Stage-2 = 5.51, Stage-3 = 7.35), whereas the expressions of both GLE (Cre17.g718500) and SPR (Cre09.g393700) - coding genes were not largely changed (Fig. 3.8A).

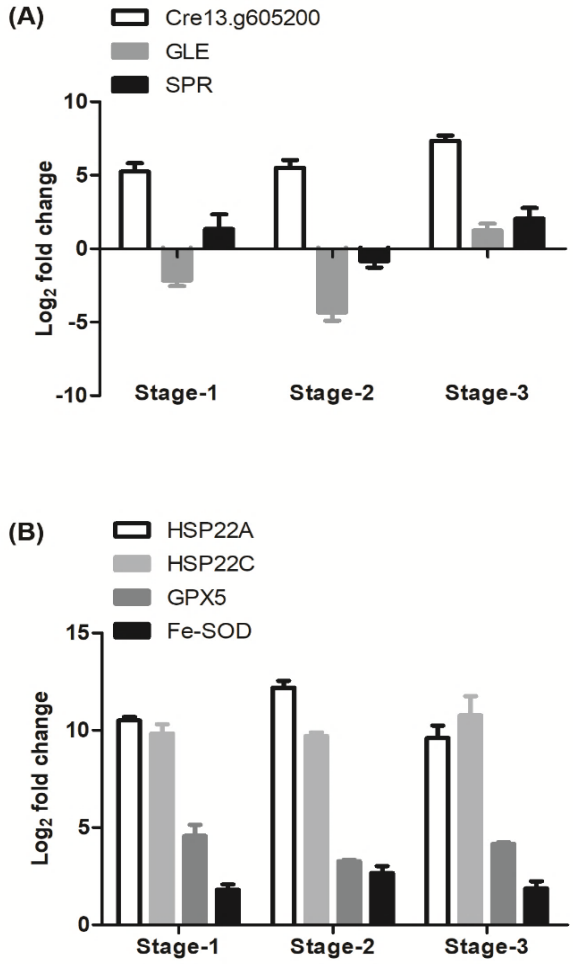

Figure 3.8. Time-course changes in gametolysin (GLE), sporangin (SPR), and Cre13.g605200 transcripts (A) HSP22A, HSP22C, GPX5, and Fe-SOD transcripts (B) following the exposure to 100 mg L^{-1} 180-nm poly(isobutylcyanoacrylate) resin nanoparticles (iBCA-NPs). Data were normalized using eukaryotic translation initiation factor 1A (EIF1A) whose expression was stable through the stages (RPKMs for EIF1A in Stage-1, -2, and -3 were 881.51 ± 23.52, 888.39 ± 36.96, and 1011.52 ± 72.74, respectively). Results are shown as the mean ratios (±SE) from three independent replicates, which were obtained using 3 independently generated samples (3 biological replicates) by quantitative reverse transcription PCR (RT-qPCR).

Moreover, genes coding for both HSPs (HSP22A and HSP22C) and redox enzymes (GPX5 and Fe-SOD) were overexpressed at all stages (Fig. 3.8B). Therefore, spectrum of the overexpressed genes was well-conserved between the two iBCA-NPs irrespective of the difference either in their size or used detergents.

3.3.12. Effect of detergents contained in the 30-nm poly(isobutylcyanoacrylate) resin nanoparticles suspension

We investigated the effect of detergents present in the 30-nm iBCA-NPs suspension by pairwise comparison of transcriptome data, one from the cells cultured in the mere TAP medium and other from the cells cultured in the TAP medium containing detergents. After 2 h, *C. reinhardtii* cells cultured in the TAP medium containing detergents showed no prominent physiological difference from those cultured in the mere TAP. In particular, the ratios of mortal, spheroplast-like, and ROS-positive cells were not prominently increased in any of the two-culture media, suggesting a negligible effect of the two applied detergents (0.003% NEOPELEX G-15 and 0.023% Tween 20).

We compared the transcriptome data obtained from cells cultured for 2 h in TAP medium either with or without the addition of detergents. We focused on 46 genes: 31 cell wall lytic enzyme-coding genes, GSTS1 gene, GPX5 gene, Fe-SOD-coding gene, and 12 HSP family genes. We found that 14 cell wall lytic enzyme-coding genes, GPX5, Fe-SOD-coding gene as well as 6 HSP-coding genes were differentially expressed (p-value < 0.05) relative to detergent addition (Appendix B, Table 5). However, their $\log_2$-FCs were recorded to be <3, except for Cre09.g407050 gene coding for cell wall lytic enzyme and Cre01.g020575 coding for HSP22D. These results show that the effect of detergents on some genes should not be neglected. However, the observed effects of detergents were considerably lower than those of nanoparticles (Table 3.2 and 3.3).

3.4. Discussion

3.4.1. Overexpression of heat shock proteins- and reactive oxygen species (ROS) scavenger-related genes

There was no critical difference recorded in the induced physiological abnormalities caused by cell coincubation with 300 mg L^{-1} 30-nm iBCA-NPs *vs*. 100 mg L^{-1} 180-nm iBCA-NPs. However, an increase in cell morality ratio was much slower after exposure to 180-nm NPs than that after exposure to 30-nm NPs. This corroborates our previous finding that cell mortality ratio increased proportionally to the invested total surface area of iBCA-NPs [10]. Moreover, prominently higher gene overexpression was detected after exposure to 30-nm NPs than after exposure to 180-nm NPs: $\log_2$-FCs for Cre13.g605200, Fe-SOD-coding, and GPX5-coding genes were 11.12, 4.75, and 6.95, respectively, using 30-nm particles at Stage-1 (Table 3.2 and 3.3), whereas the corresponding values for 180-nm particles' treatment were 5.26, 1.80, and 4.57, respectively (Fig. 3.8). Most probably, this difference reflects the extent of induced ROS as can be concluded from the steeper increase in cell mortality after the treatment with 30-nm NPs compared with treatment with 180-nm NPs.

It has been reported that a sublethal level of ROS worked as a signal [39,40] to activate pathways that bolster defense responses in land plants and multicellular animals [39,41]. The same can be applicable to *C. reinhardtii*. Enrichment of HSPs, GPX5, GST1, and Fe-SOD is extremely reasonable for the recovery from ROS damages. It has been reported that HSP22s work to prevent protein aggregation and help in refolding the misfolded proteins [42], whereas redox enzymes such as GPX5, GST1, and Fe-SOD play a role in the antioxidant defense reactions [43,44]. In *C. reinhardtii*, singlet oxygen ($^1O_2$)-induced upregulation of both GPX5- and GSTS1-coding genes has been reported [45], whereas an overexpression of GPX4- and GPX5-coding genes by H_2O_2 is also well described [46]. In our study, expression of the GPX5-

coding gene was largely enhanced (log_2-FC at Stage-1 was 6.95), whereas that of GPX4 slightly decreased (log_2-FC was −2.14 at Stage-1) after exposure to iBCA-NPs. Such a different response of these genes suggests that iBCA-NP exposure induces the generation of $^1O_2$ but not H_2O_2.

We noticed that the gene expression changes caused by ZnO nanoparticles (ZnO-NPs) are similar to those induced by iBCA-NP application. Simon et al. [47] reported the overexpression of HSP-coding genes (HSP22C, HSP70A, HSP90A, and HSP90B) and also that of ROS detoxification-related genes such as those coding for GPX5 and GSTS1 after exposure to 1 mg L^{-1} ZnO-NPs (24–72 nm). However, the intensities of their upregulation were much smaller for ZnO particles application than for the 30-nm iBCA-NPs: log_2-FCs for HSP22C, HSP70A, and HSP90A for the former were 3.87, 2.12, and 1.56, whereas these ratios for the latter were 14.21, 5.18, and 5.23 at Stage-3 (2 h exposure), respectively.

In contrast, effects of TiO_2-NP (15–31 nm diameter size, 1 mg L^{-1}, 2 h exposure) and CdTe/CdS quantum dots (QDs) (3.9–4.7 nm diameter size, 0.125 mg L^{-1}, 2 h exposure) were quite distinct from those caused either by ZnO-NPs [47] or iBCA-NPs. Intriguingly, the expressions of GPX5-, GSTS1-, HSP22A-, HSP22C-, HSP70A-, and HSP90A-coding genes were downregulated, whereas that of HSP90B was upregulated in *C. reinhardtii* by the application of TiO_2-NP and QDs [47].

Such difference may be mainly attributed to the extent of the generated ROS. In our previous paper, by microscopic observation of the DCF fluorescence-positive cells, we have shown that iBCA-NPs can induce much larger ROS production than either TiO_2-NPs or ZnO-NPs applied at the same concentration (100 mg L^{-1}) [10]. Therefore, a higher overexpression of antioxidant enzymes-coding genes after the application of iBCA-NPs relative to that of ZnO-NPs, TiO_2-NPs, or QDs might reflect the extent of the generated ROS levels.

3.4.2. Burst expression of Cre13.g605200 gene coding for gamete lytic enzyme-like activity

Cell wall of the *C. reinhardtii* is composed of hydroxyproline-rich glycoproteins [48–50]. These glycoproteins are subjected to modifications according to a life cycle stage [51–53]. Therefore, *C. reinhardtii* has three types of cell wall lytic enzymes having different specificities: Z-lysin (Cre17.g718450), which breaks off the cell wall of zygospores to liberate zoospores [30]; sporangin (V-lysin, Cre09.g393700), which mediates the breakdown of the sporangial cell wall to release daughter cells from a mother cell; and GLE (gametolysin, autolysin, Cre17.g718500), which digests the cell walls of the gametes before mating. Among these three types of enzymes, only GLE has a potential to additionally hydrolyze the cell wall of vegetative cells [54].

In our previous papers, we have demonstrated that cell wall works as a physical barrier to prevent cell death induction [10,11]. The appearance of spheroplast-like cells at Stage-1 is likely to be related to the overexpression of Cre13.g605200. This is supported by the two facts discovered in this study: first, expression of the authentic GLE-coding gene (Cre17.g718500) was limited (at Stage-1, RPKM=25.78 ± 2.81), whereas that of Cre13.g605200 was very high (at Stage-1, RPKM=411.10 ± 52.84) in the iBCA-NP-exposed cells and second, tag-insertion mutant for Cre13.g605200 showed significantly higher resistance to the nanoparticle inducing cell death than the mother strain, whereas it was not significantly changed in the GLE gene mutant (Fig. 3.6).

Nanoparticle exposure induced a prominent overexpression of Cre13.g605200 that codes for a GLE-like enzyme. However, no induction was detected for the gametogenesis-related genes whose upregulation has been reported [55,56]: no prominent gene expression changes were recorded for any genes coding for GSM1 (homeobox protein transcription factor coded by Cre08.g375400), GSP1 (homeobox transcription factor coded by Cre02.g109650),

NSG1 (unknown function, Cre17.g708750), NSG5 (ribonucleoside-diphosphate reductase R1 coded by Cre12.g492950), and NSG10 (dUTP diphosphatase coded by Cre16.g667850). This suggests that iBCA-NP exposure did not induce gametogenesis of the vegetative cells. Therefore, it can be concluded that the overexpression of Cre13.g605200 is not related to gametogenesis. This is also supported by the fact that N-starvation induces the authentic GLE-coding gene (Cre17.g718500), whereas the induction of Cre13.g605200 is limited [57].

Recently, it has been suggested that ROS functions as signaling molecules to control stress-inducible pathways in plants [39]. ROS accumulation induced by the iBCA-NP exposure suggests that overexpression of Cre13.g605200 is also intermediated by ROS signaling. This is supported by our results in which 2.5 mM H_2O_2 treatment efficiently enhanced the Cre13.g605200 expression compared with the application of 200 mM NaCl, in a situation when the induced cell mortality was ~30% for both treatments (Fig. 3.3).

It is noteworthy that the cell wall of green microalgae is seamless and the original pores residing in the cell wall have a diameter of 5-20 nm [4]. Therefore, iBCA-NPs used in this study cannot go through the cell wall without severely damaging it because even the tiniest nanoparticles present in the 30-nm iBCA-NPs are much larger than the pores (Appendix B, Fig. 1). Therefore, exerting damage to the cell wall is an essential step for nanoparticles to invade the cell interior. Moreover, via transmission electron microscopy observation, it has been shown that 30-nm iBCA-NPs-exposed cells contain nanoparticles in both cytosol and vacuoles [10]. A barrier effect of the cell wall is further supported by our previous report that cell mortality is induced in a much acute manner in the wall-less mutant compared with that in the wild type in *C. reinhardtii* [10] and in an *Emiliania huxleyi* (Haptophyta) strain bearing no coccoliths [11]. In the present study, we further reinforced the barrier effect of the *C. reinhardtii* cell wall by the fact that Cre13.g605200 mutant largely increased its resistance to nanoparticle exposure.

In this study, we addressed a hypothesis that ROS burst is caused by the nanoparticles invading the cell wall, inside of which they can bind to various proteins. It further leads to the functional loss of these proteins by alteration of their three-dimensional structures [10]. This deduction is based on the reports that cyanoacrylate nanoparticles can adsorb either bovine serum albumin (BSA) or proteins present in rat serum [58]. Furthermore, our recent paper reports that either BSA or skim milk coated 180-nm iBCA-NPs can drastically reduce the ability to induce cell death in a Haptophyta species *Prymnesium parvum* [11]. Our hypothesis, hence, contains an elegant explanation of why cell wall has a barrier effect to the nanoparticle-triggered cell death.

3.4.3. Induced necrosis-like and programmed cell death-like cell deaths by coincubation with poly(isobutylcyanoacrylate) resin nanoparticles

The stress caused by UV [59] or menadione [60] can induce PCD-like cell death in *C. reinhardtii* as exemplified by the occurrence of laddered DNA. We presume that the first response to exposure to nanoparticles is the activation of ROS-mediated signaling pathways toward resisting the limited oxidative damage, which is supported by the elevation of both redox-related and HSP-coding genes at Stage-1. Next, by the following burst of ROS, necrosis-like cell death must be induced, as represented by the smeary degraded DNA. DNA damage-induced necrosis pathway mediated by ATP depletion followed by poly(ADP-ribose) polymerase activation is well-studied [61]. Direct chemical reactions of the accumulated ROS with intracellular substances such as proteins, lipids, and DNA [62] might lead to necrosis-like cell death. However, induced cell death was shown to be partly accompanied by PCD-like cell death as observed by the slightly detected laddering DNA in the smeared DNA profiles (Fig. 3.7).

Currently, it is extremely clear that *C. reinhardtii* possesses signaling pathways for

PCD-like cell death because the key genes for PCD such as metacaspase I and II-coding genes have been detected [21,63] and appearance of laddering DNA of nucleosome units has been reported [59,60,64]. However, there are no literature data for microalgae to show primary signal pathways of the PCD and the identity of enrolled proteins. Moreover, some green microalgal species (*Ostreococcus tauri*, *O. lucimarinus*, and *Micromonas* sp. RCC299) have only the initiator metacaspase type I gene, but lack the effector metacaspase type II gene that plays a role in digesting the target proteins [63].

In this study, we recorded the chronological transcriptome changes in the iBCA-NP-treated cells, which lead to cell death that partly includes the PCD-like type. In land plants and animals, the overexpression of BAX (*Pro*), endonuclease G (*Pro*), and p53 (*Pro*) genes and downregulation of Bcl-2 (*Anti*) gene are very commonly detected as change in PCD-related gene expression in a wide range of species [65,66]. However, in *C. reinhardtii*, a decrease in both endonuclease G (*Pro*) and metacaspase II (*Pro*) was observed. Moreover, irrespective of the overexpression of a Bcl-2 family gene, *BAX1-I* (*Anti*), we could not find the target of the inhibitor protein BAX (*Pro*) or BAK (*Pro*) in the *C. reinhardtii* genome. According to these results, it can be speculated that *C. reinhardtii* have developed a unique PCD pathway that is rather different from well-described cell death strategies detected in land plants and animals. Further studies are warranted to uncover the PCD-signaling pathways in microalgae.

3.5. References

[1] X. Lu, D. Wu, Z. Li, G. Chen, Polymer Nanoparticles, in: A. Villaverde (Eds.), Progress in Molecular Biology and Translational Science, Academic Press, London, 2011, pp. 299-323. https://doi.org/10.1016/B978-0-12-416020-0.00007-3.

[2] T.J. Baker, C.R. Tyler, T.S. Galloway, Impacts of metal and metal oxide nanoparticles on marine organisms, Environ. Pollut. (2013) 1–15. https://doi.org/10.1016/j.envpol.2013.11.014.

[3] A. Nel, T. Xia, L. Mädler, N. Li, Toxic potential of materials at the nanolevel, Science 311 (2006) 622–627. https://doi.org/10.1126/science.1114397.

[4] E. Navarro, A. Baun, R. Behra, N.B. Hartmann, J. Filser, A.J. Miao, A. Quigg, P. H. Santschi, L. Sigg, Environmental behavior and ecotoxicity of engineered nanoparticles to algae, plants, and fungi, Ecotoxicology 17 (2008) 372–386. https://doi.org/10.1007/s10646-008-0214-0.

[5] P. Bhattacharya, S. Lin, J.P. Turner, P.C. Ke, Physical adsorption of charged plastic nanoparticles affects algal photosynthesis, J. Phys. Chem. C. 114 (2010) 16556–16561. https://doi.org/10.1021/jp1054759.

[6] M.A. Maurer-Jones, I.L. Gunsolus, C.J. Murphy, C.L. Haynes, Toxicity of engineered nanoparticles in the environment, Anal. Chem. 85 (2013) 3036–3049. https://doi.org/10.1021/ac303636s.

[7] F.D. Jaeghere, E. Doelker, R. Gurny, Encyclopedia of Control Drug Delivery, in: E. Mathiowitz (Ed.), Nanoparticles, John Wiley & Sons, New York, 1999, pp. 641–663.

[8] M.N.V.R. Kumar, Nano and Microparticles as Controlled Drug Delivery Devices, J. Pharm. Pharm. Sci. 3 (2000) 234-258.

[9] S. Shirotake, A new cyanoacrylate colloidal polymer with novel antibacterial mechanism and its application to infection control, J. Nanomedine Biother. Discov. 4 (2014) 1–7.

[10] D. Widyaningrum, D. Iida, Y. Tanabe, Y. Hayashi, S.D. Kurniasih, T. Ohama, Acutely induced cell mortality in the unicellular green alga *Chlamydomonas reinhardtii*

(Chlorophyceae) following exposure to acrylic resin nanoparticles, J. Phycol. 55 (2019) 118–133. https://doi.org/10.1111/jpy.12798.

[11] A.J.S. Al-Azab, D. Widyaningrum, H. Hirakawa, Y. Hayashi, S. Tanaka, T. Ohama, A resin cyanoacrylate nanoparticle as an acute cell death inducer to broad spectrum of microalgae, Algal Res. 54 (2021) 102–191. https://doi.org/10.1016/j.algal.2021.102191.

[12] N.M. Franklin, N.J. Rogers, S.C. Apte, G.E. Batley, G.E. Gadd, P.S. Casey, Comparative toxicity of nanoparticulate ZnO, bulk ZnO, and $ZnCl_2$ to a freshwater microalga (*Pseudokirchneriella subcapitata*): The importance of particle solubility, Environ. Sci. Technol. 41 (2007) 8484–8490. https://doi.org/10.1021/es071445r.

[13] V. Aruoja, H.C. Dubourguier, K. Kasemets, A. Kahru, Toxicity of nanoparticles of CuO, ZnO and TiO_2 to microalgae *Pseudokirchneriella subcapitata*, Sci. Total Environ. 407 (2009) 1461–1468.

[14] F. Li, Z. Liang, X. Zheng, W. Zhao, M. Wu, Z. Wang, Toxicity of nano-TiO_2 on algae and the site of reactive oxygen species production, Aquat. Toxicol. 158 (2015) 1–13. https://doi.org/10.1016/j.aquatox.2014.10.014.

[15] J. Zhao, X. Cao, X. Liu, Z. Wang, C. Zhang, J.C. White, B. Xing, Interactions of CuO nanoparticles with the algae *Chlorella pyrenoidosa*: adhesion, uptake, and toxicity, Nanotoxicology 10 (2016) 1297–1305. https://doi.org/10.1080/17435390.2016.1206149.

[16] J. Huang, J. Cheng, J. Yi, Impact of silver nanoparticles on marine diatom *Skeletonema costatum*, J. Appl. Toxicol. 36 (2016) 1343–1354. https://doi.org/10.1002/jat.3325.

[17] Y. Wang, X. Zhu, Y. Lao, X. Lv, Y. Tao, B. Huang, J. Wang, J. Zhou, Z. Cai, TiO_2 nanoparticles in the marine environment: Physical effects responsible for the toxicity on algae *Phaeodactylum tricornutum*, Sci. Total Environ. 565 (2016) 818–826.

https://doi.org/https://doi.org/10.1016/j.scitotenv.2016.03.164.

[18] P. Couvreur, B. Kante, M. Roland, P. Guiot, P. Bauduin, P. Speiser, Polycyanoacrylate nanocapsules as potential lysosomotropic carriers: preparation, morphological and sorptive

properties, J. Pharm. Pharmacol. 31 (1979) 331–332. https://doi.org/10.1111/j.2042- 71 58.1979.tb13510.x.

[19] G. Yordanov, Poly(alkyl cyanoacrylate) nanoparticles as drug carriers 33 years later, Bulg. J. Chem. 1 (2012) 61-72. https://www.researchgate.net/publication/260795492.

[20] W. Strober, Trypan Blue Exclusion Test of Cell Viability, Curr. Protoc. Immunol. 111 (2015) A3.B.1-A3.B.3. https://doi.org/10.1002/0471142735.ima03bs111.

[21] S.S. Merchant, S.E. Prochnik, O. Vallon, E.H. Harris, S.J. Karpowicz, G.B. Witman, A. Terry, A. Salamov, L.K. Fritz-laylin, L. Maréchal-drouard, W.F. Marshall, L. Qu, D.R. Nelson, A.A. Sanderfoot, M.H. Spalding, V.V Kapitonov, Q. Ren, P. Ferris, E. Lindquist, H. Shapiro, S.M. Lucas, J. Grimwood, The Chlamydomonas Genome Reveals the Evolution of Key Animal and Plant Functions, Science 318 (2007) 245–252.

[22] S. Anders, W. Huber, Differential expression analysis for sequence count data, Nature Precedings. (2010) 1.

[23] M.W. Pfaffl, A new mathematical model for relative quantification in real-time RT-PCR, Nucleic Acids Res. 29 (2001) e45-e45.

[24] S.V. Pollock, B. Mukherjee, J. Bajsa-Hirschel, M.C. Machingura, A. Mukherjee, A.R. Grossman, J.V. Moroney, A robust protocol for efficient generation, and genomic characterization of insertional mutants of *Chlamydomonas reinhardtii*, Plant Methods. 13 (2017). https://doi.org/10.1186/s13007-017-0170-x.

[25] J.D. Thompson, D.G. Higgins, T.J. Gibson, CLUSTAL W: Improving the sensitivity of progressive multiple sequence alignment through sequence weighting, position-specific gap penalties and weight matrix choice, Nucleic Acids Res. 22 (1994) 4673–4680. https://doi.org/10.1093/nar/22.22.4673.

[26] S. Kumar, G. Stecher, M. Li, C. Knyaz, K. Tamura, MEGA X: Molecular evolutionary genetics analysis across computing platforms, Mol. Biol. Evol. 35 (2018) 1547–1549. https://doi.org/10.1093/molbev/msy096.

[27] T. Kubo, The structure and function of the matrix metalloproteinase gene family in *Chlamydomonas reinhardtii*, Protozool. J. 39 (2006) 47–51.

[28] C. Tallant, A. Marrero, F.X. Gomis-Rüth, Matrix metalloproteinases: Fold and function of their catalytic domains, Biochim. Biophys. Acta - Mol. Cell Res. 1803 (2010) 20–28. https://doi.org/10.1016/j.bbamcr.2009.04.003.

[29] J. Felsenstein, Evolutionary Trees from DNA Sequences: A Maximum Likelihood Approach, J. Mol. Evol. 17 (1981) 368-376.

[30] U.G. Schlösser, Algal wall-degrading enzymes — autolysines, in: W. Tanner, F. A. Loewus (Eds.), Encyclopedia of plant physiology new series, Springer, Berlin, Heidelberg, New York, 1981, pp. 333–351.

[31] L. Jaenicke, W. Kuhne, R. Spessert, U. Wahle, S. Waffenschmidt, Cell-wall lytic enzymes (autolysins) of *Chlamydomonas reinhardtii* are (hydroxy)proline-specific proteases, J. Eur. Biochem. 170 (1987) 485-491.

[32] X. Li, W. Patena, F. Fauser, R.E. Jinkerson, S. Saroussi, M.T. Meyer, N. Ivanova, J.M. Robertson, R. Yue, R. Zhang, J. Vilarrasa-Blasi, T.M. Wittkopp, S. Ramundo, S.R. Blum, A. Goh, M. Laudon, T. Srikumar, P.A. Lefebvre, A.R. Grossman, M. C. Jonikas, A genome-wide algal mutant library and functional screen identifies genes required for

eukaryotic photosynthesis, Nat. Genet. 51 (2019) 627–635. https://doi.org/10.1038/s41588-019-0370-6.

[33] M.D. Jacobson, M. Weil, Programmed cell death review in animal development, Cell 88 (1997) 347-354.

[34] Y. Sun, Y. Zhao, X. Hong, Z. Zhai, Cytochrome c release and caspase activation during menadione-induced apoptosis in plants, FEBS Lett. 462 (1999) 317–321.

[35] M. Elbaz, A. Avni, M. Weil, Constitutive caspase-like machinery executes programmed cell

death in plant cells, Cell Death Differ. 9 (2002) 726–733. https://doi.org/10.1038/sj.cdd.4401030.

[36] N.V. Chichkova, S.H. Kim, E.S. Titova, M. Kalkum, V.S. Morozov, Y.P. Rubtsov, N.O. Kalinina, M.E. Taliansky, A.B. Vartapetian, A Plant Caspase-Like Protease Activated during the Hypersensitive Response, Plant Cell 16 (2004) 157–171. https://doi.org/10.1105/tpc.017889.

[37] A.H. Wyllie, Glucocorticoid-induced thymocyte apoptosis is associated with endogenous endonuclease activation, Nature 284 (1980) 555–556. https://doi.org/10.1038/284555a0.

[38] E.A. Prokhorova, A.Y. Egorshina, B. Zhivotovsky, G.S. Kopeina, The DNA-damage response and nuclear events as regulators of nonapoptotic forms of cell death, Oncogene 39 (2020) 1–16. https://doi.org/10.1038/s41388-019-0980-6.

[39] K. Apel, H. Hirt, Reactive oxygen species: Metabolism, oxidative stress, and signal transduction, Annu. Rev. Plant Biol. 55 (2004) 373–399. https://doi.org/10.1146/annurev.arplant.55.031903.141701.

[40] C.H. Foyer, G. Noctor, Redox homeostasis and antioxidant signaling: A metabolic interface between stress perception and physiological responses, Plant Cell 17 (2005) 1866–1875. https://doi.org/10.1105/tpc.105.033589.

[41] G. Storz, L.A. Tartaglia, B.N. Ames, Transcriptional regulator of oxidative stress-inducible
genes: Direct activation by oxidation, Science 248 (1990) 189–194. https://doi.org/10.1126/science.2183352.

[42] G. Morrow, M. Samson, S. Michaud, R.M. Tanguay, Overexpression of the small mitochondrial Hsp22 extends Drosophila life span and increases resistance to oxidative stress., FASEB J. 18 (2004) 598–599. https://doi.org/10.1096/fj.03-0860fje.

[43] E. Pigeolet, P. Corbisier, A. Houbion, D. Lambert, C. Michiels, M. Raes, M.D. Zachary, J. Remacle, Glutathione peroxidase, superoxide dismutase, and catalase inactivation by peroxides and oxygen derived free radicals, Mech. Ageing. Dev. 51 (1990) 283-297.

[44] J.M. Matés, C. Pérez-Gómez, I.N. De Castro , Antioxidant enzymes and human diseases Antioxidant Enzymes and Human Diseases, Clin. Biochem. 32 (1999) 595–603. https://doi.org/10.1016/S0009-9120(99)00075-2.

[45] H.K. Ledford, B.L. Chin, K.K. Niyogi, Acclimation to Singlet Oxygen Stress in *Chlamydomonas reinhardtii*, Eukaryot. Cell 6 (2007) 919–930. https://doi.org/10.1128/EC.00207-06.

[46] I.K. Blaby, C.E. Blaby-Haas, M.E. Pérez-Pérez, S. Schmollinger, S. Fitz-Gibbon, S.D. Lemaire, S.S. Merchant, Genome-wide analysis on *Chlamydomonas reinhardtii* reveals the impact of hydrogen peroxide on protein stress responses and overlap with other stress transcriptomes, Plant J. 84 (2015) 974–988. https://doi.org/10.1111/tpj.13053.

[47] D.F. Simon, R.F. Domingos, C. Hauser, C.M. Hutchins, W. Zerges, K.J. Wilkinson, Transcriptome sequencing (RNA-seq) analysis of the effects of metal nanoparticle exposure on the transcriptome of *Chlamydomonas reinhardtii*, Appl. Environ. Microbiol. 79 (2013) 4774–4785. https://doi.org/10.1128/AEM.00998-13.

[48] D.H. Miller, I.S. Mellman, D.T.A. Lamport, M. Miller, The chemical composition of the cell wall of *chlamydomonas gymnogama* and the concept of a plant cell wall protein, J. Cell Biol. 63 (1974) 420–429. https://doi.org/10.1083/jcb.63.2.420.

[49] U.W. Goodenough, J.E. Heuser, The Chlamydomonas cell wall and its constituent glycoproteins analyzed by the quick-freeze, deep-etch technique, J. Cell Biol. 101 (1985) 1550–1568. http://rupress.org/jcb/article-pdf/101/4/1550/371890/1550.pdf.

[50] J.H. Lee, S. Waffenschmidt, L. Small, U. Goodenough, Between-species analysis of short-repeat modules in cell wall and sex-related hydroxyproline-rich glycoproteins of Chlamydomonas, Plant Physiol. 144 (2007) 1813–1826. https://doi.org/10.1104/pp.107.100891.

[51] J.P. Woessner, U.W. Goodenough, Molecular Characterization of a Zygote Wall Protein: An Extensin-Like Molecule in *Chlamydomonas reinhardtii*, The plant cell 1 (1989) 901-911.

[52] J.P. Woessner, U.W. Goodenough, Zygote and vegetative cell wall proteins in *Chlamydomonas reinhardtii* share a common epitope, (SerPro)x, Plant Science 83 (1992) 65-76.

[53] L. Suzuki, J.P. Woessner, H. Uchida, H. Kuroiwa, Y. Yuasa, S. Waffenschmidt, U.W. Goodenough, T. Kuroiwa, A zygote-specific protein with hydroxyproline-rich glycoprotein domains and lectin-like domains involved in the assembly of the cell wall of *Chlamydomonas reinhardtii* (Chlorophyta), J. Phycol. 36 (2000) 571-583.

[54] H. Claes, Autolyse der zellwand bei den gameten von *Chlamydomonas reinhardii*, Arch.

Für Mikrobiol. 78 (1971) 180–188. https://doi.org/10.1007/bf00424874.

[55] J. Abe, T. Kubo, Y. Takagi, T. Saito, K. Miura, H. Fukuzawa, Y. Matsuda, The transcriptional program of synchronous gametogenesis in *Chlamydomonas reinhardtii*, Curr. Genet. 46 (2004) 304–315. https://doi.org/10.1007/s00294-004-0526-4.

[56] J. Abe, T. Kubo, T. Saito, Y. Matsuda, The Regulatory Networks of Gene Expression during the Sexual Differentiation of *Chlamydomonas reinhardtii* , as Analyzed by Mutants for Gametogenesis, Plant Cell Physiol. 46 (2005) 312–316. https://doi.org/10.1093/pcp/pci025.

[57] N.R. Boyle, M.D. Page, B. Liu, I.K. Blaby, D. Casero, J. Kropat, S.J. Cokus, A. Hong-hermesdorf, J. Shaw, S.J. Karpowicz, S.D. Gallaher, S. Johnson, C. Benning, M. Pellegrini, A. Grossman, S.S. Merchant, Three Acyltransferases and Nitrogen-responsive Regulator Are Implicated in Nitrogen Starvation-induced Triacylglycerol Accumulation in Chlamydomonas, J. Biol. Chem. 287 (2012) 15811–15825. https://doi.org/10.1074/jbc.M111.334052.

[58] A.K.O. Åslund, E. Sulheim, S. Snipstad, E. Von Haartman, H. Baghirov, N. Starr, M. Kvale Løvmo, S. Lelú, D. Scurr, C.D.L. Davies, R. Schmid, Ý. Mørch, Quantification and Qualitative Effects of Different PEGylations on Poly(butyl cyanoacrylate) Nanoparticles, Mol. Pharm. 14 (2017) 2560–2569. https://doi.org/10.1021/acs.molpharmaceut.6b01085.

[59] S. Moharikar, J.S. D'Souza, A.B. Kulkarni, B.J. Rao, Apoptotic-like cell death pathway is induced in unicellular chlorophyte *Chlamydomonas reinhardtii* (Chlorophyceae) cells following UV irradiation: Detection and functional analyses, J. Phycol. 42 (2006) 423–433. https://doi.org/10.1111/j.1529-8817.2006.00207.x.

[60] V.L. Sirisha, M. Sinha, J.S. D'Souza, Menadione-induced caspase-dependent

programmed cell death in the green chlorophyte *Chlamydomonas reinhardtii*, J. Phycol. 50 (2014) 587–601. https://doi.org/10.1111/jpy.12188.

[61] O. Surova, B. Zhivotovsky, Various modes of cell death induced by DNA damage, Oncogene 32 (2013) 3789–3797. https://doi.org/10.1038/onc.2012.556.

[62] P. Moradas-Ferreira, V. Costa, P. Piper, W. Marger, The molecular defences against reactive oxygen species in yeast, Mol. Microbiol. 19 (1996) 651–658.

[63] C.J. Choi, J.A. Berges, New types of metacaspases in phytoplankton reveal diverse origins
of cell death proteases, Cell Death Dis. 4 (2013) e490-e490. https://doi.org/10.1038/cddis.2013.21.

[64] S.L. Vavilala, K.K. Gawde, M. Sinha, J.S. D'Souza, Programmed cell death is induced by hydrogen peroxide but not by excessive ionic stress of sodium chloride in the unicellular
green alga *Chlamydomonas reinhardtii*, Eur. J. Phycol. 50 (2015) 422–438.https://doi.org/10.1080/09670262.2015.1070437.

[65] R. Hückelhoven, BAX Inhibitor-1 , an ancient cell death suppressor in animals and plants with prokaryotic relatives, Apoptosis 9 (2004) 299–307.

[66] M.J. Akhtar, M. Ahamed, S. Kumar, M.M. Khan, J. Ahmad, S.A. Alrokayan, Zinc oxide nanoparticles selectively induce apoptosis in human cancer cells through reactive oxygen species, Int. J. Nanomed. 7 (2012) 845. https://doi.org/10.2147/IJN.S29129.

CHAPTER FOUR: GENERAL CONCLUSION

The intensive use of ENPs in industrial and medical applications and their inadequate disposal into the environment raise the concern of their toxic effect on living organisms. In this study, acrylic resin nanoparticles derived from isobutyl cyanoacrylate monomers (iBCA-NPs) were tested for their physiological and molecular effect on different algal species. It was found that iBCA-NPs induced acute cell death in different algal species belonging to the SAR and Hacrobia clades. The induced cell death was accompanied by ROS accumulation, where the ROS level increased along with an increase of the cell death ratio. However, the addition of an ROS scavenger (NAC) significantly reduced the cell death ratio. Moreover, disorders of both mitochondria and chloroplast structures in *R. atrorosea* cells were detected using TEM images. The variation in the algal cell covering structure indicates different sensitivities to iBCA-NPs. High sensitivity to iBCA-NPs was detected in species bearing no cell covering or a cell covering that easily allows the invasion of NPs, suggesting that the target of NPs to induce cell death, most probably proteins, is located inside the cell walls.

IBCA-NPs also induced the expression of antioxidant enzymes and HSP genes in *C. reinhardtii*. Overexpression of these genes enables cells to cope with oxidative stress caused by NPs. Besides that, one of the cell wall hydrolytic enzyme-coding genes, Cre13.g605200, was largely overexpressed. The tag-insertion mutants of this gene showed remarkable resistance to nanoparticle-induced cell death, suggesting that overexpression of this gene is essential to induce efficient cell death by the exposure of iBCA-NPs. Moreover, the status of isolated DNA following the exposure to iBCA-NPs indicated that iBCA-NPs induced necrosis-like cell death, which is partly accompanied by PCD-like cell death.

APPENDIX A: SUPPORTING FIGURES AND VIDEOS FOR CHAPTER TWO

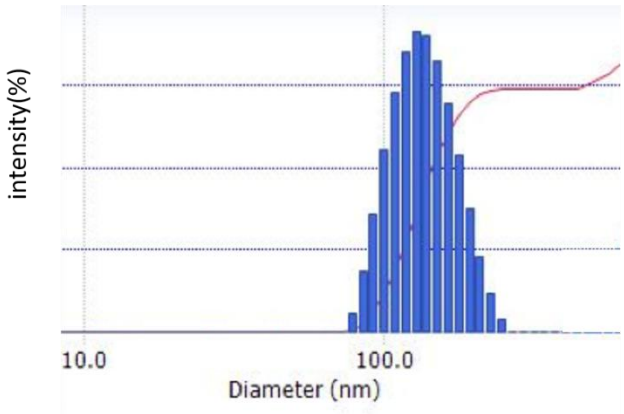

Figure 1. Particle size distribution of poly(isobutylcyanoacrylate) resin nanoparticles (iBCA-NPs) measured based on the dynamic light scattering method. Red line shows accumulated intensity.

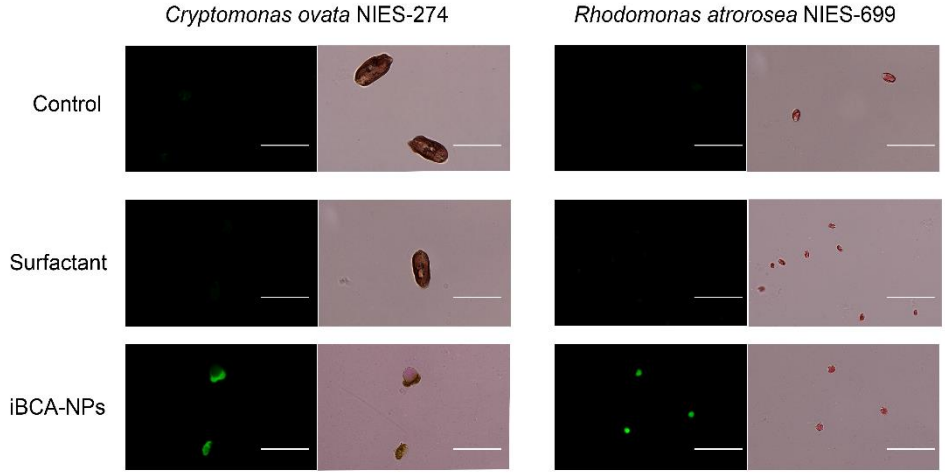

Figure 2. 2',7'- dichlorofluorescein (DCF) fluorescence observed in *Cryptomonas ovata* NIES-274 (Cryptophyta) and *Rhodomonas atrorosea* NIES-699 (Cryptophyta) after a 1-h exposure to poly(isobutylcyanoacrylate) resin nanoparticles (iBCA-NPs) at 100 mg L^{-1}. Left panels show fluorescence images, while right panels are bright-field images. Control, cells were cultured in a normal medium. Surfactant, cells were cultured in the dextran-containing medium. Bar, 20 µm.

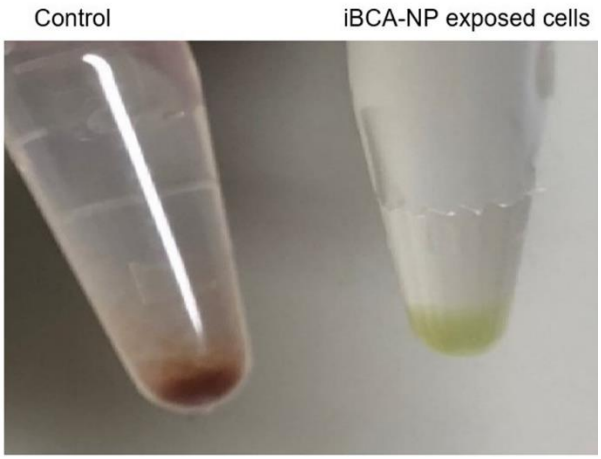

Figure 3. Changes in the color of *Rhodomonas atrorosea*. Cells were exposed to poly(isobutylcyanoacrylate) resin nanoparticles (iBCA-NPs) at 100 mg L^{-1} for 24 h and then centrifuged. Control, cells not exposed to iBCA-NPs.

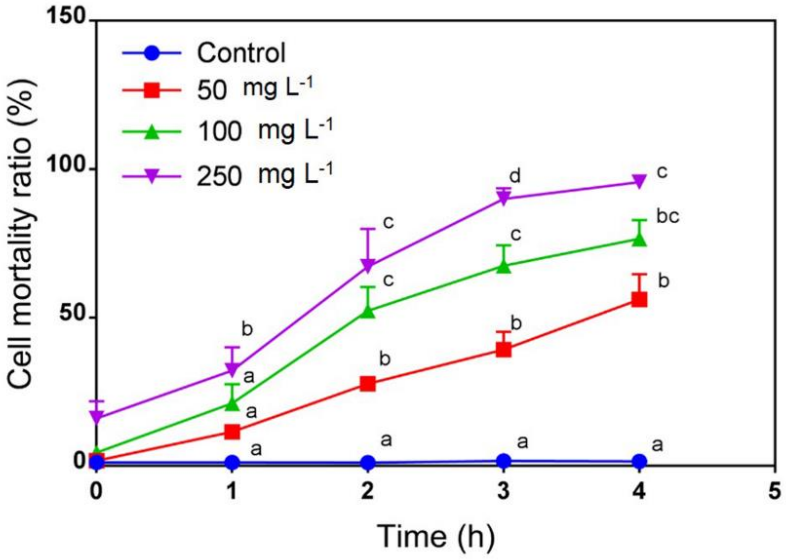

Figure 4. Time-course changes in cell mortality in *Prymnesium parvum* by the exposure of different concentrations (w/v) of poly(isobutylcyanoacrylate) resin nanoparticles (iBCA-NPs). Results are shown as the mean ratios (± SE) from three independent experiments. Values with different superscript letters are significantly different at each measured time point ($p < 0.05$).

Video 1 (A).mp4

Video 1A. Dark field microscopic observation for the collision of poly(isobutylcyanoacrylate) resin nanoparticles (iBCA-NPs) with the cells of *Prymnesium parvum*.

Video 1 (B).mp4

Video 1B. Dark field microscopic observation for the abonormal swimming pattern and the apperance of protoplast-like cells of *Prymnesium parvum* following 1 h exposure to poly(isobutylcyanoacrylate) resin nanoparticles (iBCA-NPs).

APPENDIX B: SUPPORTING FIGURES AND TABLES FOR CHAPTER THREE

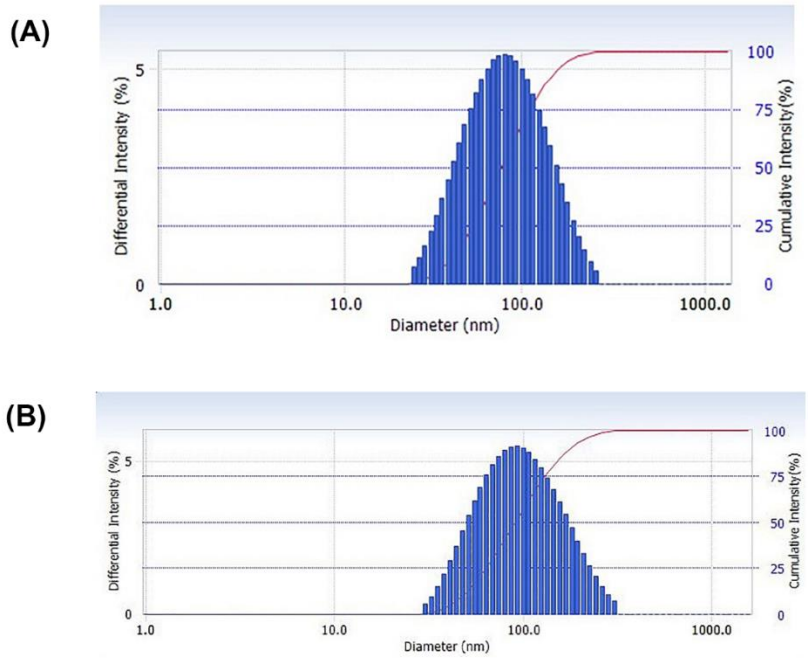

Figure 1. Particle size distribution of 30 nm-sized poly(isobutylcyanoacrylate) resin nanoparticles (iBCA-NPs). (A) Particle size distribution of 1% 30 nm-sized iBCA-NPs measured immediately after synthesis. (B) Particle size distribution of 1% 30 nm-sized iBCA-NPs measured after two cycles of sedimentation. Red line shows cumulative intensity.

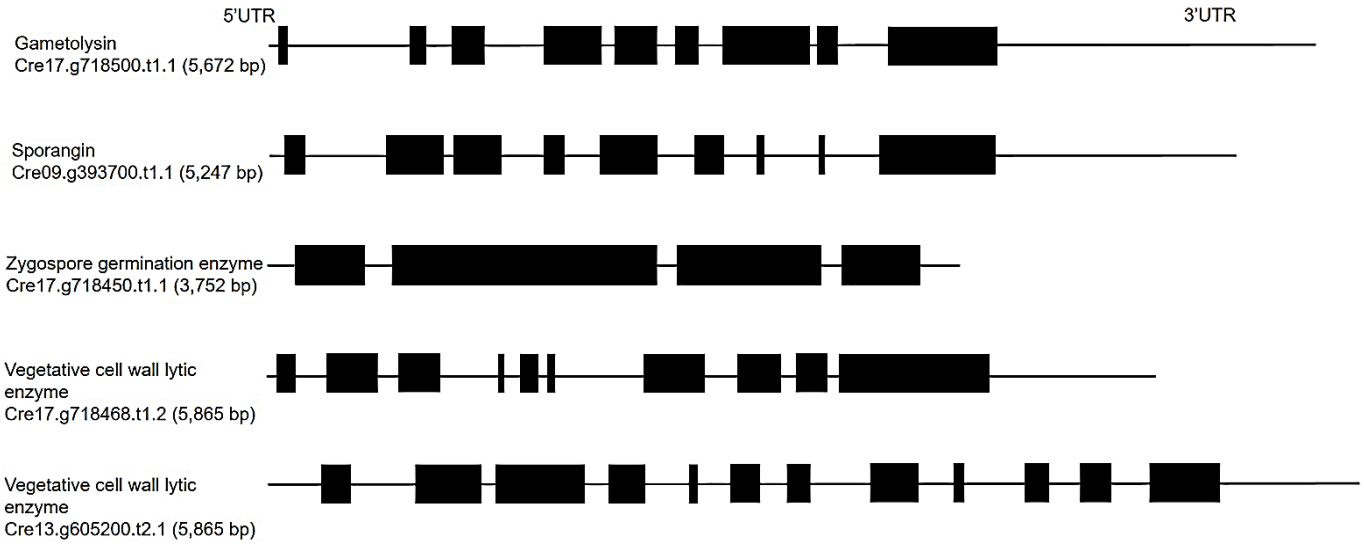

Figure 2. Exon-intron arrangement in cell wall hydrolytic enzymes-coding genes. Exons are shown as black rectangles, while introns are presented as solid lines. UTR, untranslated region.

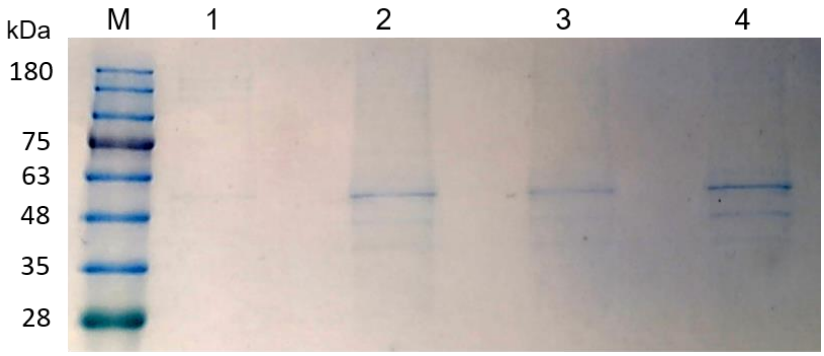

Figure 3. SDS-polyacrylamide gel electrophoresis of the partially purified Cre13.g605200 enzyme. Enzyme fraction from TAP cultured control cells containing detergents (lane 1); enzyme fraction from treated cells with 300 mg L^{-1} of 30-nm poly(isobutylcyanoacrylate) resin nanoparticles (iBCA-NPs) (lanes 2-4); M, protein marker.

Table 1. List of primer sequences used for quantitative reverse transcription PCR (RT-qPCR).

Gene ID	Annotated gene function	Forward primer (5'-3')	Reverse Primer (5'-3')
Cre13.g605200	Matrix metalloproteinase	AAGTTCTCAAACCCCGACCG	GTGCCCTCCTTGGTGTCAAA
Cre09.g393700	Matrix metalloproteinase (Autolysin type)	TTGAGTACGGCGACCAGACC	GTTGGCGACGGTGAGGTTTC
Cre17.g718500	Matrix metalloproteinase, gamete lytic enzyme (G-lysin)	AATCCTTCCAGGTTCGGTGCC	GTGGGCGAATCCAACGGAAG
Cre07.g318800	Heat shock protein 22A	CGCGCCTATGGACATCATCG	GCCTCCTTGGTGGTGTGAGA
Cre03.g145787	Heat shock protein 22C	GGGTCCCACAGCTAAAAGGC	CCCCCTGACGTGACAAAGAC
Cre10.g458450	Glutathione peroxidase	AGTCTGATGTGGCTGTGCGA	ATATGTACGGGCCTCGGTGC
Cre10.g436050	Fe superoxide dismutase	CCGTGATAGCCTGGTTTCGC	GCATGATCTGGGGGAGTGGT
Cre02.g103550	Eukaryotic translation initiation factor 1A, EIF1A	AGTATGCCCAAGTGATCCGC	CCTCATCCGCTGTGTACTTCAT

Table 2. Ratios of cell mortality induced by 30-nm poly(isobutylcyanoacrylate) resin nanoparticles (iBCA-NPs)

Treatment time	Cell mortality ratio[a]
10 min (Stage-1)	2.67 ± 0.98
60 min (Stage-2)	15.00 ± 1.41
120 min (Stage-3)	32.33 ± 1.19

[a] Results are shown as the mean ratios (±SE) from three independent experiments.

Table 3. Ratios of 2',7'- dichlorofluorescein (DCF) fluorescence positive cells induced by 30-nm poly(isobutylcyanoacrylate) resin nanoparticles (iBCA-NPs).

Treatment time	2',7'- dichlorofluorescein (DCF) fluorescence positive cells ratio[a]
10 min (Stage-1)	0.67 ± 0.24
60 min (Stage-2)	9.67 ± 0.85
120 min (Stage-3)	24.00 ± 0.82

[a] Results are shown as the mean ratios (±SE) from three independent experiments.

Table 4. Ratios of cell mortality induced by 180-nm poly(isobutylcyanoacrylate) resin nanoparticles (iBCA-NPs)

Treatment time	Cell mortality ratio[a]
60 min (Stage-1)	2.00 ± 0.47
120 min (Stage-2)	14.00 ± 1.69
180 min (Stage-3)	31.67 ± 3.60

[a] Results are shown as the mean ratios (±SE) from three independent experiments

Table 5. List of genes of which expressions were significantly changed in TAP culture condition with and without detergents.

Gene ID	Annotated gene function	Log_2-FC	*p*-value
Cre03.g170850	Matrix metalloproteinase	1.80	2.49×10^{-29}
Cre05.g232600	Gametolysin/Lysin	2.36	1.40×10^{-15}
Cre06.g278152	Gametolysin/Lysin	-1.13	3.25×10^{-08}
Cre06.g278164	Gametolysin/Lysin	-1.05	4.33×10^{-3}
Cre07.g333400	Matrix metalloproteinase	0.67	1.89×10^{-4}
Cre09.g393700	Matrix metalloproteinase (Autolysin type)	0.84	8.98×10^{-07}
Cre09.g396772	Similar to Gametolysin and Autolysin	-0.65	1.52×10^{-2}
Cre09.g407050	Matrix metalloproteinase	5.05	7.24×10^{-17}
Cre10.g421350	Matrix metalloproteinase	1.82	1.73×10^{-14}
Cre11.g467684	Gametolysin/Lysin	-0.67	3.32×10^{-3}
Cre16.g680902	Gametolysin/Lysin	1.26	9.58×10^{-05}
Cre17.g708450	Matrix metalloproteinase	2.83	1.78×10^{-34}
Cre17.g718468	Gametolysin/Lysin	0.58	8.68×10^{-4}
Cre17.g718500	Matrix metalloproteinase, gamete lytic enzyme (G-lysin)	0.58	2.59×10^{-3}
Cre10.g436050	Fe superoxide dismutase	0.51	1.00×10^{-3}
Cre10.g458450	Glutathione peroxidase	0.52	3.71×10^{-3}
Cre01.g020575	Heat shock protein 22D (HSP22D)	3.16	9.95×10^{-3}
Cre14.g617450	Heat shock protein 22E (HSP22E)	1.62	1.47×10^{-09}
Cre14.g617400	Heat shock protein 22F (HSP22F)	2.15	9.18×10^{-13}
Cre08.g372100	Heat shock protein 70A (HSP70A)	-0.45	3.33×10^{-3}
Cre16.g677000	Heat shock protein 70E (HSP70E)	-0.49	1.15×10^{-3}
Cre09.g386750	Heat shock protein 90A (HSP90A)	-0.36	1.97×10^{-2}

Video 1.mp4

Video 1. *Chlamydomonas reinhardtii* cells exposed to the detergent-reduced 30-nm poly(isobutylcyanoacrylate) resin nanoparticles (iBCA-NPs) at a concentration of 300 mg L^{-1} for 3 min.

Video 2.mp4

Video 2. A *Chlamydomonas reinhardtii* cell exposed to detergent-reduced 30-nm poly(isobutylcyanoacrylate) resin nanoparticles (iBCA-NPs) at a concentration of 300 mg L^{-1} for 60 min. The bright spots in the enlarged vacuole in Brownian motion are nanoparticles.

ACHIEVEMENTS

List of publications

- A.J.S. Al-Azab, D. Widyaningrum, H. Hirakawa, Y. Hayashi, S. Tanaka, T. Ohama, A resin cyanoacrylate nanoparticle as an acute cell death inducer to broad spectrum of microalgae, Algal Res. 54 (2021) 102–191.
- A.J.S. Al-Azab, Y. Aoki, F.D. Sarian, Y. Sori, D. Widyaningrum, T. Yamasaki, F. Kong, T. Ohama, Chronological transcriptome changes induced by exposure to cyanoacrylate resin nanoparticles in *Chlamydomonas reinhardtii*, Algal Res. (*Under review*)

Conferences

- A.J.S. Alazab, D. Widyaningrum, Y. Hayashi, T. Ohama. Acutely induced burst ROS generation and cell death on board algal species by resin nanoparticle exposure. 5th International Volvox Conference. 26th-29th July 2019, Tokyo, Japan. (Oral)